ANL-HEP-PR--90-28

DE90 012153

ANALYTIC MULTI-REGGE THEORY AND THE POMERON IN QCD—PART I*

ALAN R. WHITE
High Energy Physics Division
Argonne National Laboratory
Argonne, IL 60439

Abstract

The formalism of Analytic Multi-Regge Theory is developed as a basis for the study of abstract Critical and Super-Critical Pomeron high-energy behavior and for related studies of the Regge behavior of spontaneously broken gauge theories and the Pomeron in QCD.

Asymptotic domains of analyticity for multiparticle amplitudes are shown to follow from properties of Field Theory and S-Matrix Theory. General asymptotic dispersion relations are then derived for such amplitudes in which the spectral components are described by the graphical formalism of hexagraphs. Further consequences are distinct Sommerfeld- Watson representations for each hexagraph spectral component, together with a complete set of angular momentum plane unitarity equations which control the form of all multi-Regge amplitudes. Because of this constraint of "Reggeon Unitarity" the Critical Pomeron solution of the Reggeon Field Theory gives the only known "non-trivial" unitary high-energy S-Matrix.

By exploiting the full structure of multi-Regge amplitudes as the Pomeron becomes Super-Critical, the *simultaneous* modification of hadrons and the Pomeron can be studied. The result is a completely consistent description of the Super-Critical Pomeron appearing in hadron scattering. Reggeon Unitarity is satisfied in the Super-Critical Phase by the appearance of a massive "gluon" (Reggeised vector particle) coupling pair-wise to the Pomeron.

*Work supported by the U.S. Department of Energy, Division of High Energy Physics, Contract W-31-109-ENG-38.

DISCLAIMER

1. INTRODUCTION

QCD is now firmly established as the gauge theory of the strong interaction. It is commonly believed that the theory can be calculated in the ultra-violet region via the parton model and perturbation theory and that in the infra-red region it can at least be approximated via lattice gauge theory. An optimist might believe that it is only a matter of time before the continuum limit of lattice QCD is proved to exist, giving a confining, unitary, theory of hadrons and giving the parton model at short distances. This article is most directly aimed at the pessimist (or realist) who is persuaded (persuadable) that coupling the current infra-red and ultra-violet understanding of QCD is a major challenge for which new technology may be at least desirable, if not mandatory. The general purpose of the article, which will be published in two separate parts, is to provide a comprehensive analysis and review of how Analytic Multi-Regge Theory, when applied to the problem of the Pomeron in QCD, provides both new technology and a simultaneous confrontation with infra-red and ultra-violet properties of the theory.

A primary ambition of the article, and of this first part in particular, is to demonstrate that the vacuum quantum number multi-Regge region of the strong-interaction multiparticle S-Matrix is close to being determined by the very powerful general principles of analyticity and unitarity. We can then argue that in this truly mixed infra-red/ultra-violet kinematical regime, unitarity provides an explicit challenge to the complete formulation of QCD. This argument will provide the dominant theme of the second part of the article, which will contain all the analysis of gauge theories and of QCD in particular. We shall see that ultimately confinement, chiral symmetry-breaking, asymptotic freedom and the parton-model, and even the quark flavor spectrum all couple together in the problem of obtaining a fully unitary high-energy S-Matrix within QCD.

During the barren years of quantum field theory (for the strong interaction) the most sophisticated analyticity methods were developed[1,2] to study multi-Regge behavior and its inter-relation with unitarity. However, the resulting formalism is not well-known, nor is its underlying basis well understood. Consequently the early Sections of this article will be devoted to a broad and fairly comprehensive development of the subject. The essential results are first that in the multi-Regge asymptotic regime there are relatively simple many-variable domains of analyticity and corresponding multiparticle dispersion relations

are valid. Secondly consequent generalised Sommerfeld-Watson representations exist which lead to asymptotic behavior strongly constrained by "cross-channel" multiparticle unitarity continued in the complex angular momentum plane. At the Regge pole level the asymptotic amplitudes obtained from these representations were shown[1,3,4,5] to coincide (in all essential respects) with those calculated directly from "dual models". Such amplitudes are, of course, now understood as tree-level string theory amplitudes and so it follows that the multi-Regge form of string theory amplitudes is just that imposed by the requirements of analyticity and unitarity. Not surprisingly these requirements do not determine, or even constrain, the number and nature of the quantum numbers involved in a string theory.

The strongest constraints are actually on multi-Regge behavior involving the Pomeron—where no quantum numbers are exchanged. The concept of the Pomeron was originally purely phenomenological. It was introduced[6] as a Regge pole with vacuum quantum numbers which is responsible for the energy independence (up to logarithms) of total cross-sections. However, it became clear, even before the advent of QCD, that the Pomeron is at the core of a fundamental high-energy, strong-interaction, "vacuum problem". This is the problem of producing a *non-trivial* high-energy S-Matrix which is consistent with both direct-channel and *cross-channel* unitarity. We shall call a high-energy S-Matrix *non-trivial* if *all total and inclusive cross-sections do not go to zero asymptotically.* Producing such an S-Matrix is a "vacuum problem" in that those channels which are related to physical cross-sections via optical theorems necessarily involve "vacuum" quantum number exchange. It is the fundamental importance of angular momentum plane unitarity[1,7] (Reggeon Unitarity) for a non-trivial high-energy S-Matrix that suggests the problem is best analysed in the language of Regge theory and the Pomeron. However, the derivation of further "direct-channel" unitarity constraints[8–11] and several "no-go theorems"[4,12,13] emphasised that even in this formalism finding a solution would be far from easy.

Note that since the resulting large transverse momentum cross-sections do not decrease with energy, the requirement within QCD that perturbation theory and the parton-model are valid in the ultra-violet region actually determines that the high-energy S-Matrix must be non-trivial. Therefore QCD must provide a solution to the full high-energy vacuum problem if it is indeed a complete theory of the strong interaction with all the properties we would like! As we already implied above we shall find that within QCD the high-energy vacuum problem is intimately related to the full vacuum problem.

The basic reason that Pomeron amplitudes are so constrained, and the high-energy problem correspondingly difficult, is that "multi-Pomeron" exchanges (Regge Cuts) are also required by unitarity and they are necessarily as important in the asymptotic S-Matrix as single Pomeron exchange. Consequently there is an unavoidable "strong-coupling" problem - the major constraint on which is that of Reggeon Unitarity. This is explicitly satisfied in the (perturbative) formalism of Pomeron Reggeon Field Theory.[13,14] Indeed it was a very elegant application[16,17] of renormalisation group methods to the Reggeon Field Theory, in the mid-70's, which finally produced an infra-red fixed-point, scaling solution of Reggeon Unitarity for the Pomeron. This solution, the "Critical Pomeron", is a vital part of the basic argument which this article advances. We shall emphasise that the Critical Pomeron is both completely formulated and absolutely calculable and also gives the only known non-trivial unitary high-energy S-Matrix. We shall argue both that it is crucial to the consistency of QCD that the Critical Pomeron be the true high-energy behavior and also that QCD explains why the Critical Pomeron occurs!

The foremost problem posed by our general purpose is clearly that of making direct contact between the abstract Pomeron formalism developed before QCD and the explicit formulation of a non-abelian gauge theory. It is quite probable that a large N topological expansion has a straightforward correspondence with the general Pomeron Reggeon Field Theory perturbation expansion[18]. However, this correspondence is only qualitative and certainly does not allow us to discuss the detailed dynamical question of the Criticality of the Pomeron. Fortunately a direction in which to proceed is provided by the answer to another question which was also posed, and studied, before the advent of QCD.

As part of its formulation it is clear that the Critical Pomeron is a "phase-transition" point for a class of "Sub-Critical" Pomeron theories in which the asymptotic S-Matrix is trivial - that is total cross-sections go to zero asymptotically as a power of the energy (the power decreasing to zero as the critical point is approached). The question is whether there exists a "Super-Critical Phase" and if so what are its distinguishing properties. There was much controversy surrounding this subject in the late 70's. Several authors[19–21] advocated an "Expanding Disc" solution of the problem which (at least) saturates the energy dependence of the Froissart bound and so potentially gives a non-trivial S-Matrix in the sense discussed above. We argued then (and have re-emphasised recently[22] in the context of minijet models) that the large transverse momentum dependence of the Expanding Disc inevitably violates Reggeon Unitarity. Indeed this was the case for all explicit versions of this solution that

could be constructed[21].

We should point out that our criticism of the Expanding Disc "solution" of Reggeon Field Theory applies to all high-energy models or "theories" giving Froissart bound saturating energy dependence ("Froissarton" behavior). That is such behavior is almost certainly in direct contradiction with angular momentum plane unitarity and therefore is inconsistent with the basic analyticity and crossing properties of the hadron S-Matrix. Indeed, if this form of high-energy behavior could be made to satisfy some form of Reggeon Unitarity, all of our discussion of the constraints placed on QCD in the multi- Regge region would be empty. It is almost trivial to obtain Froissarton behavior as a first approximation in a wide variety of circumstances and if there were no problem with unitarity there is little doubt that it would arise as the exact high-energy behavior in almost all such circumstances. It would then be futile to look for any deep constraint on a theory by studying the high-energy S-Matrix. This is clearly the very opposite of our point of view. We believe the constraint of producing a unitary Pomeron is the deepest of constraints on a theory. (As an aside we might mention that the problem of producing a consistent reggeised graviton is a generalised Super-Critical Pomeron problem in string theories, whose solution probably involves the sister trajectories and hence[23] the detailed algebraic structure of such theories, in an intricate manner. This almost certainly places a very strong constraint on such theories—perhaps even selecting the desired *unique* theory!)

Our major contribution[24] to the Super-Critical Pomeron controversy was to advocate a solution to the problem which is again characterised by asymptotically decreasing cross-sections, that is a "trivial" high-energy S-Matrix. The distinction from the Sub-Critical phase is the presence of a "Pomeron Condensate" together with an odd-signature component of the Pomeron associated with a vector particle. At the Critical point the vector particle decouples while its mass simultaneously goes to zero. The problem with this solution was always that we were unable to find a formulation for introducing the Pomeron Condensate which unambiguously defined the graphical rules of the theory and clearly satisfied Reggeon Unitarity. Nevertheless we became convinced that this solution described the (partial) deconfinement of a gauge theory and that the Reggeised massive vector particle we had found emerging out of the Critical Pomeron would provide a key to the exact nature of such an underlying theory. We then began studying the possible connection of the Regge behavior of massive gauge theories to the high-energy behavior of QCD. Our hope was that we would uncover the Super-Critical Pomeron theory we had proposed and that the ambiguity

in the rules would somehow be resolved by the gauge theory context. A number of articles published over the years[25-27] have gradually elaborated the physics that we have come to believe underlies the relation of the Super-Critical Pomeron to spontaneously broken QCD. This relationship will, of course, be extensively covered in the second part of this article.

As our direct study of the Pomeron within QCD developed we found that the inevitable confrontation with confinement involved several deep issues that actually required a full exploitation of multi-Regge theory for their resolution. Specifically, it was necessary to simultaneously study both the formation of hadrons (as Reggeons) and the Pomeron by studying appropriate multi-Regge amplitudes. We then realised that almost the same issues were involved in the ambiguities of defining the Super-Critical Phase and so their resolution should be similar. Following this idea through, we have now found that if we consider a multi-Regge amplitude in which we can simultaneously study the modification of the Pomeron and the modification of hadrons by the Pomeron, then the introduction of a Pomeron Condensate leads to an unambiguous theory. (In this context a hadron is simply a massive particle lying on a Regge trajectory). The full discontinuity structure of multi-Regge amplitudes and Regge cuts is involved in the formulation but the outcome is a straightforward set of graphical rules. Reggeon Unitarity is explicitly satisfied, with the properties of the resulting Super-Critical Pomeron exactly as we had previously conjectured.

It seems therefore that, after more than ten years of (intermittent) study, we can finally claim to have solved the problem of the Super-Critical Pomeron. The description of this solution actually provides a self-contained motivation for this part of our article in that all of the analyticity properties and multi-Regge theory that we develop and review are necessary background for the presentation of the Super-Critical Pomeron. However, this material will also be an essential background for our analysis of QCD in the second part of the article. More importantly perhaps we believe that the abstract formalism of Analytic Multi-Regge Theory will eventually prove to be very powerful for studying many aspects of gauge theories, string theories and perhaps more general theoretical formalisms. Most of the review material incorporated in this article is not appropriately presented elsewhere and it surely provides an essential basis for future development of the subject.

We shall discuss explicitly the relationship between the phase structure of QCD and the Pomeron phase transition in the second part of the article. This will make it clear that the Super-Critical Pomeron provides a vital bridge between the perturbative Regge behavior

of an entirely massive gauge theory (in which the gauge symmetry is completely broken) and the Pomeron of unbroken QCD. That is the Super-Critical Pomeron describes a *partial* breaking of the SU(3) gauge symmetry of QCD down to SU(2). The extraction of the theory with unbroken SU(2) symmetry from completely massive (spontaneously broken) QCD is an infra-red problem that will be a major topic in part two.

The outline of this Part is as follows. We begin in Section 2 with a description of the multiparticle angular variables that we utilise for all of the analyticity and Regge theory analysis. The introduction of these variables is extensively described in several articles[1,4,28,29]. However, there is almost no usage of them in current research work. We give a brief but complete, in principle, description which is aimed directly at the applications in the following Sections. The over-riding virtue of the angular variables is that they provide a complete and *unconstrained* set of independent Lorentz-invariant variables for a general N-point amplitude.

Section 3 is devoted to a description of the domains of analyticity of multiparticle amplitudes and related asymptotic dispersion relations. We discuss the basis of these properties in Field theory and S-Matrix theory. Both the generality of the material and the presentation distinguish this Section from previous related discussions. The Section closes with a complete description, utilising "hexagraphs"[1], of the break-up of a general multiparticle amplitude into spectral components via an asymptotic dispersion relation. The essence of the general multi-Regge theory developed in Section 4 is that each hexagraph spectral component has a distinct Sommerfeld-Watson Representation utilising distinct Froissart-Gribov Continuations. We emphasise the inter-relation of the particle pole structure of a hexagraph spectral component with the asymptotic discontinuity structure. This inter-relation is essential in the formulation of the Super-Critical Pomeron. We also note a connection with the structure of sister Regge trajectory contributions in multiparticle string-theory amplitudes.

The complete Reggeon Unitarity equation for a general hexagraph Froissart-Gribov amplitude is the subject of Section 5. That angular momentum plane unitarity is effectively diagonalised by the break-up of a general amplitude into hexagraph spectral components is an essential element in the derivation. In Section 6 we move on to the relationship between Reggeon Unitarity and Reggeon Field Theory for the Pomeron. We then present a brief review of both the formulation and some key features of the Critical Pomeron.

Section 7 contains our new formulation of the Super-Critical Pomeron. An important point is that once all of the necessary background multi-Regge theory is in place, it is clear

that the appropriate "classical solution" defining the Pomeron condensate is a symmetric stationary point which always appeared to have many virtues as a candidate "vacuum" but was thought to give an unstable perturbation expansion[30]. The new formulation we present produces a straightforwardly stable expansion with the unstable classes of graphs simply absent.

Section 8 summarises our view of the general significance of the Pomeron phase transition for the high-energy vacuum problem, in preparation for the analysis of QCD in the second part of the article.

2. MULTIPARTICLE KINEMATICS

Regge theory is, in a sense, generalized partial-wave analysis. Not surprisingly therefore to apply such an analysis to a multiparticle amplitude we must first introduce a set of angular variables. Although we shall make little direct use of these variables in the second part of the article, involving the analysis of QCD, they play a basic role in the initial dispersion theory and complex angular momentum theory. Therefore a reader wishing to understand these basic formalisms must have a working knowledge of the angular variables. We shall therefore elaborate their properties rather more pedantically than in previous articles. We shall do this by first giving an excessively pedantic treatment of elastic scattering which will then generalize in a straightforward manner.

2.1 Elastic Scattering

A four-point amplitude is a function of the four on-mass-shell momenta satisfying

$$p_i^2 = m_i^2 \qquad i = 1, 2, 3, 4 \tag{2.1}$$

which if incoming particles carry positive energy and outgoing particles carry negative energy satisfy momentum conservation in the form

$$\sum_{i=1}^{4} p_i = 0 \tag{2.2}$$

There are three obvious Lorentz-invariant variables

$$s = (p_1 + p_2)^2, \qquad t = (p_1 + p_3)^2 \quad \text{and} \quad u = (p_1 + p_4)^2 \tag{2.3}$$

which, of course, satisfy

$$s + t + u = \sum_{i=1}^{4} m_i^2. \tag{2.4}$$

If p_1 and p_2 are incoming particles (and for simplicity we take $m_i^2 = m^2 \quad i = 1, \ldots 4$) then the physical region is

$$\text{I}: \quad s \geq 4m^2, \qquad t, u < 0. \tag{2.5}$$

There are two other physical regions in which p_1 and p_4, and p_1 and p_3, are respectively incoming momenta, that is

$$\text{II}: \quad u \geq 4m^2, \qquad t, s < 0, \tag{2.6}$$

$$\text{III}: \quad t \geq 4m^2, \qquad s, u < 0. \tag{2.7}$$

We introduce the t-channel center-of-mass scattering angle by the following procedure. First we define Lorentz frames $\tilde{F}_1, \ldots, \tilde{F}_4$ in which the external momenta p_i respectively have the *standard* form

$$p_i^0 = (m, 0, 0, 0). \tag{2.8}$$

Next we define further standard frames F_1 and F_2 in which $Q = (p_1 + p_3)$ has the standard form

$$Q^0 = (Q, 0, 0, 0) \qquad t = Q^2 > 0. \tag{2.9}$$

In F_1 we also require that p_1 and p_3 lie in the z-t plane. Therefore to transform from frame $\tilde{F}_1$ to F_1 we can apply a boost $a_z(\zeta)$ in the z-t plane such that

$$p_1 = a_z(\zeta)p_1^0 = (m\cosh\zeta, 0, 0, m\sinh\zeta) \qquad \cosh\zeta = \frac{Q}{2m}. \tag{2.10}$$

In F_2 we similarly require that p_2 and p_4 lie in the $(z$-$t)$ plane, so that p_2 in particular has the form (2.10) but with the sign of the time component reversed.

Since Q has the form Q^0 in both frame F_1 and F_2 it follows that these two frames differ by a Lorentz transformation g such that

$$gQ^0 = Q^0. \tag{2.11}$$

That is g belongs to the "little group" of Q^0 which, since Q^0 is timelike, implies that

$$g \in \mathrm{SO}(3). \tag{2.12}$$

We can parameterize SO(3) as

$$g = u_z(\mu)u_x(\theta)u_z(\nu) \qquad \begin{matrix} 0 \le \theta < \pi \\ 0 \le \nu,\ \mu \le 2\pi \end{matrix}, \tag{2.13}$$

where u_z and u_x are respectively rotations about the z and x axes.

We can express invariant variables in terms of μ, θ, and ν by computing all the relevant external momenta in one particular standard frame. To compute s, for example, we can compute p_1 and p_2 in frame F_1. p_1 already has the form (2.10), while p_2 has this form in frame F_2. Therefore we apply g to p_2 in the form (2.10) to obtain its form in F_1. That is we first calculate

$$u_z(\nu)(-m\cosh\zeta, 0, 0, m\sinh\zeta) = (-m\cosh\zeta, 0, 0, m\sinh\zeta), \tag{2.14}$$

and then

$$u_x(\theta)(-m\cosh\zeta, 0, 0, m\sinh\zeta) = (-m\cosh\zeta, 0, m\sinh\zeta\sin\theta, m\sinh\zeta\cos\theta), \tag{2.15}$$

and finally applying $u_z(\mu)$ gives

$$p_2 = (-m\cosh\zeta, m\sinh\zeta\sin\theta\sin\mu, m\sinh\zeta\sin\theta\cos\mu, m\sinh\zeta\cos\theta). \tag{2.16}$$

Utilizing (2.10) and (2.16) directly we find that

$$s = (p_1 + p_2)^2 = -2m^2\cosh^2\zeta - 2m^2\sinh^2\zeta\cos\theta + 2m^2 \tag{2.17}$$

$$= -2m^2\sinh^2\zeta(1 + \cos\theta) \tag{2.18}$$

$$= \frac{(4m^2 - t)}{2}(1 + \cos\theta). \tag{2.19}$$

Similarly we find

$$u = (p_1 + p_4)^2 = \frac{(4m^2 - t)}{2}(1 - \cos\theta). \tag{2.20}$$

Clearly we recognize θ as the usual t-channel center of mass scattering angle which we have simply introduced in a rather elaborate way. Note that while the invariants s and u are independent of the azimuthal angles μ and ν, these angles would appear in the spin-dependence of amplitudes if we considered particles with spin. Analogous angles will play an important role in the multiparticle amplitudes we consider shortly.

Note that the constraint (2.4) is automatically satisfied by the parameterization (2.19) and (2.20) and so t and $z = \cos\theta$ can be used as independent *unconstrained* variables. The three physical regions are then

$$\begin{aligned} &\text{I.} \quad t < 0, \quad z \geq 1, \\ &\text{II.} \quad t < 0, \quad z \leq -1 \\ &\text{III.} \quad t \geq 4m^2 \quad -1 \leq z \leq 1. \end{aligned} \tag{2.21}$$

Since (2.19) and (2.20) express $\cos\theta$ as a function of invariant variables only it is clear that although introduced in a frame-dependent manner it is really a Lorentz-invariant variable. We refer to I and II as *direct channels*. Regge singularities in the *cross-channel* or t-channel III describe high-energy scattering in the direct channels.

We can also introduce the variables t and z in the direct channels. Since $t < 0$ we replace the standard form (2.9) in the frames F_1 and F_2 by

$$Q^0 = (0, 0, 0, Q) \qquad t = -Q^2 < 0. \tag{2.22}$$

We change (2.10) only in that $\sinh\zeta = Q/2m$ (instead of $\cosh\zeta$). (2.12) is replaced by

$$g \in \mathrm{SO}(2,1), \tag{2.23}$$

and so we write

$$g = u_z(\mu)a_x(\beta)u_z(\nu) \qquad \begin{matrix} -\infty < \beta < \infty \\ 0 \le \mu, \nu \le 2\pi \end{matrix}, \tag{2.24}$$

where a_x is now a boost in the $x - t$ plane. In frame F_1, (2.16) is replaced by (note that p_2 is now an incoming momentum)

$$p_2 = (m\cosh\zeta\cosh\beta,\ m\cosh\zeta\sinh\beta\cos\mu,\ m\cosh\zeta\sinh\beta\sin\mu,\ m\sinh\zeta)\,, \tag{2.25}$$

so that now

$$s = (p_1 + p_2)^2 = 2m^2\cosh^2\zeta\cosh\beta - 2m^2\sinh^2\zeta + 2m^2 \tag{2.26}$$

$$= \frac{(4m^2 - t)}{2}(\cosh\beta + 1)\,, \tag{2.27}$$

and so we can directly identify $z = \cosh\beta$ and, of course, recover the parameterization (2.21) of the s-channel physical region. To recover the parameterization (2.21) of the u-channel we can simply add the "TCP" transformation

$$g : z = \cosh\beta \to -z \tag{2.28}$$

as an extension of SO(2,1) and include the s and u-channels in the same little group parameterization.

It will also be useful for the following to extend our elastic scattering kinematical analysis to the unphysical situation of particles with spacelike masses. That is we now consider replacing (2.8) by

$$p_i^0 = (0, 0, 0, p) \qquad -p^2 = m^2 < 0. \tag{2.29}$$

If Q remains spacelike we now replace (2.10) by

$$p_1 = u_y(\phi)p_1^0 = (0, p\sin\phi, 0, p\cos\phi) \qquad \cos\phi = \frac{Q}{2P}. \tag{2.30}$$

To obtain the equivalence of the independence of μ and ν in (2.17)–(2.20) we must replace the parameterization (2.13) of SO(2,1) by one of the form

$$g = a_y(\alpha)\tilde{g}a_y(\gamma) \qquad -\infty < \alpha, \gamma < \infty. \tag{2.31}$$

In fact, if we choose $\tilde{g} \equiv a_x(\beta)$ we do not cover the whole group. Instead we have to use both

$$\tilde{g} \equiv a_x(\beta) \qquad -\infty < \beta < \infty \qquad \text{allowing both } \cosh\beta \geq 1 \text{ and } \cosh\beta \leq -1$$

and

$$\tilde{g} \equiv u_z(\theta) \qquad 0 \leq 0 \leq 2\pi. \tag{2.32}$$

Repeating (2.14) to (2.16) gives that in F_1, for $\tilde{g} = a_x(\beta)$,

$$p_2 = (p\sin\phi\sinh\beta\cosh\alpha,\ p\sin\phi\cosh\beta,\ p\sin\phi\sinh\beta\sinh\alpha,\ -p\cos\phi) \tag{2.33}$$

or for $\tilde{g} = u_z(\theta)$

$$p_2 = (p\sin\phi\sin\theta\sinh\alpha,\ p\sin\phi\cos\theta,\ p\sin\phi\sin\theta\cosh\alpha,\ -p\cos\phi) \tag{2.34}$$

and hence

$$s = -2p^2\sin^2\phi\, z + 2p^2\cos^2\phi - 2p^2 \tag{2.35}$$

$$= \frac{(4m^2 - t)}{2}(z + 1), \tag{2.36}$$

where now $z = \cosh\beta$ *and* $z = \cos\theta$ in the parameterization (2.32). In effect the three physical ranges of z appearing in (2.21) all describe "physical" real momenta when the external masses are spacelike.

Finally we note that we can also consider one set of external momenta, p_1 and p_3 say, to be timelike (and sum to a spacelike vector) while allowing the remaining two momenta to be spacelike. In this case we could repeat the above analysis using yet another parameterization of SO(2,1) namely

$$g = u_z(\mu)a_x(\beta)a_y(\gamma) \qquad -\infty < \beta, \gamma < \infty \tag{2.37}$$

$$0 \leq \mu \leq 2\pi.$$

Our next task is to generalize the above discussion to an arbitrary multiparticle amplitude.

2.2 Toller Diagrams and Little Group Variables

For a multiparticle amplitude there are many possible sets of angular variables.[1,4,28,29] They are distinguished by the *Toller diagram* with which they are associated. A Toller diagram is a tree diagram with *only three-point vertices.* For every Toller diagram there is a distinct set of angular variables and, as we shall describe in the next Section, a distinct asymptotic dispersion relation. We use a general formalism to introduce the variables and use the above discussion to be more specific when necessary.

For an N-point amplitude we denote the external momenta as P_i, $i = 1, \ldots, N$ and introduce internal momenta Q_j, $j = 1, \ldots, N-3$ for each internal line of the Toller diagram as illustrated in Fig. 2.1. The Q_j are defined by imposing momentum conservation at each vertex (following the momentum flow of the incoming momenta). Next we introduce *three standard* Lorentz frames at each vertex (including the external vertices) in each of which one of the three momenta entering the vertex has a standard form. To be specific we can utilize (2.9) ((2.8)) if Q_j (P_i) is timelike or (2.22) ((2.29)) if Q_j (P_i) is spacelike. We denote as g_j the Lorentz transformation—associated with the internal line j—which transforms between the two standard frames for Q_j defined respectively at the two vertices to which the line j is attached. Since Q_j has the same form Q_j^0 in both standard frames g_j necessarily belongs to the little group of Q_j^0 implying (as above) that

$$\begin{aligned} &g_j \in \mathrm{SO}(2,1) \text{ if } Q_j \text{ is spacelike} \\ &g_j \in \mathrm{SO}(3) \text{ if } Q_j \text{ is timelike.} \end{aligned} \tag{2.38}$$

We also introduce the Lorentz transformations ζ_{jk} transforming between the standard frames defined for Q_j and Q_k respectively, at the same vertex. Note that ζ_{jk} is a function of $t_j = Q_j^2$, $t_k = Q_k^2$ and $t_\ell = (Q_j + Q_k)^2$ only. In analogy with (2.10) and (2.14)–(2.16) we can combine the g_j and ζ_{jk} (together with ζ_{ij} transformations defined analogously to the ζ_{jk}, but at external vertices) to determine any of the external momenta in any of the standard frames associated with the Toller diagram. Consequently for the N-point amplitude M_N we can write

$$M_N(p_1, \ldots, p_N) \equiv M_N(t_1, \ldots, t_{N-3}, g_1, \ldots, g_{N-3}). \tag{2.39}$$

If we initially consider all the Q_j to be timelike then we can use the parameterization (2.13) for the g_j. We can also take all the ζ_{jk} and ζ_{ij} to be boosts $a_z(\zeta)$ in the z-t plane. In this case the u_z rotations clearly commute with the a_z and as a result the external invariant variables depend only on combinations $w_{jk} = \mu_j - \nu_k$ of the azimuthal angles. (This is a generalization of the independence of s and u of μ and ν in (2.19) and (2.20)). The net effect is that the angular variables for each Toller diagram reduce always to the $(3N-10)$ independent variables which we know it is possible to find for an N-point amplitude. There are always

$$\left.\begin{array}{ll} (N-3) & t_i \text{ variables } (\equiv Q_i^2) \\ (N-3) & z_j \text{ variables } (\equiv \cos\theta_j) \\ (N-4) & u_{jk} \text{ variables} (\equiv e^{i w_{jk}}) \end{array}\right\} (3N-10) \text{ variables.} \tag{2.40}$$

Just as t and z were an unconstrained, Lorentz invariant, independent set of variables for the elastic amplitude, so for each Toller diagram the t_j, z_j, and u_{jk} variables are an unconstrained Lorentz invariant set for the N-point amplitude. given the complicated (Gram-determinant) constraints satisfied by the complete set of momentum or invariant variables for a general amplitude, this is a remarkable simplification, which is particularly important for the dispersion relations we describe in the next Section.

Before discussing the details of spacelike kinematics for a general Toller diagram we first introduce an extended tree-diagram notation which can be used to distinguish both the "direct channels" in which the Q_j are spacelike and the "cross-channels" in which these momenta are timelike.

2.3 Hexagraphs, Cross-Channels, Direct Channels and Twisting

We begin by first introducing a set of *planar Toller diagrams* for each Toller diagram. These are obtained by considering all scattering processes for which *all* the Q_j are spacelike. Each distinct process is then drawn as proceeding via the particular Toller diagram, but in a *plane* and with the incoming particle lines drawn vertically entering the diagram from the bottom and the outgoing particles similarly exiting from the top. The Q_j lines are drawn horizontal when they don't meet internal vertices and close to horizontal when they do. An example of the resulting set of *planar* Toller diagrams obtained from a simple Toller diagram is shown in Fig. 2.2. We shall not distinguish processes differing by the TCP transformation of incoming particles into outgoing particles. The set of planar Toller diagrams is in one to

one correspondence with the set of *direct channels* for a general Toller diagram.

From the set of planar Toller diagrams we generate a further set of diagrams called *hexagraphs*. A hexagraph has the same number of vertices as the original Toller diagram but all lines are drawn either horizontal or at 60° (or 120°). Hexagraphs are constructed by substituting for each of the vertices of a planar Toller diagram the sets of vertices shown in Fig. 2.3 (As illustrated the number of vertices substituted depends on the number of external lines entering the vertex.) By joining the available vertices with horizontal lines in all possible manners the complete set of hexagraphs is formed. Examples of this construction are shown in Fig. 2.4 and 2.5. If incoming particles are now considered to enter a hexagraph from the left of the diagram and outgoing particles to exit from the right then (up to a TPC transformation) each hexagraph represents a unique *cross-channel*. To illustrate this we can think of each internal horizontal line of the diagram as representing a resonance and each vertex as representing resonance formation or decay. For this to be kinematically possible, if Q_j is the horizontal momentum line entering a vertex and Q_{j+1} and Q_{j+2} the other two momenta we must have

$$Q_j > Q_{j+1} + Q_{j+2}, \tag{2.41}$$

and so

$$\lambda(t_j, t_{j+1}, t_{j+2}) = t_j^2 + t_{j+1}^2 + t_{j+2}^2 - 2t_jt_{j+1} - 2t_{j+1}t_{j+2} - 2t_{j+2}t_j \tag{2.42}$$

$$= -(Q_j + Q_{j+1} + Q_{j+2})(Q_j + Q_{j+1} - Q_{j+2})$$

$$\times (Q_j - Q_{j+1} + Q_{j+2})(-Q_j + Q_{j+1} + Q_{j+2}) \tag{2.43}$$

$$> 0 \tag{2.44}$$

That is $\lambda > 0$ is satisfied at all vertices in a cross-channel. However, distinct cross-channels can be distinguished by which factors in (2.43) are positive and which negative at each vertex. This is what the hexagraph describes. The horizontal line at the vertex is the largest momentum.

Note that the hexagraph can also be used to count the variables of the Toller diagram. That is each θ_j (and each t_j) can be associated with the corresponding horizontal line of the hexagraph, while each ω_{jk} can be associated with an internal sloping line. In this case the θ_j can be thought of as conjugate to the angular momentum of the corresponding resonance while the ω_{jk} are conjugate to the helicity of the corresponding resonance. Of course, the scattering process does not have to take place by the resonance formation illustrated by the hexagraph—it is simply that this process is kinematically possible.

Although a hexagraph is drawn in a plane the scattering process described is not at all planar. Indeed if one half of a hexagraph is rotated through 180° (perpendicular to the plane of the paper) about one horizontal line relative to the other half so that the diagram is again drawn in a plane as illustrated in Fig. 2.6, the same cross-channel is described. Therefore each cross-channel is described by a class of hexagraphs related by twisting. The process of twisting a hexagraph (or a planar Toller diagram) about a horizontal line is, however, important for distinguishing direct channels because it defines the multiparticle generalization of signature. Note that the (unique) direct channel associated with a hexagraph is immediately obtained by simply recovering the original planar Toller diagram from the hexagraph.

The angular variables can be straightforwardly introduced in any physical region by the procedure described above. In general some of the little groups will be spacelike and some will be timelike, that is some g_j will belong to SO(2,1) and some to SO(3). Also even if all the Q_j meeting at a vertex are spacelike the vertex may still be timelike in that (2.41) is satisfied. In general we call a vertex *timelike* if $\lambda(t_j, t_{j+1}, t_{j+2}) > 0$ and *spacelike* if $\lambda(t_j, t_{j+1}, t_{j+2}) < 0$. For spacelike internal lines joining two timelike vertices the parameterization (2.24) of SO(2,1) must be used, if a timelike and spacelike vertex are joined (2.37) must be used while for two spacelike vertices (2.32) has to be used.[31]

For our purposes it will be sufficient to describe as direct-channels those (parts of) physical regions in which all the Q_j are spacelike and *all* the *internal vertices* are *spacelike*. We can then generalize (2.21) to say that in each *cross-channel*, in addition to (2.44) we have

$$t_j \geq 4m^2, \quad -1 \leq z_j \leq 1, \quad -1 \leq \cos\omega_{jk} \leq 1 \tag{2.45}$$

while in each *direct-channel*, (2.44) is reversed and also

$$t_j < 0, \quad z_j \geq 1 \text{ or } \leq -1 \quad \cosh\omega_{jk} \geq 1 \text{ or } \leq -1. \tag{2.46}$$

(Although for vertices with just one external particle we must retain $-1 \leq \cos\omega_{jk} \leq 1$ to remain in a physical region.) A *twist* about a horizontal line of a hexagraph changes the sign of the corresponding z_j and, for any sloping line attached directly to this line (not via a vertex), the sign of the corresponding ω_{jk}.

2.4 Invariants and Angular Variables

Some detailed calculations of expressions for invariant variables in terms of angular

variables can be found in Ref. 2. Here we simply list some properties that are particularly important in the following.

2a) If we define $v_j = e^{i\theta_j}$, that is $z_j = \frac{1}{2}\left(v_j + v_j^{-1}\right)$, and u_{jk} as above then all factors of i in expressions for invariants (coming from $\sin\theta_j$ and $\sin\omega_{jk}$) cancel. The relation between all invariants and the u's and v's is real and analytic.

2b) When all the v_j's are large (or all the z_j's) we obtain for an invariant $s_{mn} = (p_m + p_n)^2$

$$\begin{aligned}\frac{s_{mn}}{2m^2} \sim \sinh\zeta_{mj_1} v_{j_1} (\cosh\zeta_{j_1 j_2} + \cos\omega_{j_1 j_2}) v_{j_2} \cdots v_{j_{r-1}} \\ \times \left(\cosh\zeta_{j_{r-1} j_r} + \cos\omega_{j_{r-1} j_r}\right) v_{j_r} \sinh\zeta_{j_r n},\end{aligned} \tag{2.47}$$

which implies that for any invariant $s_{mn\cdots r} = (p_m + p_n + \ldots + p_r)^2$

$$\frac{s_{mn\ldots r}}{2m^2} \underset{z_j \to \infty}{\sim} \forall_j \; f(\underset{\sim}{t}, \underset{\sim}{\omega}) z_{j_1} z_{j_2} \cdots z_{j_s}, \tag{2.48}$$

where now $j_1, j_2, \ldots, j_s$ denotes the *longest* path through the tree diagram linking any two of the external momenta contained in $s_{mn\cdots r}$.

2c) When all the u_{jk}'s are large we similarly obtain

$$\begin{aligned}\frac{s_{mn}}{2M^2} \sim \sinh\zeta_{mj_1} \sin\theta_{j_1} u_{j_1,j_2} (\cos\theta_{j_2} + 1) u_{j_2,j_3} \cdots u_{j_{r-2},j_{r-1}} \\ \times \left(\cos\theta_{j_{r-1}} + 1\right) u_{j_{r-1},j_r} \sin\theta_{j_r} \sinh\zeta_{j_r n}.\end{aligned} \tag{2.49}$$

2d) When $z_i = v_j = \pm 1$ ($\theta_j = 0, \pi$) the associated line can be contracted out of the tree diagram for the purpose of calculating invariants. The azimuthal angles at the contracted vertices are added or subtracted according to whether $z_j = \pm 1$.

2e) Similarly when $z_j = \pm 1$, $z_{j+1} = \pm 1$ and $\cos\omega_{j,j+1} = \pm 1$ both the j and $j+1$ lines can be contracted from the diagram and under analogous conditions any number of lines can be contracted out.

2f) If p_n and p_m are separated by one internal line only, then s_{nm} is linearly related to the associated z (simple examples of this being (2.19) and (2.20)).

It will be important in the following that the singularities of amplitudes as functions of the invariant variables have a very similar asymptotic structure in terms of either the z_j variables or the u_{jk} variables because of the similarity of (2.47) and (2.49).

3. Multiparticle Asymptotic Dispersion Relations

Any standard book on elementary Regge theory covers the relationship between the analyticity properties of (four-particle) momentum-space amplitudes and complex angular momentum theory. However, the development of a comparable relationship for multiparticle amplitudes took many years since the relevant analyticity properties are much more complicated. In particular it is necessary to concentrate on "asymptotic analyticity properties". To explain this concept and also to give a self-contained development for those who wish to avoid going back to the "standard" books of the 60's we first describe in detail the asymptotic dispersion relation for an elastic amplitude.[2]

3.1 The Asymptotic Dispersion Relation for Elastic Scattering

Consider a scalar (for simplicity) elastic scattering amplitude $A(s,t)$. The analyticity property most immediately derived from field theory[32] is "cut-plane analyticity" for large s at spacelike t. That is $A(s,t)$ has a domain of analyticity

$$D = \{|s| > s_0,\ \mathrm{Im}\, s \neq 0,\ t \text{ fixed} < 0\}\,. \tag{3.1}$$

Applying the Cauchy formula to the contour shown in Fig. 3.1 gives

$$A(s,t) = \frac{1}{2\pi i}\int_{I_+} \frac{ds'\Delta(s',t)}{(s'-s)} + \frac{1}{2\pi i}\int_{I_-} \frac{ds'\Delta(s',t)}{(s'-s)} + \frac{1}{2\pi i}\int_{\substack{|s'|=R\\ |s'|=s_0}} ds' \frac{A(s',t)}{(s'-s)}, \tag{3.2}$$

where

$$\Delta(s,t) = A(s+i\,0,t) - A(s-i\,0,t) = 2i\,\mathrm{Im}\,A(s,t). \tag{3.3}$$

In early applications of dispersion relations the third term in (3.2) played a crucial role in relating low and high energy data.[33] Consequently it was important to know the precise details of the low-energy cut structure. However, if we are *interested only in the leading Regge behavior* of the amplitude then we need just the first two terms and as the following argument shows the third term can be ignored. Suppose that

$$A(s,t)\underset{|s|\to\infty}{\sim} \beta_+(t)s^{\alpha(t)} + \beta_-(t)(-s)^{\alpha(t)}, \tag{3.4}$$

(there could also be additional $\ln s$ dependence—the important feature is that the power behavior is t-dependent) and suppose also that somewhere in an interval $t_a < t < t_b$ (which

could even be complex) $\alpha(t)$ increases through -1. In the full interval

$$\frac{1}{2\pi i}\int_{|s'|=S_0} ds' \frac{A(s',t)}{(s'-s)} \underset{|s|\to\infty}{\sim} O\left(\frac{1}{s}\right), \tag{3.5}$$

while in some subinterval

$$\frac{1}{2\pi i}\int_{|s'|=R} \frac{ds' A(s',t)}{(s'-s)} \underset{R\to\infty}{\sim} R^{\alpha(t)} \to 0 \qquad \mathrm{Re}\,\alpha(t) < -1. \tag{3.6}$$

Consequently we can begin with $\mathrm{Re}\,\alpha(t) < -1$ and take $R \to \infty$ leaving only the integral over $|s'| = s_0$ in (3.1). Analytic continuation to $\mathrm{Re}\,\alpha(t) > -1$ then gives that the first two terms dominate and we can write

$$A(s,t) = \frac{1}{2\pi i}\left(\int_{I_+} + \int_{I_-}\right) \frac{ds'\Delta(s',t)}{(s'-s)} + A_0, \tag{3.7}$$

where A_0 gives sub-dominant asymptotic behavior provided $\mathrm{Re}\,\alpha(t) > -1$ and the I_+ and I_- integrals are *defined* by analytic continuation from $\mathrm{Re}\,\alpha(t) < -1$. The integrals I_+ and I_- are over the intervals (s_0, ∞) and $(-\infty, -s_0)$ respectively, with the precise value of s_0 being irrelevant. (3.7) is the simplest example of an "asymptotic dispersion relation".

We should emphasize that the asymptotic dispersion relation is not qualitatively different from the exact dispersion relation. It simply drops some irrelevant details from the complete relation (irrelevant for our purposes, that is). We do not mean to imply that the asymptotic dispersion relation is in any sense "only valid asymptotically".

3.2 Analyticity Properties of Many-Particle Amplitudes

The analytic structure of many-particle amplitudes is much more complicated than that of elastic amplitudes and for many years physicists despaired of deriving any generalization of (3.2). An N-point amplitude is a function of $3N - 10$ independent variables only but there are $\sim N!$ invariants with threshold singularities in each of them. Even if some invariants are fixed (away from their thresholds) there is still an enormous complexity of simple thresholds to consider. In addition there is a very rich structure of higher-order Landau singularities for many-particle amplitudes. Finally the many variable generalization of Cauchy's theorem (which we discuss shortly) is in general very difficult to apply. Altogether it seemed that any simple generalization of (3.2) was very unlikely to exist.

Fortunately if we consider (3.7) rather than (3.2) we can find a generalization which is precisely what we require to provide a general basis for multi-Regge theory. Our major purpose will be to simply describe the structure of the resulting "asymptotic dispersion relations". Our intention is to exploit this structure in our development of multi-Regge theory rather than to dwell on an axiomatic derivation of the relations. Nevertheless we do want to describe why we believe they are natural consequences of the two most well-established formalisms used for deriving analyticity properties, that is Axiomatic Field Theory (AFT) and Axiomatic S-Matrix Theory (AST). We shall therefore briefly review what can be said with respect to deriving the dispersion relations within each formalism. Of course, AFT and AST are, as far as is known, mutually consistent and in a sense complimentary to each other.

Note that as in our discussion of (3.7), we do not expect the asymptotic dispersion relations for multiparticle amplitudes to be only valid asymptotically. We expect their essential structure to be preserved at finite momenta but with a multitude of (for our purposes) "inessential complications".

3.3 Axiomatic Field Theory

AFT has many starting points and distinct formalisms within it. However, the basic ingredient is always space-time fields $\phi_i(x)$ which as operators can create (or destroy) the particles of the theory from (or into) the vacuum. As an imposition of *microcausality* such fields are *assumed to commute* at space-like separations

$$[\phi_i(x),\ \phi_j(y)] = 0 \qquad (x-y)^2 < 0 \quad \forall i,j. \tag{3.8}$$

In this case the S-Matrix elements of the theory can be related by reduction formulae to the Fourier transforms of "retarded" Greens functions, the simplest example of which is

$$G(p) = \int d^4x e^{ip\cdot x}\langle 0|\theta(x_0)\phi(x)\phi(0)|0\rangle, \tag{3.9}$$

(where $\theta(y) = 1,\ y > 0;\ \theta(y) = 0,\ y < 0$). Provided that the retarded Greens functions are well-defined distributions—that is they are polynomially bounded—then their Fourier transforms have extensive analyticity domains because of the convergence provided by the Fourier exponential factors of the form $\exp[ip\cdot x]$. For example $G(p)$ is analytic in the "forward-tube"

$$(\mathrm{Im}\, p)^2 > 0 \qquad \mathrm{Im}\, p_0 > 0. \tag{3.10}$$

The general AFT program formulated by Bros, Epstein and Glaser[32,34-36] introduces a complete set of "Generalized Retarded Functions" (GRF's) defined from all the field-operators in the theory. Each GRF is analytic in a particular tube or "cone" which is a generalization of (3.10). In addition each GRF gives an S-Matrix element as a boundary-value from within this tube. For an N-point amplitude a general tube is defined by

$$\left(\sum_{\Delta} \mathrm{Im}\, p_i\right)^2 > 0 \qquad \sum_{\Delta} \mathrm{Im}\, p_{i0} \gtrless 0 \quad \forall \Delta, \tag{3.11}$$

where Δ is any channel, that is any subset of the external momenta $p_1 \ldots p_N$, and (3.11) must be satisfied with either the $>$ or the $<$ sign operative in the second term for all Δ. Distinct tubes and therefore distinct GRF's are then defined by the possible combinations of choices for the $\gtrless$ signs. By use of the "Edge of the Wedge" theorem[34] it is straightforward to extend analyticity within the tubes to "partial tubes" in which any of the p_i are real and spacelike. If all of the p_i are real and spacelike then all the GRF's defined from a given set of field operators coincide. This implies that they are all (off mass-shell) continuations of the same analytic function.

For the 4-point amplitude we can use our kinematic analysis of Section 3.2 for spacelike external momenta to immediately see the origin of the dispersion relation (3.2). Going to frame F_1 we have by definition that p_1 and p_3 are spacelike and have the form

$$p_1 = (0, 0, p\sin\phi, p\cos\phi), \qquad p_3 = (0, 0, -p\sin\phi, p\cos\phi), \tag{3.12}$$

while (2.33) gives, on taking $\alpha = \gamma = 0$

$$p_2 = (p\sin\phi\sinh\beta,\ p\sin\phi\cosh\beta, 0, -p\cos\phi) \tag{3.13}$$

$$p_4 = (-p\sin\phi\sinh\beta, -p\sin\phi\cosh\beta, 0, -p\cos\phi) \tag{3.14}$$

If we allow $z = \cosh\beta$ to be complex so that

$$2\,\mathrm{Im}\, z = \mathrm{Im}\cosh\beta = \mathrm{Im}\left[\rho e^{i\delta} + \frac{1}{\rho}e^{-i\delta}\right] = \left[\rho - \frac{1}{\rho}\right]\sin\delta \tag{3.15}$$

$$2\,\mathrm{Im}\sinh\beta = \mathrm{Im}\left[\rho e^{i\delta} + \frac{-1}{\rho}e^{-i\delta}\right] = \left[\rho + \frac{1}{\rho}\right]\sin\delta \tag{3.16}$$

then all momenta apart from p_2 and p_4 are real and spacelike and

$$\mathrm{Im}\, p_2 = -\mathrm{Im}\, p_4 = \frac{p\sin\phi}{2}\sin\delta\left(\left[\rho + \frac{1}{\rho}\right], \left[\rho - \frac{1}{\rho}\right], 0, 0\right). \tag{3.17}$$

Consequently

$$(\mathrm{Im}\, p_2)^2 = (\mathrm{Im}\, p_4)^2 > 0 \quad \mathrm{Im}\, p_{20} = -\mathrm{Im}\, p_{40} \sim \mathrm{Im}\, z. \tag{3.18}$$

That is the cut z-plane and hence, from (2.19), the cut s-plane is contained in the analyticity domain given by the GRF (partial) tubes.

We see that the analyticity domain of Fig. 3.1 is obtained straightforwardly from AFT for spacelike masses. It is nevertheless a major exercise in the use of analytic completion theorems to show[32,34] that this domain survives the continuation onto the physical mass shell. In a sense the continuation on mass-shell could be sidestepped for our purposes. We have no intention of being rigorous in our analysis since we intend in any case to input the assumption of Regge behavior. (When analyzing non-abelian gauge theories we shall discuss the extent to which this is an assumption.) As we shall see our major interest is in the analytic structure of reggeon amplitudes. Since the reggeons carry spacelike momenta we could derive their analyticity properties directly from field-theory amplitudes with spacelike external momenta simply by assuming that the reggeons couple directly to spacelike states.

The analysis of (3.12)–(3.18) extends naturally to an N-point amplitude regarded as a function of the $(N-3)$ z_j-variables if all the external p_i and all the internal Q_j are spacelike. From (3.15)– (3.18) we see that applying a complex boost to a real spacelike momentum vector automatically takes the momentum vector into a tube of the form (3.10). More generally if the imaginary part of the initial four momentum already satisfies (3.10) and in addition the *real part* is a *spacelike vector* then both properties are preserved by a complex boost. As a result the application of successive "complex z_j" transformations—with the $\cosh \omega_{jk}$ and t_j kept real—automatically takes all the momenta involved into a tube of the form (3.11). Since the product of z_j transformations satisfies

$$\cosh\left[\beta_j + \beta_{j+1} + \beta_{j+2} + \cdots + \beta_{j+r}\right] \underset{z_j, z_{j+1}, z_{j+2}, \ldots \to \infty}{\sim} \cosh\beta_j \cosh\beta_{j+1} \ldots \cosh\beta_{j+r} \tag{3.19}$$

$$\equiv z_j z_{j+1} \ldots z_{j+r}, \tag{3.20}$$

the result is that analyticity in the tubes (3.11) transfers "asymptotically" into analyticity in the "z_j-cones" bounded by the "cuts"

$$\mathrm{Im}\left(\prod_{\Delta} z_j\right) = 0 \quad \forall \Delta, \tag{3.21}$$

where now Δ is any subset of $j = 1, \ldots, N-3$ associated with *adjacent* lines in the Toller diagram. Note that we would also obtain a very similar cut structure asymptotically in terms of the u_{jk} variables.

The analyticity domain given by the compliment of (3.21) is just what we require to write the asymptotic dispersion relations we shall describe. From (2.48) it is clear that all normal threshold cuts, that is

$$\mathrm{Im}\, S_{mn\ldots r} = 0 \qquad \forall mn\ldots r, \tag{3.22}$$

lie asymptotically within the cuts (3.21). Consequently analyticity outside of the cuts (3.21) provides a natural generalization of the cut-plane analyticity for the four-point amplitude illustrated in Fig. 3.1

To the extent that we are prepared to ignore (or sidestep) the very considerable problem of analytic continuation in the masses the above description shows why the dispersion relations are a natural consequence of AFT. (Although a much more detailed discussion of the relationship between (3.11) and (3.21) could clearly be given.) We shall postpone discussion of the structure of the discontinuities across the branch cuts (3.21) until after our discussion of S-Matrix theory.

3.4 Axiomatic S-Matrix Theory

Axiomatic S-Matrix Theory (AST) has been given a solid foundation[37] by starting from the principle of *macrocausality*. This principle says that all interactions between particles fall-off exponentially under space-time dilations unless the interaction can be transmitted by the exchange of (interacting) stable particles. This leads to the existence of (infinitesimal) domains of analyticity for S-Matrix elements in the immediate neighborhood of physical regions. Note that while macrocausality is thought to be consistent with the microcausality property of AFT a direct relationship has yet to be established. It is thought that unitarity of the S-Matrix has to be combined with the microcausality property of AFT to derive macrocausality. This is effectively the purpose of the "non-linear program" of AFT in which "asymptotic completeness" is added as an additional axiom to allow the mixing of unitarity properties with the off-shell analyticity domains of AFT.

Given the local analyticity which follows from macrocausality it is possible, within AST, to study the minimal singularity structure required by unitarity and to analyze the

discontinuity formulae implied. A heuristic way to understand the basic results[37,38] of AST is as follows. First write the S-Matrix as $S = 1 + R^+$ and its Hermitian conjugate as $S^+ = 1 - R^-$. The unitarity equation $SS^+ = 1$ can be written formally as

$$R^+ = \frac{R^-}{1 - R^-} \tag{3.23}$$

$$= \sum (R^-)^n. \tag{3.24}$$

Using a conventional bubble diagram notation for R^+ and R^- and inserting intermediate states into (3.24) we obtain for a general connected part of R^+

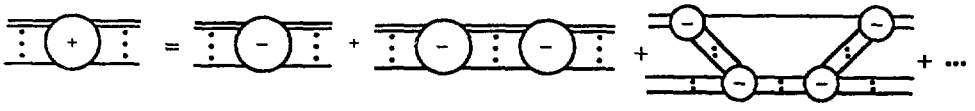

$$= \sum B^-, \tag{3.25}$$

where the sum is over all kinematically possible connected (minus) bubble diagram functions. (Note that all internal lines are on mass-shell in such diagrams.)

The series (3.25) displays explicitly all possible normal-threshold *and higher-order* Landau singularities, in the sense that new terms appear in the series whenever such a (generalized) threshold is passed. The sum of these new terms actually defines the discontinuity at such a threshold. As a result the total discontinuity across all thresholds in a particular channel is then defined as the sum of all terms in (3.25) which have a phase-space integration in the relevant channel. Extending this argument multiple discontinuities can be defined from (3.25) by keeping those term which have *all* the corresponding phase-space integrations. Consequently it is possible to given an S-Matrix definition of amplitudes on all sides of normal threshold cuts. The main consequence is that there are *good* and *bad* boundary-values onto the "unphysical" sides of normal threshold cuts.

Amplitudes obtained as bad boundary-values have the very undesirable property that the higher-order Landau singularities they contain produce multiple complex cuts extending from the real normal threshold cuts as illustrated in Fig. 3.2. Conversely the good boundary-value amplitudes have a neighborhood of analyticity close to the physical region.

The higher-order Landau singularities are real and contained within the (product of) the normal thresholds.

To write a dispersion relation we clearly require global analyticity properties of the kind discussed above. To "derive" global analyticity domains from AST necessarily requires some form of *maximal analyticity* assumption or principle. The simplest such principle is that all S-Matrix amplitudes with the same number of external particles are boundary-values of the same analytic function (generalized crossing) and have *only* those *singularities required by unitarity.* Adopting this principle the analyticity domain of Fig. 3.1 for the elastic amplitude can be *derived* by first showing that the infinitesimal analyticity domain illustrated in Fig. 3.3 and involving both physical and unphysical sides of the normal threshold cuts, is consistent with unitarity. This is in fact the case since there are no bad boundary-values for the elastic amplitude. Consequently maximal analyticity says that the infinitesimal domain of Fig. 3.3 (derived from microcausality plus unitarity) can be extended to the global domain of Fig. 3.1.

Generalizing this last argument to multiparticle amplitudes requires that we start with infinitesimal domains analogous to those shown in Fig. 3.3. We can then appeal to maximal analyticity to extend such domains to global domains if and only if there are no complex cuts extending uncontrollably out into the complex plane. Consequently an AST derivation[1] of the asymptotic dispersion relations amounts to demonstrating that bad boundary-values are not involved in the analyticity domain utilized. Remarkably, adding imaginary parts to z_j variables (only) does not allow invariants to acquire bad boundary-value imaginary parts. We shall not attempt to prove this in general here but instead give an elementary example. For the 2–4 amplitude shown in Fig. 3.4 a bad boundary-value is

$$s + i0,\ \sigma + i0,\ s_1 - i0,\ s_2 - i0, \tag{3.26}$$

whereas in the asymptotic limit associated with the Toller diagram of Fig. 3.1 we have from (2.48)

$$s \sim z_1 z_2 z_3,\ s_1 \sim z_1 z_2,\ s_2 \sim z_2 z_3,\ \sigma \sim z_2, \tag{3.27}$$

and no combination of imaginary part signs for the z_j's will give (3.26).

We see therefore that the dispersion relations follow in AST from maximal analyticity plus the existence of good boundary-values. (The details, of course, depend on some further properties which we discuss shortly.) At first sight the principle of maximal analyticity may seem somewhat arbitrary. However, it is satisfied, to the extent of existing knowledge, by

all Feynman diagrams and therefore in perturbation theory to all orders (ignoring possible complications from renormalization and regularization) when the S-Matrix can be defined. (Of course, the S-Matrix is not defined perturbatively in QCD because of infra-red divergences.) There is also a body of knowledge on how the "physical solution" of any differential equation is always "maximally analytic" as a function of the parameters involved. In fact this line of argument is brought to its most sophisticated by Japanese mathematicians who have suggested (and in some cases demonstrated) that the discontinuity formulae satisfied by S-Matrix elements can be regarded as infinite order "pseudo-differential" equations. The maximal analyticity assumption then appears closely related to Sato's conjecture[39] that the S-Matrix is a holonomic microfunction—that is it is a solution of a maximally over-determined system of pseudo-differential equations.

The most complete argument for the dispersion relations perhaps comes from combining the AFT and AST arguments. That is the AFT analysis shows that the needed global analyticity domains are present for spacelike masses while the AST analysis shows that these domains are not violated by any singularities emerging from the physical regions on mass-shell. Since it is very hard (if not impossible) to imagine any source of singularities disconnected from the physical regions the AST analysis shows the AFT domains should be preserved on mass-shell.

Our next task will be to describe the asymptotic relations in detail. (Afterwards we will briefly comment on the extent to which we can derive them directly for the study of QCD which is our ultimate purpose.) For each multiparticle amplitude there will be a separate dispersion relation for each Toller diagram introduced in the last Section. (Although as we shall describe some individual contributions can appear in more than one dispersion relation.)

The dispersion relation for a particular Toller diagram is derived by regarding the N-point amplitude as a function of the t_i, z_j and u_{jk} variables introduced in the last Section. That is we write

$$M(p_1,\ldots,p_N) \equiv M(t_1,\ldots,t_{N-3},\ z_1,\ldots,z_{N-3},\ u_{12},\ldots,u_{N-4,N-3}). \qquad (3.28)$$

We then fix all t_i in a direct-channel region. We further fix the u_{jk} at physical values and regard the amplitude as a function of the $(N-3)$ z_i-variables, to which we apply the many-variable generalization of the Cauchy formula—that is the "Bargman-Weil" integral formula.

We begin by describing this formula in the most directly applicable manner.[2]

3.5 The Bargman-Weil Formula

Suppose a function $f(\underset{\sim}{z}) = f(z_1, \ldots, z_n)$ is analytic in a domain D that is the whole space $\mathbf{C}^n$ minus a set of cuts c_m where

$$c_m = \left\{ \underset{\sim}{z} \in \mathbf{C}^n; \quad \operatorname{Im} s_m(\underset{\sim}{z}) = 0 \right\}. \tag{3.29}$$

(Clearly we anticipate that s_m is an invariant variable and c_m the corresponding normal threshold cut.) If I^λ is the intersection of n such cuts we define the multiple discontinuity at $\underset{\sim}{z} \in I^\lambda$ as

$$\Delta^\lambda(\underset{\sim}{z}) = \sum (-1)^{n'} f\left(\underset{\sim}{z}(\operatorname{Re} s_{\lambda_1} \pm i0, \ldots, \operatorname{Re} s_{\lambda_n} \pm i0) \right), \qquad \lambda \equiv (\lambda_1, \ldots, \lambda_n) \tag{3.30}$$

where the sum is over all combinations of $\pm$ signs and n' is the number of minus signs. The theorem says we can write

$$f(\underset{\sim}{z}) = \sum_\lambda f^\lambda(\underset{\sim}{z}) + f^0(\underset{\sim}{z}), \tag{3.31}$$

where the sum is over all sets of n cuts λ and f^0 includes possible contributions from intersections of less than n cuts together with the "sphere" at infinity and

$$f^\lambda(\underset{\sim}{z}) = \frac{1}{(2\pi i)^n} \int_{\underset{\sim}{z}' \in I^\lambda} dz_1' \ldots dz_n' \Delta^\lambda(\underset{\sim}{z}') \times \det\left(\underset{\sim}{q}^{\lambda_1}, \underset{\sim}{q}^{\lambda_2}, \ldots \underset{\sim}{q}^{\lambda_n} \right). \tag{3.32}$$

The generalized dispersion denominators $\underset{\sim}{q}^{\lambda_m}$ must satisfy

$$\underset{\sim}{q}^{\lambda_m}(\underset{\sim}{z}, \underset{\sim}{z}') \cdot (\underset{\sim}{z}' - \underset{\sim}{z}) = 1. \tag{3.33}$$

We would ultimately like the contributions (3.32) expressed as integrals over the invariant variables s_{λ_m}. If we simply change variables to the s_{λ_m} and write (3.32) in the

form

$$f^{\lambda}\left(\underset{\sim}{z}(s_\lambda)\right) = \frac{1}{(2\pi i)^n}\int_{\underset{\sim}{z}'\in I^\lambda} ds'_{\lambda_1}\dots ds'_{\lambda_n}\left(\frac{\partial \underset{\sim}{z}}{\partial s_\lambda}\right)_{\underset{\sim}{z}=\underset{\sim}{z}'} \Delta^{\lambda}(s'_\lambda)\frac{D^\lambda(\underset{\sim}{z},\underset{\sim}{z}'(s'_\lambda))}{(s'_{\lambda_1}-s_{\lambda_1}(\underset{\sim}{z}))\dots(s'_{\lambda_n}-s_{\lambda_n}(\underset{\sim}{z}))}, \tag{3.34}$$

(3.33) will be satisfied if the numerator $D^\lambda(\underset{\sim}{z},\underset{\sim}{z}')$ is the determinant of any set of functions $p^\lambda_{m\ell}$ satisfying

$$s_{\lambda_m}(\underset{\sim}{z}) - s_{\lambda_m}(\underset{\sim}{z}') = \sum_\ell p^\lambda_{\ell m}(\underset{\sim}{z},\underset{\sim}{z}')(z_\ell - z'_\ell). \tag{3.35}$$

Note that this implies that

$$D^\lambda(\underset{\sim}{z},\underset{\sim}{z}) = \frac{\partial s_\lambda}{\partial \underset{\sim}{z}}. \tag{3.36}$$

In a general application of the Bargman-Weil formula the numerator $D^\lambda(\underset{\sim}{z},\underset{\sim}{z}')$ can be very complicated (if the $s_{\lambda_m}(\underset{\sim}{z})$ are sufficiently complicated functions). However, in the special circumstance that the s_{λ_m} are simple polynomials (or entire functions) of the z_j we can expect to write

$$D^\lambda(\underset{\sim}{z},\underset{\sim}{z}') = D^\lambda(\underset{\sim}{z},\underset{\sim}{z}) + \left[s_{\lambda_1}(\underset{\sim}{z}) - s_{\lambda_1}(\underset{\sim}{z}')\right] E^\lambda_1(\underset{\sim}{z},\underset{\sim}{z}') + \dots + \left[s_{\lambda_n}(\underset{\sim}{z}) - s_{\lambda_n}(\underset{\sim}{z}')\right] E^\lambda_n(\underset{\sim}{z},\underset{\sim}{z}'), \tag{3.37}$$

where the $E^\lambda_m(\underset{\sim}{z},\underset{\sim}{z}')$ are also polynomials (or entire functions). Substituting (3.37) into (3.34) the first term gives a very simple expression

$$f^{\lambda}\left(\underset{\sim}{z}(s_\lambda)\right) = \frac{1}{(2\pi i)^n}\int_{I^\lambda} ds'_{\lambda_1}\dots ds'_{\lambda_n}\frac{\Delta^\lambda(s'_\lambda)}{\left(s'_{\lambda_1}-s_{\lambda_m}(\underset{\sim}{z})\right)\dots\left(s'_{\lambda_n}-s_{\lambda_n}(\underset{\sim}{z})\right)}, \tag{3.38}$$

while the remaining terms in (3.37) cancel at least one denominator in (3.34) and so can be included in the f^0 term appearing in (3.31).

Our assumption of multi-Regge asymptotic behavior which generalizes (3.4) (and which we describe in greater detail in later Sections) will be that

$$f(\underset{\sim}{z}) \equiv M(\underset{\sim}{t},\underset{\sim}{z},\underset{\sim}{u})\underset{z_1,\dots,z_{N-3}\underset{\sim}{\to}\infty}{\sim} \prod_{j=1}^{N-3}(z_j)^{\alpha_j(t_j)} \tag{3.39}$$

(where again there may also be $(\ln z_j)^{B_j}$ factors). Since this asymptotic form represents a function with $n \equiv (N-3)$ cuts in the z_j-variables it can only originate from the $f^\lambda(\underset{\sim}{z})$ terms in (3.31). Also in the same sense that s_0 was irrelevant in (3.7), non-leading functions of the z_j appearing in the $s_{\lambda_m}(\underset{\sim}{z})$ can be dropped in writing that part of the $f^\lambda(\underset{\sim}{z})$ which can generate the asymptotic form (3.39). Consequently we can write as an asymptotic dispersion relation

$$M(\underset{\sim}{t},\underset{\sim}{z},\underset{\sim}{u}) = \sum_\lambda M^\lambda(\underset{\sim}{t},\underset{\sim}{z},\underset{\sim}{u}) + M^0(\underset{\sim}{t},\underset{\sim}{z},\underset{\sim}{u}), \tag{3.40}$$

where we can use the asymptotic form (2.48), which expresses all invariants as *polynomials* in the z_j, to justify writing each of the $M^\lambda(\underset{\sim}{t},\underset{\sim}{z},\underset{\sim}{u})$ in the simple form (3.38). $M^0(\underset{\sim}{t},\underset{\sim}{z},\underset{\sim}{u})$ contains all non-leading multi-Regge behavior. Therefore the problem of writing the full asymptotic dispersion relation reduces to enumerating the complete set of multiparticle discontinuities (3.30).

3.6 The Steinmann Relations and Multiple Discontinuity Formulae

From the AFT analysis in Section 3.3 leading to (3.21) it is clear that all of the multiple discontinuities involved lie in the set (3.21). At first sight this implies that too many cuts intersect to apply the Bergman-Weil formula. However, *the Steinmann relations* imply that only $(N-3)$-fold multiple discontinuities occur. In AFT the Steinmann relations are linear relations between the GRF's involved as boundary-values in the distinct tubes (3.11). Multiple discontinuities are defined in analogy with (3.30) as multiple differences between GRF's with $\pm i\,0$ replaced by $\gtrless$ for the subsets Δ of (3.11). The Steinmann relations simply state that there is *no double discontinuity for two overlapping channels.*

In the AFT context a channel is a subset of the external momenta $p_1 \ldots p_{N-3}$ and two channels overlap if they include common momenta but neither set is contained entirely in the other. If all the Q_j of a Toller diagram are spacelike and all the external momenta p_i are also spacelike, then each maximal set of non-overlapping channels can be characterized by a *conjugate* Toller diagram—that is a tree diagram which again contains only three-point-vertices but which has no internal lines in common with the original Toller diagram. The non-overlapping channels are the internal momenta of the conjugate diagram. Since there are again $(N-3)$ internal lines it is clear that all multiple discontinuities involve only $(N-3)$ (or less) channels.

Within AFT therefore the multiple discontinuities contributing to (3.40) for a particular Toller diagram are in one to one correspondence with the "conjugate" set of Toller diagrams. The discontinuities can be directly evaluated in terms of GRF's or, if complete sets of states corresponding to the tree diagram are inserted, as products of amplitudes.[36] Of course, all of the AFT formalism is for spacelike masses and if physical intermediate states are used we are effectively assuming asymptotic completeness.

Within AST a channel refers to an invariant (the "mass" of the momentum involved in the AFT formalism) and multiple discontinuities involve the definition (3.30). It is nontrivial to show[1] that the Steinmann relations can be analogously applied as above because and only because just good boundary-value amplitudes are involved. The multiple discontinuity formulae derived[37,38] can also be shown to be identical to those derived in the AFT context. Consequently the identical asymptotic dispersion relation is derived off mass-shell from the AFT formalism and on mass-shell from the AST formalism.

A further feature of the *asymptotic* nature of the dispersion relation is that *many invariant* cuts coincide asymptotically. Because of (2.48) all invariants $S_{mn\ldots r}$ having the same longest path through the Toller diagram (linking any two of the external momenta) coincide asymptotically. However, only multiple discontinuities involving $(N-3)$ *asymptotically* distinct invariant cuts can contribute to the multi-Regge behavior (3.39). Therefore we further modify our description of (3.40) by insisting that the M^λ originate from $N-3$-fold discontinuities involving asymptotically distinct cuts only. This brings us to our final classification of discontinuities.

3.7 Hexagraph Classification of Multiple Discontinuities

Given a particular hexagraph we define an *allowable* discontinuity as in any channel defined by a set of external particles such that the minimal path (cut) drawn through the graph connecting *all* the particles involved enters and exits only between 60° lines as illustrated in Fig. 3.5.

Any set of $(N-3)$ non-overlapping cuts which are asymptotically distinct with respect to a particular Toller diagram correspond to a unique hexagraph if all $(N-3)$ cuts are required to be *allowable*. This is because allowing each cut to enter and exit appropriately, determines the choice of hexagraph vertices at each vertex of the Toller diagram.

Consequently we can re-express the asymptotic dispersion relation (3.40) in the final form

$$M(p_1,\dots p_N) = \sum_{H\in T} M^H(p_1,\dots,p_N) + M^0, \tag{3.41}$$

where M^0 again contains all non-leading multi-Regge behavior and the sum is over all hexagraphs H generated by the Toller diagram T. Each "hexagraphical component" M^H is further written as

$$M^H = \sum_{C\in H} M^C(p_1,\dots,p_N), \tag{3.42}$$

where now the sum is over all sets C of $(N-3)$ asymptotically distinct, non-overlapping, cuts which are (all) allowable cuts of the hexagraph. If we denote the invariant cuts of a particular C as $(s_1,\dots,s_{N-3})$ then from (3.38) we can write

$$M^C(p_1,\dots,p_N) = \frac{1}{(2\pi i)^{N-3}}\int \frac{ds_1'\dots ds_{N-3}'\Delta^C(\underset{\sim}{t},\underset{\sim}{w},s_1',s_2',\dots,s_{N-3}')}{(s_1'-s_1)(s_2'-s_2)\dots(s_{N-3}'-s_{N-3})}, \tag{3.43}$$

where from (3.30)

$$\Delta^C(\underset{\sim}{t},\underset{\sim}{w},s_1\dots,s_{N-3}) = \sum(-1)^{n'}M(\underset{\sim}{t},\underset{\sim}{w},s_1\pm i0,s_2\pm i0,\dots,s_{N-3}\pm i0), \tag{3.44}$$

and the asymptotic relation (2.48) is used to change variables from $z_1,\dots,z_{N-3}$ to $s_1,\dots,s_{N-3}$.

(3.41)–(3.44) is our final complete description of the asymptotic dispersion relation for an N-point amplitude associated with each Toller diagram. Clearly it is trivial to introduce the simple (unique) Toller diagram for the elastic amplitude such that (3.7) is expressed in the form (3.40)–(3.44) showing that we have indeed formulated a direct multiparticle generalization of (3.7). We close by discussing briefly the extent to which we expect the foregoing discussion to apply either directly or indirectly to QCD.

The S-Matrix of QCD presumably involves hadrons only and it is quite possible, if not probable, that hadrons are not describable by off mass-shell fields of the kind required to apply the AFT formalism above. In this case we would have to appeal to the AST formalism alone. (Of course, we have emphasized that the AFT results can be viewed as simply making plausible the maximal analyticity assumption of AST.) However, the starting point for our direct construction of the Pomeron in QCD will be the perturbative Regge behavior of the spontaneously broken massive theory. The perturbation theory of a (completely massive)

spontaneously broken gauge theory should satisfy all the assumptions of the AFT (and the AST) formalism. In this case all of the asymptotic dispersion relation formalism and all of the following multi-Regge theory should directly apply—given that the perturbative high-energy behavior does indeed sum up to Regge behavior, as all existing calculations imply.

4. PARTIAL-WAVE EXPANSIONS, FROISSART-GRIBOV CONTINUATIONS AND SOMMERFELD-WATSON TRANSFORMATIONS

In this Section we shall set up the basic machinery for applying complex angular momentum theory to many-particle amplitudes. An essential feature of the formalism is that each hexagraph amplitude has a distinct Sommerfeld-Watson (S-W) representation and each multiple discontinuity (that is each term in the asymptotic dispersion relation) corresponds to a distinct analytically continued Froissart-Gribov (F-G) partial-wave amplitude. Again we begin by briefly reviewing the elementary elastic scattering formalism.

4.1 Elastic Scattering

The familiar partial-wave expansion is

$$A(z,t) = \sum_{\ell=0}^{\infty}(2\ell+1)a_\ell(t)P_\ell(z), \tag{4.1}$$

where the $P_\ell(z)$ are Legendre polynomials and

$$a_\ell(t) = \frac{1}{2}\int_{-1}^{+1} dz A(z,t)P_\ell(z) \tag{4.2}$$

$$= \int_C dz A(z,t)Q_\ell(z), \tag{4.3}$$

where C is the contour shown in Fig. 4.1. Moving this contour out using Cauchy's theorem gives (if, for simplicity, we ignore A_0 in (3.7))

$$a_\ell(t) = \frac{1}{2\pi}\int_{\Delta\neq 0} dz\, Q_\ell(z)\Delta(z,t). \tag{4.4}$$

Since the second-type Legendre function $Q_\ell(z)$ satisfies

$$Q_\ell(z) \underset{|\ell|\to\infty}{\sim} \frac{1}{\ell^{1/2}}\exp\left[\ell \ln\left[z-(z^2-1)^{1/2}\right]\right], \tag{4.5}$$

it follows that if $a_\ell(t)$ is defined for complex ℓ from (4.3) then the contribution from the right-hand cut

$$a_\ell^R(t) = \frac{1}{2\pi}\int_{I+} dz' Q_\ell(z')\Delta(z',t) \tag{4.6}$$

satisfies the Carlson condition for uniqueness (cf a function defined initially for integer ℓ only), that is

$$\left|a_\ell^R(t)\right| \underset{\substack{\ell\to\infty \\ \mathrm{Re}\,\ell>0}}{\lesssim} e^{\theta|\ell|} \qquad \theta < \frac{\pi}{2}. \tag{4.7}$$

Using the further property that for integer ℓ

$$Q_\ell(z) = (-1)^{\ell+1} Q_\ell(-z), \tag{4.8}$$

we can define "signatured" F-G continuations from even and odd ℓ respectively, that is

$$a_\ell^\pm(t) = \left[a_\ell^R(t) \pm a_\ell^L(t)\right]/2, \tag{4.9}$$

where $a_\ell^L(t)$ is defined exactly the same as $a_\ell^R(t)$ but with $Q_\ell(z) \to Q_\ell(-z)$, that is

$$a_\ell^L(t) = -\frac{1}{2\pi}\int_{I-} dz' Q_\ell(-z')\Delta(z',t). \tag{4.10}$$

Behavior of the form (4.7) for $a_\ell^\pm(t)$ allows us to make a S-W transformation and rewrite (4.1) as

$$A(z,t) = \int \frac{d\ell(2\ell+1)}{\sin\pi\ell} \sum_\pm a_\ell^\pm(t)\left[p_\ell(z) \pm p_\ell(-z)\right], \tag{4.11}$$

or equivalently

$$A(z,t) = A_R(z,t) + A_L(z,t) \tag{4.12}$$

$$= \int \frac{d\ell(2\ell+1)}{\sin\pi\ell} a_R(\ell,t)p_\ell(z) + \int \frac{d\ell(2\ell+1)}{\sin\pi\ell} a_L(\ell,t)p_\ell(-z). \tag{4.13}$$

Comparing (4.13) and (4.11) we see that the signatured representation can be viewed simply as a consequence of the right-hand and left-hand cuts having identical representations apart from the change of sign of z. The importance of signature is, of course, that t-channel unitarity equations are diagonalized by signatured partial-wave amplitudes. We shall discuss this further in the next Section.

4.2 Multiparticle Partial-Wave Expansions

It is straightforward to generalize (4.1) to an N-point amplitude expressed as a function of a particular set of Toller variables since (4.1) is simply a special case of harmonic

analysis on SO(3). For a general function $f(g)$ on SO(3) we can write

$$f(g) = \sum_{\ell=0}^{\infty} \sum_{|n|,|n'|\leq\ell} D^{\ell}_{nn'}(g) a_{\ell nn'}, \tag{4.14}$$

where the $D^{\ell}_{nn'}(g)$ are representation functions. In particular for the parameterization (2.13) we have

$$D^{\ell}_{nn'}(g) = e^{in\mu} d^{j}_{nn'}(\theta) e^{in'\nu}. \tag{4.15}$$

Since $d^{j}_{00}(\theta) = p^{j}(\cos\theta)$, (4.14) gives (4.1) for a function that is independent of μ and ν.

Using (4.14) we can write immediately

$$\begin{aligned} M_N(\underset{\sim}{t}, g_1, \ldots, g_{N-3}) = \sum_{\ell_1=0}^{\infty} \sum_{|n_1|,|n_1'|\leq\ell_1} \cdots \sum_{\ell_{N-3}=0}^{\infty} \sum_{|n_{N-3}|,|n_{N-3}'|\leq\ell_{N-3}} \\ D^{\ell_1}_{n_1 n_1'}(g_1) \ldots D^{\ell_{N-3}}_{n_{N-3},n_{N-3}'}(g_{N-3}) a_{\ell_1,n_1,n_1',\ldots,\ell_{N-3},n_{N-3},n_{N-3}'}(\underset{\sim}{t}). \end{aligned} \tag{4.16}$$

Since each M_N in fact depends only on combinations of the azimuthal angles μ_j and ν_j there is an additional constraint on the sums on n_j, n_j' in (4.16). If we temporarily adopt the convention that at a vertex where lines j, k, ℓ meet, the Lorentz transformations g_j, g_k, g_ℓ are defined to transform *from* this particular vertex *to* adjacent vertices then this constraint takes the form

$$n_j + n_k + n_\ell = 0. \tag{4.17}$$

After this constraint is imposed there are $(N-4)$ independent n and n' indices in (4.16) (considering spinless external particles) which are "conjugate" to the $(N-4)$ independent azimuthal angles ω_{jk} discussed in the last Section.

For a particular hexagraph we can associate each ℓ_j with the corresponding horizontal line of the graph and an appropriately chosen $n_{jk} \equiv n_j$ with each sloping line of the graph. With the resonance interpretation of the hexagraph discussed in Section 2.3 the ℓ_j's are the angular momentum of the relevant resonance while the n_j's are the corresponding helicities. It is then helpful to identify three subgraphs contained in a general hexagraph and to rebuild the partial-wave expansion (4.16) using a partial-wave for each subgraph.

A T-graph is, as illustrated in Fig. 4.2, analogous to a 2-2 scattering amplitude. If

the scattering takes place through a state (resonance) with angular momentum ℓ_j then

$$T_{\ell_j} \sim d^{\ell_j}_{n_j,n'_j}(z_j) \equiv d^{\ell_j}_{n_{j_1}+n_{j_2},n'_{j_1}+n'_{j_2}}(z_j), \tag{4.18}$$

where n_{j_1}, n_{j_2} and n'_{j_1}, n'_{j_2} are the helicity indices associated with the sloping lines of the T-graph and ℓ_j is the angular momentum associated with the central horizontal line.

A D-graph is, as illustrated in Fig. 4.3, analogous to a decay of a state (resonance) with angular momentum ℓ_j and helicity n_j, that is

$$D_{\ell_j} \sim e^{in_j\omega_j} d^{\ell_j}_{n_j,n'_j}(z_j) \equiv u_j^{n_j} d^{\ell_j}_{n_j,n'_{j_1}+n'_{j_2}}(z_j). \tag{4.19}$$

A V-graph is, as illustrated in Fig. 4.4, analogous to a virtual transition, that is

$$V_{\ell_j} \sim e^{in_j\omega_j} d^{\ell_j}_{n_j,n'_j}(z_j) e^{in'_j\omega'_j} \equiv u_j^{n_j} d^{j}_{n_j,n'_j}(z_j)(u'_j)^{n'_j}. \tag{4.20}$$

The partial-wave expansion (4.14) is reproduced by choosing a particular hexagraph of the original Toller diagram, writing T_{ℓ_j}, D_{ℓ_j} and V_{ℓ_j} factors for each corresponding subgraph of the hexagraph (identifying n_j and n'_j labels where appropriate) multiplying by a partial-wave amplitude and summing over ℓ_j, n_j and n'_j labels.

It is, of course, trivial that a Toller diagram partial-wave expansion can be rewritten in a distinct way for each hexagraph. What is non-trivial is that this will allow us to write a distinct S-W transform for each hexagraph amplitude. Before discussing this in detail we first discuss the transform[40] of the simple Fourier sums that are involved in the expansion (4.16).

4.3 The Sommerfeld-Watson Transform of a Fourier Series

Consider the expansion

$$f(u) = \sum_{n=-\infty}^{\infty} a_n u^n, \tag{4.21}$$

which we assume converges in some annulus around $|u| = 1$. If $f(u)$ has the cut-plane analyticity illustrated in Fig. 4.5, then we can write

$$f(u) = f_>(u) + f_<(u), \tag{4.22}$$

where

$$f_{\gtrless}(u) = \frac{1}{2\pi} \int_{I^+_{\gtrless} + I^-_{\gtrless}} \frac{du'}{(u'-u)} \Delta(u'). \tag{4.23}$$

$I^+_{\gtrless}$ is the right-hand cut in $|u| \gtrless 1$ and $I^-_{\gtrless}$ the corresponding left-hand cut. Since

$$a^{>}_n = \frac{1}{2\pi} \int_{|u|=1} du\, u^{-n-1} f_>(u), \tag{4.24}$$

the contour can be closed to zero for $n < 0$, while for $n > 0$ the contour can be moved out to give

$$a^{>}_n = \frac{1}{2\pi} \int_{I^+_> + I^-_>} du\, v^{-n-1} \Delta(u). \tag{4.25}$$

Consequently signatured continuations can be defined as above

$$a^{>}_{\pm}(n) = \int_{I^+_>} du\, u^{-n-1} \Delta(u) \pm \int_{I^-_>} du (-u)^{-n-1} \Delta(u), \tag{4.26}$$

and an S-W transform written

$$f_>(u) = \int\limits_{\mathrm{Re}\, n\, =\, -1/2} \frac{dn}{\sin \pi n} \sum_{\tau=\pm 1} a^{>}_{\tau}(n) \left[(-u)^n + \tau u^n\right]. \tag{4.27}$$

Clearly it is straightforward to derive a similar representation for $f_<(u)$ in terms of signatured continuations $a^{<}_{\pm}(n)$. However, if we wish to study the asymptotic limit $|u| \to \infty$, we can move the contour to the left in (4.27) giving contributions from the singularities of $a^{>}_{\tau}(n)$ *and* from the poles of the $[\sin \pi n]^{-1}$ factor. These last contributions will be inverse powers of u which will in general simply cancel the series expansion of $f_<(u)$. Therefore the $|u| \to \infty$ "Regge behavior" of $f(u)$ (given by the dynamical singularities of $a^{\gtrless}_{\tau}(n)$) is entirely contained in the representation(4.27). Of course, for an amplitude that is a function of $\cos\omega = \frac{1}{2}\left(u + \frac{1}{u}\right)$ the behavior as $|u| \to \infty$ must be identical to that for $|u| \to 0$.

4.4 Problems for Many-Variable Transforms

Each hexagraph (amplitude) has multiple discontinuities in $(N-3)$ variables (if the t-variables are below threshold), while there are $(2N-7)$ angular variables available to

describe the corresponding cuts. From (4.3)-(4.13) or (4.23)-(4.27) it is clear that the existence of a continuation to complex angular momentum or helicity (and the subsequent S-W representation) is a direct reflection of cut-plane analyticity in the corresponding complex plane. It might seem therefore that the most obvious multiparticle procedure would be to simply look for a continuation to complex values of each of the $(N-3)$ ℓ_j as a reflection of the $(N-3)$-fold multiple discontinuities. However, it is clear from (3.21) that we have something more complicated than simple cut-plane analyticity in each z_j-variable. To illustrate some of the issues involved we consider first a function $f(u_1, u_2)$ of two u-type variables.

If $f(u_1, u_2)$ is analytic for $|u_1|, |u_2| \sim 1$ then we can write

$$f(u_1, u_2) = \sum_{n_1=-\infty}^{+\infty} \sum_{n_2=-\infty}^{\infty} u_1^{n_1} u_2^{n_2} a_{n_1 n_2}. \tag{4.28}$$

Suppose also that for large u_1 and u_2 there are (right-hand) cuts in the planes

$$\mathrm{Im}\, u_1 = 0, \quad \mathrm{Im}\, u_1 u_2 = 0 \tag{4.29}$$

associated with the asymptotic behavior

$$f(u_1, u_2) \underset{\substack{|u_1|\to\infty \\ |u_2|\to\infty}}{\sim} u_1^{\alpha}(u_1 u_2)^{\beta} \stackrel{?}{\equiv} u_1^{\alpha+\beta} u_2^{\beta}. \tag{4.30}$$

From (4.23)-(4.27) it is clear that we should simply take f to be a function of u_1 and $u_1 u_2$ and carry out the corresponding S-W transform, that is we rewrite (4.28) as

$$f(u_1, u_2) = \sum_{n_2=-\infty}^{+\infty} \sum_{n_1-n_2=-\infty}^{+\infty} u_1^{n_1-n_2}(u_1 u_2)^{n_2} a_{n_1 n_2} \tag{4.31}$$

$$= \int_{\mathrm{Re}\, n_2=-1/2} \frac{dn_2}{\sin \pi n_2} \int_{\mathrm{Re}(n_1-n_2)=-1/2} \frac{dn_1}{\sin \pi(n_1-n_2)} u_1^{n_1} u_2^{n_2} a(n_1, n_2)$$

$$+ \left(\sum_{n_2=-\infty}^{-1} \sum_{n_1-n_2=-\infty}^{+\infty} + \sum_{n_2=-\infty}^{+\infty} \sum_{n_1-n_2=-\infty}^{-1} \right) u_1^{n_1} u_2^{n_2} a_{n_1 n_2} \tag{4.32}$$

(for simplicity we have omitted signature). Pulling the n_1 and n_2 contours to the left we expect to pick up poles at $n_1 = \alpha + \beta$ and $n_2 = \beta$ while the contributions of the poles at integer n_2 and $n_1 - n_2$ are cancelled by the sums in (4.32). Consequently we obtain

$$f(u_1, u_2) \sim R_{\alpha+\beta,\alpha} \frac{u_2^{\alpha}(u_1 u_2)^{\beta}}{\sin \pi(\alpha+\beta) \sin \pi\beta}. \tag{4.33}$$

From this simple manipulation there are a number of general points we can make. Firstly we note that the "kinematic poles" or "phase-factors" $[\sin\pi(\alpha+\beta)]^{-1}$ and $[\sin\pi\beta]^{-1}$ arising from the S-W procedure actually distinguish in which variables the asymptotic cut structure appears even though the location of the helicity (or angular momentum) plane singularities does not. Secondly we see that only a subset of the sums in the partial-wave expansion is responsible for building up the asymptotic behavior that is of interest. In this case it is the subset

$$n_2 \geq 0, \quad n_1 \geq n_2. \tag{4.34}$$

If the function $f(u_1, u_2)$ also had branch-points (with a simultaneous discontinuity) in u_2 and u_1u_2 than the corresponding asymptotic behavior would be generated from the part of the partial-wave expansion satisfying (4.34) but with n_1 and n_2 interchanged. Note that the FG continuation $a(n_1, n_2)$ has to be defined as a two variable generalization of (4.25) that is (for right-hand cuts only)

$$a(n_1n_2) = \int\limits_{\substack{u_1>u_1^0 \\ u_1u_2>(u_1u_2)^0}} du_1du_2\,\Delta(u_1, u_1u_2)u_1^{-n_1-1}u_2^{-n_2-1}, \tag{4.35}$$

and this will *only* satisfy the Carlson condition for uniqueness (4.7), in the half-planes corresponding to (4.34). To obtain the formula (4.35) it is necessary to apply the Bargman-Weil theorem (3.32) (which can be regarded as the many-variable generalization of Cauchy's theorem) to the two-variable version of (4.24). In fact this is straightforward because there are no singularities of $u_1^{-n_1-1}u_2^{-n_2-1}$ in the finite u_1 or u_2 planes that would interfere with the two-variable contour manipulation.

This last point has a very important general significance because if we were to attempt a two-variable generalization of (4.2)–(4.10), the singularities of $Q_\ell(z)$ at $z = \pm 1$ would *directly prevent* the appropriate *two-variable* contour manipulation. (In addition to integrals over the double discontinuities of the function there would be integrals over single discontinuities together with a discontinuity of one of the $Q_\ell(z)$). As a result it is essentially impossible to define a simultaneous continuation to complex values of two or more ℓ_j variables (we shall qualify this shortly). Fortunately we can exploit the similarity of the analytic structure with respect to the z_j and u_{jk} variables emphasized in the last two Sections and obtain multiple helicity continuations even though multiple angular momentum continuations cannot be defined.

The above discussion is intended to explain in general terms why the distinct sets of cuts associated with each term in the multiparticle dispersion relation (3.42) require a distinct S-W transform procedure. One important property of the hexagraph notation is that it classifies together all those sets of cuts for which continuations in the same helicity and angular momentum variables are made. However, distinct sets of cuts associated with the same hexagraph do differ in terms of constraints of the form (4.34) on the parts of the partial-wave expansion that are S-W transformed. We shall first give the rules for which continuations exist for a particular hexagraph amplitude and then briefly outline how we demonstrate the existence of such continuations.

4.5 Froissart-Gribov Continuations for Hexagraph Amplitudes

As is clear from subsection 4.3 the negative helicity terms in all partial-wave expansions can be handled analogously to the positive helicity sums and simply produce cancellations in all discussions of asymptotic behavior. Therefore we shall adopt conventions for azimuthal angles that allow us to always consider all helicities to be positive in the following. We describe the rules for F-G continuations in terms of the T, D and V subgraphs of a hexagraph.

In each V_j we can take n_j complex with $(\ell_j - n_j)$ and $(n_j - n'_j)$ held fixed at integer values. In each D_j we take n_j and n'_j complex with $(\ell_j - n_j)$ held fixed at an integer value. In each T_j we can take all three of ℓ_j, n_j and n'_j complex. (Note that each n-label appears in two subgraphs, although the corresponding u is associated with only one subgraph.) These rules imply that the helicity labels, which are attached to sloping lines of the hexagraph, are always coupled (that is differ only by an integer) to the angular momentum associated with the corresponding horizontal line of the hexagraph.

It is interesting to note that the continuations we make correspond, in the case when no v'_j's are present in the hexagraph, to continuing the total cross-channel angular momentum to complex values, together with all the helicities of (cross-channel) subchannels. In no case is the angular momentum of a subchannel continued separately from the helicity. When V_j's are present the total angular momentum of the cross-channel is not used as a variable. Instead, the scattering can be regarded as made up of subprocesses for which the total angular momenta and subchannel helicities are analytically continued.

We begin the general construction of F-G amplitudes by discussing the V_j subgraphs

first. For simplicity consider a hexagraph $A^H(\underset{\sim}{z},\underset{\sim}{u},\underset{\sim}{t})$ with a single V_j subgraph, for example that shown in Fig. 4.6. We consider first the analyticity properties of the partial-wave amplitude obtained by performing just the z_j-integration, that is we consider

$$A^H_{\ell_j n_j n'_j}\left(z_1,\ldots,z_{j-1},z_{j+1},\ldots,\underset{\sim}{u},\underset{\sim}{t}\right)=\int_{-1}^{+1}dz_j d^{\ell_j}_{n_j n'_j}(z_j)A^H(\underset{\sim}{z},\underset{\sim}{u},\underset{\sim}{t}). \tag{4.36}$$

The cuts of $A^H_{\ell_j n_j n'_j}$ include those of A^H which are independent of z_j together with branch cuts arising from collisions of the branch points of A_H with the end-points $z_j=\pm 1$. It is important that because of the allowable discontinuity rule of Section **3.7**, A^H has no cuts depending on just z_j (and no other angular variables) and also no cuts depending on u_j but not u'_j (or vice-versa). (Both of these features follow because a path defining an allowable discontinuity cannot exit at either of the vertices to which the V_j graph is attached.) The location of the resulting end-point branch cuts can then be determined by simply contracting out the j-line of the hexagraph to effectively give a smaller hexagraph as described in 2d. The resulting branch-cuts will be functions of the variables $u\equiv u_j u'_j$ or $u'\equiv u_j/u'_j$ depending on whether they are generated at the $z_j=+1$ or $z_j=-1$ end-points respectively. The cuts which are functions of u will have no double discontinuity with those which are functions of u' since they are generated at distinct end-points. If we now carry out the u_j and u'_j projections we can write

$$\begin{aligned}a^H_{jnn'}&=\int\limits_{\substack{|u_j|=1\\|u'_j|=1}}du_j du'_j u_j^{-n_j-1}\left(u'_j\right)^{-n'_j-1}A^H_{jnn'}\\&=\frac{1}{2}\int\limits_{\substack{|u|=1\\|u'|=1}}dudu'u^{-\frac{1}{2}(n_j+n'_j)-1}(u')^{-\frac{1}{2}(n_j-n'_j)-1}A^H_{jnn'}.\end{aligned} \tag{4.37}$$

By moving the u-contour out to enclose the cuts of $A^H_{jnn'}$ we can define a F-G continuation to complex $n_j+n'_j$ with $n_j-n'_j$ fixed at an integer value. We cannot simultaneously move out the u'-contour because of the absence of double discontinuities in u and u'. This absence also implies that $a^H_{jnn'}(\underset{\sim}{z},\underset{\sim}{u},\underset{\sim}{t})$ will have branch-cuts in only those invariant variables which are independent of both u and u'. Effectively then $a^H_{jnn'}$ has the branch-cut structure of the two hexagraphs which are joined by the V_j-graph in the original hexagraph. In the case of

Fig. 4.6 this is the two hexagraphs of Fig. 4.7. Clearly for hexagraphs with many v_j's we proceed similarly to the above and arrive at an amplitude with the cut-structure of a product of hexagraphs all containing no v_j subgraphs.

We now have to consider only hexagraphs that contain a single T subgraph with an arbitrary number of D-graphs attached to each leg as illustrated in Fig. 4.8 [The most general hexagraph contains an arbitrary number of such structures connected by V-graphs.] The corresponding F-G amplitude can be defined straightforwardly by simply applying the analogue of (4.2)–(4.4) to the z_i projection associated with the T graph *after* applying (4.23)–(4.27) to each of the u_j-projections associated with the D-graphs. We need only the generalization of (4.2)–(4.3) which is provided by the formula

$$\begin{aligned}\underset{-1\le z\le 1}{\text{disc}}\left[(1+z)^{\frac{n+n'}{2}}(1-z)^{\frac{n-n'}{2}}e^j_{nn'}(z)\right] &= \frac{1}{2}(1+z)^{\frac{-n-n'}{2}}(1-z)^{\frac{n'-n}{2}}d^j_{nn'}(z) \quad n>n' \\ &\equiv P^{j-n}(z),\end{aligned} \tag{4.38}$$

where $P^{j-n}(z)$ is a polynomial for $j-n=N$ an integer and $e^j_{nn'}(z)$ is a "second-type" representation function. The appropriate powers of $(1+z)$ and $(1-z)$ needed to apply this formula always emerge, if the integrals over the u-variables are performed first, because of the factors $\sin\theta_{j_1}$, $(\cos\theta_{j_2}+1)$ etc. appearing in (2.49). The asymptotic behavior needed to check the Carlson condition is

$$e^j_{nn'}(z) \underset{|j|\to\infty}{\sim} j^{\frac{-1}{2}}e^{j\ln\left[z-(z^2-1)^{1/2}\right]}, \tag{4.39}$$

which is a simple extension of (4.5). In general the additional factors in (4.38) will imply the Carlson condition is satisfied in the half-plane

$$\text{Re}(j-n)>0. \tag{4.40}$$

An additional property of the $e^j_{nn'}(z)$ and $d^j_{nn'}(z)$ functions that we shall need in the following is their "fixed-pole" structure. At the "nonsense" point $j=n-1$, $e^j_{nn'}(z)$ has an inverse square-root branch-point and

$$(1+z)^{\frac{n+n'}{2}}(1-z)^{\frac{n-n'}{2}}e^j_{nn'}(z) \underset{j\to n-1}{\longrightarrow} \frac{[\Gamma(j+n+1)\Gamma(j-n+1)\Gamma(j+n'+1)\Gamma(j-n'+1)]^{1/2}}{2^{1-n}\Gamma(2j+2)}. \tag{4.41}$$

It will also be important that $d^j_{nn'}(z)$ has an inverse square-root branch point at $j = n' - 1$ and when also $j = n$ we have a particularly simple result, that is

$$(1+z)^{\frac{-n-n'}{2}}(1-z)^{\frac{n'-n}{2}} d^j_{nn'}(z) = \frac{1}{2^n}\left[\frac{\Gamma(j+n+1)\Gamma(j-n'+1)}{\Gamma(j+n'+1)\Gamma(j-n+1)}\right]^{1/2}. \tag{4.42}$$

The F-G continuation of a hexagraph of the form of Fig. 4.8 has the general form

$$\begin{aligned}&\int_\Delta dz(1+z)^{n_1+n_2+n_3+n_4}(1-z)^{n_1+n_2-n_3-n_4} e^j_{n_1+n_2,n_3+n_4}(z)\\ &\times \prod_{j=1}^{M}\int_{\underset{\sim}{\Delta}^M} du_j u_j^{-n_j-1}\prod_j\int_{-1}^{+1} dz_j d^{\ell_j}_{n_j,n'_j} A^H(z,z_1,\ldots,u_1,\ldots,\underset{\sim}{t}),\end{aligned} \tag{4.43}$$

where the integration over the region $\Delta \times \underset{\sim}{\Delta}^M$ will be around the non-zero multiple discontinuities Δ^c of A_H. From (4.41) and (4.42) the continuation to $\ell, n_1, \ldots, n_M$, complex (from $n_1 + n_2 > n_3 + n_4$, say) and with $\ell_1 - n_1, \ldots, \ell_M - n_M$ kept fixed has branch-points at

$$\ell = n_1 + n_2 - 1, \quad n_1 = \ell_1 = n_5 + n_6 - 1, \ldots. \tag{4.44}$$

The "residue" at the product of such singularities reduces (apart from a normalization factor due to (4.41) and (4.42)) to the simple integral

$$\sum_{C\in H}\int ds'_1 \ldots ds'_{M+1} D(z,u_1,\ldots u_M,s'_1,\ldots,s'_{M+1})\Delta^C(s'_1,\ldots,s'_{M+1}), \tag{4.45}$$

where Δ^C is given by (3.44) and $D(z,\underset{\sim}{u},\underset{\sim}{s'})$ is the relevant Jacobian. For large z and $\underset{\sim}{u}$ this Jacobian is simply a product of factors $\left[\sqrt{t_j}\,\lambda^{-1/2}(t_j,t_{j+1},t_{j+2}\right]$ for each vertex of the hexagraph.

To obtain a signatured F-G amplitude we have to add together all hexagraphs related by twisting—with a positive or negative sign for each twist (according to the signature associated with the line twisted). For the residues at a nonsense singularity to not cancel (by virtue of a contour in (4.45) being closable to zero), the nonsense point must be *wrong-signature*. For example, the nonsense singularity at $\ell = n_1 + n_2 - 1$ in (4.44) will be wrong-signature if $\tau\tau_1\tau_2 = -1$ where τ, τ_1 and τ_2 are the signatures associated with ℓ, n_1

and n_2 respectively. "Nonsense, wrong-signature, fixed-poles", which are products of the branch-points we have discussed, will play a vital role in the generation of Regge cuts in unitarity integrals discussed in the next Section.

Since there is only one z-integration manipulated in arriving at (4.43) there is, as discussed above, no multivariable problem. Similarly there is no such problem for the simultaneous continuation to complex values of ℓ_j's corresponding to T-graphs linked by V-graphs (together with some number of D-graphs in general)—this being the only exception to the statement in subsection 4.4 that two or more ℓ_j's cannot be simultaneously continued. This exception is possible because as we have described there is effectively a factorization of the cut-structure involved.

Signature is introduced in general into the F-G and S-W transformation procedure by adding together all hexagraphs differing simply by a twist as described in Section 3. A single twist can be treated as simply changing the sign of the angular variable (associated with the line about which the twist is made) whose conjugate variable (ℓ_j or n_j) is taken complex. In effect then (4.9) and (4.13) simply generalize by the presence of corresponding minus signs associated with twisting—the twist of the hexagraph representing the right-hand cut in the elastic amplitude to give the left-hand cut hexagraph being the simplest example of a twist.

The F-G amplitudes define by the above procedure will satisfy the Carlson uniqueness condition only in appropriate half-planes in analogy with (4.34). This will determine the form of the corresponding S-W transformation as we will illustrate on some examples in the next subsection.

4.6 Sommerfeld-Watson Representations of Hexagraph Amplitudes

Rather than giving a general description of the construction of S-W representations we shall give a detailed description of the representations for a small number of individual hexagraphs. This will illustrate the general construction but will also enable us to make some important special comments associated with the particular hexagraphs we choose.

Consider first the Toller diagram of Fig. 2.2. There are three z_j variables, two u_{jk} variables and three t_j-variables. Altogether there are thirty-two hexagraphs associated with this Toller diagram (if we distinguish hexagraphs differing by a twist) all of which are drawn in Fig. 2.5. The sets of branch-cuts in each type of hexagraph are illustrated in Fig. 4.9. As illustrated in Fig. 4.9*a* each of the hexagraphs in Fig. 2.5*a* has only one sets of cuts, as

do each of the graphs in Fig. 2.5*d*. Similarly Fig. 4.9*a* illustrates that all the hexagraphs of Fig. 2.5*c* also contain only one set of cuts. In contrast half of the hexagraphs of Fig. 2.5*b* contain three sets of cuts as illustrated in Figs. 4.9*b–d* while the other half contain the two sets illustrated in Figs. 4.9*e* and *f*. Altogether the thirty-two hexagraphs generate forty-four sets of three cuts and so there are forty-four terms in the corresponding asymptotic dispersion relation as described in Ref. 2.

We describe first the S-W representation for the first hexagraph of Fig. 2.5*a* which has the cut structure shown in Fig. 4.9*a*. The angular variables and corresponding angular momenta and helicity labels are shown in Fig. 4.10. This hexagraph contains one T-graph and two D-graphs and so the partial-wave expansion has the form

$$A_H(z_1,z_2,z_3,u_1,u_2,t_1,t_2,t_3) = \sum_{\underset{\sim}{\ell}\,\underset{\sim}{n}} T_{\ell_1} D_{\ell_2} D_{\ell_3} a_{\underset{\sim}{\ell}\,\underset{\sim}{n}} \tag{4.46}$$

$$= \sum_{\underset{\sim}{\ell}\,\underset{\sim}{n}} d^{\ell_1}_{0,n_1}(z_1) u_1^{n_1} d^{\ell_2}_{n_1,n_2}(z_2) u_2^{n_2} d^{\ell_3}(z_3) a_{\underset{\sim}{\ell}\,\underset{\sim}{n}}(\underset{\sim}{t}). \tag{4.47}$$

A F-G continuation can be defined to complex ℓ_1, n_1 and n_2. The corresponding asymptotic cut structure is in the variables z_1, u_1 and u_2 and is given by (in the limit $z_1, u_1, u_2 \to \infty$)

$$S_{23} = (P_2+P_3)^2 \sim z_1 \tag{4.48}$$

$$S_{236} = (P_2+P_3+P_6)^2 \sim y_{12} \equiv \left[\left(z_1^2-1\right)^{1/2}\left(z_2^2-1\right)^{1/2}\right] u_1 \tag{4.49}$$

$$S_{15} = (P_1+P_5)^2 \sim y_{123} \equiv \left[\left(z_1^2-1\right)^{1/2}\left(\left(z_3^2-1\right)^{1/2}\right] u_1 u_2 \tag{4.50}$$

From the F-G formula, or by comparing with (4.31)–(4.34) we see that we can expect the analogous constraints to (4.34) following from the asymptotic relations (4.48)–(4.50) to be

$$\ell_1 \geq n_1, \quad n_1 \geq n_2, \quad n_2 \geq 0, \tag{4.51}$$

that is the F-G formula would show that it is in the three complex half-planes

$$\mathrm{Re}(\ell_1 - n_1) \geq 0, \quad \mathrm{Re}(n_1 - n_2) \geq 0, \quad \mathrm{Re}\, n_2 \geq 0, \tag{4.52}$$

that the Carlson condition for uniqueness is satisfied. The corresponding S-W transform is

$$A_H = \frac{1}{8} \int_{\mathrm{Re}\, n_2 = -\frac{1}{2}} \frac{dn_2\, u_2^{n_2}}{\sin \pi n_2} \int_{\mathrm{Re}(n_1 - n_2) = -\frac{1}{2}} \frac{dn_1\, u_1^{n_1}}{\sin \pi (n_1 - n_2)} \int_{\mathrm{Re}(\ell_1 - n_1) = -\frac{1}{2}} \frac{d\ell_1 d^{\ell_1}_{0,n_1}(z_1)}{\sin \pi (\ell_1 - n_1)}$$

$$\times \sum_{\substack{\ell_2 - n_1 = N_1 = 0 \\ \ell_3 - n_2 = N_2 = 0}}^{\infty} d^{\ell_2}_{n_1,n_2}(z_2) d^{\ell_3}_{n_2,0}(z_3) a_{N_2 N_3}(\ell_1, n_1, n_2, \underset{\sim}{t})$$

$$+ \widetilde{\sum}_{\underset{\sim}{\ell}\,\underset{\sim}{n}} T_{\ell_1} D_{\ell_2} D_{\ell_3} a_{\underset{\sim}{\ell}\,\underset{\sim}{n}}(\underset{\sim}{t}), \tag{4.53}$$

where the sum $\widetilde{\sum}$ is over that part of (4.47) not reproduced by the integrals in (4.53). As discussed above we expect $\widetilde{\sum}$ to simply cancel non-Regge behavior produced from the integrals in the asymptotic limits we study.

From the definitions of $P^N(z)$, y_{12} and y_{123} in (4.38), (4.49) and (4.50) respectively we can rewrite (4.53) in the form

$$A_H = \int \frac{dn_2 dn_1 d\ell_1}{\sin \pi n_2 \sin \pi (n_1 - n_2) \sin \pi (\ell_1 - n_1)} y_{123}^{n_2}\, y_{12}^{n_1 - n_2} P^{\ell_1 - n_1}(z_1)$$

$$\times \sum_{N_1, N_2 = 0}^{\infty} P^{N_1}(z_2) P^{N_2}(z_3) a_{N_1 N_2}(\ell_1, n_1, n_2, \underset{\sim}{t}) \tag{4.54}$$

$$+ \widetilde{\sum} T_{\ell_1} D_{\ell_2} D_{\ell_3} a_{\underset{\sim}{\ell}\,\underset{\sim}{n}}(\underset{\sim}{t}),$$

where now, since all of the asymptotic cut structure of A_H has been represented by the S-W integrals we expect the polynomial sums over N_1 and N_2 to be convergent in the asymptotic regions we study.

Unitarity determines (see the next Section and Ref.1) that the Regge singularities of $a_{N_1 N_2}(\ell_1, n_1, n_2)$ occur at values of $\ell_1, \ell_2 = n_1 + N_1$ and $\ell_3 = n_2 + N_2$. As a consequence an asymptotic expansion for the multi-Regge region $z_1, z_2, z_3 \to \infty$, with u_1 and u_2 fixed, can be obtained by pulling back the ℓ_1, n_1 and n_2 contours in (4.54). In particular Regge poles at $\ell_1 = \alpha_1$, $\ell_2 = \alpha_2$, $\ell_3 = \alpha_3$ will give

$$A_H \underset{\substack{z_1 \to \infty \\ z_2 \to \infty \\ z_3 \to \infty}}{\sim} \sum_{N_1, N_2 = 0}^{\infty} \frac{\beta^{\alpha_1 \alpha_2 \alpha_3}_{N_1, N_2} P^{N_1}(z_2) P^{N_2}(z_3)}{\sin \pi \alpha_3 \sin \pi (\alpha_2 - \alpha_3) \sin \pi (\alpha_1 - \alpha_2)} z_1^{\alpha_1} (z_2 u_1)^{\alpha_2 - N_1} (z_3 u_2)^{\alpha_3 - N_2} \tag{4.55}$$

$$\sim \frac{z_1^{\alpha_1} z_2^{\alpha_2} z_3^{\alpha_3}}{\sin\pi\alpha_3 \sin\pi(\alpha_2-\alpha_3)\sin\pi(\alpha_1-\alpha_2)} \sum_{N_1=N_2=0}^{\infty} \beta_{N_1 N_2}^{\alpha_1\alpha_2\alpha_3} u_1^{\alpha_2-N_1} u_2^{\alpha_3-N_2}. \tag{4.56}$$

Again we see that the $[\sin\pi\alpha_3]^{-1}, [\sin\pi(\alpha_2-\alpha_3)]^{-1}, \ldots$ factors reflect the asymptotic cut structure of A_H. In fact the Steinmann relations discussed in the last Section determine that this must be the case. To see this we rewrite (4.56) in the form

$$A_H \sim z_1^{\alpha_1-\alpha_2}(z_1 z_2 u_1)^{\alpha_2-\alpha_3}(z_1 z_2 z_3 u_1 u_2)^{\alpha_3} V_{\alpha_1\alpha_2\alpha_3}(u_1,u_2) \tag{4.57}$$

$$\sim (S_{23})^{\alpha_1-\alpha_2}(S_{236})^{\alpha_2-\alpha_3}(S_{15})^{\alpha_3} V_{\alpha_1\alpha_2\alpha_3}(u_1,u_2), \tag{4.58}$$

which implies that asymptotically

$$\underset{S_{23}}{\text{disc}}\, a_H \sim \sin\pi(\alpha_1-\alpha_2) A_H \tag{4.59}$$

$$\underset{S_{236}}{\text{disc}}\, a_H \sim \sin\pi(\alpha_2-\alpha_3) A_H \tag{4.60}$$

$$\underset{S_{15}}{\text{disc}}\, a_H \sim \sin\pi\alpha_3 A_H. \tag{4.61}$$

Consequently each discontinuity cancels one of the poles in the α_j-variables—which for the purposes of the Steinmann relations we regard as poles in the t_j-variables. Therefore the triple discontinuity of A_H indeed has no poles in the t_j-variables. Since the t_j-channels overlap the discontinuity channels, the Steinmann relations imply this must be the case.

In the "helicity-pole" limit z_1, u_2, $u_3 \to \infty$ we obtain from the same Regge poles a very similar (but simpler) expression to (4.58) by again pulling back the ℓ_1, n_2 and n_3 contours in (4.54) giving

$$A_H \underset{\substack{z_1\to\infty \\ u_2\to\infty \\ u_3\to\infty}}{\sim} \frac{z_1^{\alpha_1-\alpha_2} y_{12}^{\alpha_2-\alpha_3} y_{123}^{\alpha_3} \beta_{00}^{\alpha_1\alpha_2\alpha_3}}{\sin\pi\alpha_3 \sin\pi(\alpha_2-\alpha_3)\sin\pi(\alpha_1-\alpha_2)} \tag{4.62}$$

$$\sim s_{23}^{\alpha_1-\alpha_2} s_{236}^{\alpha_2-\alpha_3} s_{15}^{\alpha_3} \frac{\beta_{00}^{\alpha_1\alpha_2\alpha_3}}{\sin\pi\alpha_3 \sin\pi(\alpha_2-\alpha_3)\sin\pi(\alpha_1-\alpha_2)}. \tag{4.63}$$

So in terms of invariants we have the same result as (4.58) but with the distinction that the vertex function involved is a single (analytically-continued) partial-wave amplitude. This emphasizes the close relationship between the u_j-dependence and z_j-dependence of amplitudes in the asymptotic region which is, of course, a consequence of the presence of only $(N-3)$ cuts (in general) for $(2N-7)$ variables. It will be very important in the following that helicity-pole limits have the advantage of isolating a single partial-wave amplitude. This

is because the unitarity properties of such an amplitude can be straightforwardly studied. Note that the helicity-pole limit (4.62) is not a physical region limit although for the more complicated hexagraphs studied in later Sections the analogous limits will be.

We consider next the first hexagraph of Fig. 2.5*b* whose cut structure is shown in Fig. 4.9*b–d*. This is a more complicated example since there are three sets of cuts contained in the same hexagraph. Fig. 4.9*b* gives cuts in

$$S_{36} \sim z_2 \tag{4.64}$$

$$S_{236} \sim y_{12} \tag{4.65}$$

$$S_{15} \sim y_{123} \tag{4.66}$$

Fig. 4.9*c* gives cuts in

$$S_{36} \sim z_2 \tag{4.67}$$

$$S_{364} \sim \left[\left(z_2^2-1\right)^{1/2}\left(z_3^2-1\right)^{1/2}\right] u_2 \equiv y_{23} \tag{4.68}$$

$$S_{15} \sim y_{123} \tag{4.69}$$

while 4.9*d* gives cuts in

$$S_{26} = (P_2+P_4)^2 \sim y_{12} \tag{4.70}$$

$$S_{34} = (P_3+P_5)^2 \sim y_{23} \tag{4.71}$$

$$S_{15} = y_{123} \tag{4.72}$$

For all three cases the F-G continuation made is to complex n_1, n_2 and ℓ_2 with $\ell_1 - n_1 = N_1$and $\ell_3 - n_2 = N_2$ held fixed at integer values. However, the set of asymptotic cuts (4.64)-(4.66) leads to the constraints (analogous to (4.34))

$$\ell_2 \geq n_1, \quad n_1 \geq n_2, \quad n_2 \geq 0 \tag{4.73}$$

and the corresponding S-W transform is

$$\begin{aligned} A_H = \frac{1}{8}\int \frac{dn_2 dn_1 d\ell_2}{\sin\pi n_2 \sin\pi(n_1-n_2)\sin\pi(\ell_2-n_1)} y_{123}^{n_2} y_{12}^{n_1-n_2} P^{\ell_2-n_1}(z_2) \\ \times \sum_{N_1,N_2=0}^{\infty} P^{N_1}(z_1)P^{N_2}(z_3) a_{N_1N_2}\left(\ell_2, n_1, n_2, \underset{\sim}{t}\right) \\ + \widetilde{\sum} D_{\ell_1} T_{\ell_2} D_{\ell_3} a_{\underset{\sim}{\ell}\underset{\sim}{n}}(\underset{\sim}{t}), \end{aligned} \tag{4.74}$$

which is very similar to (4.54). The S-W transform for the sets of cuts (4.67)–(4.69) is the same but with $n_1 \leftrightarrow n_2$.

The S-W transform of the dispersion integral corresponding to (4.70)–(4.72) has, however, some distinctive features. The Carlson condition requires that the S-W transform be made on the half-plane sums

$$\ell_2 - n_1 \geq 0, \quad \ell_2 - n_2 \geq 0, \quad n_1 + n_2 - \ell_2 \geq 0, \tag{4.75}$$

while the distinct analytic definition of $d^{\ell}_{n_1 n_2}(z)$ for $n_1 \gtrless n_2$ requires that we treat these two cases separately. In practice there will be two terms in the transform, with the first having the form

$$\begin{aligned}\frac{1}{8} \int_{\substack{\mathrm{Re}(\ell_1 - n_1) = -\frac{1}{2} \\ \mathrm{Re}(n_1 - n_2) = -\frac{1}{2} \\ \mathrm{Re}(n_1 + n_2 - \ell_2) = -\frac{1}{2}}} & \frac{dn_1 dn_2 d\ell_2}{\sin\pi(\ell_2 - n_1)\sin\pi(n_1 - n_2)\sin\pi(n_1 + n_2 - \ell_2)} y_{123}^{n_2} y_{12}^{n_1 - n_2} P^{\ell_2 - n_1}(z_2) \\ & \times \sum_{N_1, N_2 = 0}^{\infty} P^{N_1}(z_1) P^{N_2}(z_3) a_{N_1 N_2}(\ell_2, n_1, n_2, \underset{\sim}{t}) \\ & + \widetilde{\sum},\end{aligned} \tag{4.76}$$

while the second has the same form but again with $n_1 \leftrightarrow n_2$.

Consider now the contribution of Regge poles at $\ell_1 = \alpha_1$, $\ell_2 = \alpha_2$, $\ell_3 = \alpha_3$, to the helicity-pole limit z_2, u_1, $u_2 \to \infty$ of (4.76). Pulling back the ℓ_2, n_1 and n_2 contours as usual gives

$$\sim y_{123}^{\alpha_3} y_{12}^{\alpha_1 - \alpha_3} z_2^{\alpha_2 - \alpha_1} \frac{\beta_{00}^{\alpha_1 \alpha_2 \alpha_3}}{\sin\pi(\alpha_2 - \alpha_1)\sin\pi(\alpha_1 - \alpha_3)\sin\pi(\alpha_1 + \alpha_3 - \alpha_2)}. \tag{4.77}$$

Since

$$y_{12} y_{23} \underset{z_2 \to \infty}{\sim} z_2 y_{123}, \tag{4.78}$$

it is straightforward to rearrange the power behavior in (4.77) to give, from (4.70)–(4.72)

$$\sim S_{15}^{\alpha_3 + \alpha_1 - \alpha_2} S_{26}^{\alpha_2 - \alpha_3} S_{34}^{\alpha_2 - \alpha_1} \frac{\beta_{00}^{\alpha_1 \alpha_2 \alpha_3}}{\sin\pi(\alpha_2 - \alpha_1)\sin\pi(\alpha_1 - \alpha_3)\sin\pi(\alpha_1 + \alpha_3 - \alpha_2)}, \tag{4.79}$$

which cannot be the complete asymptotic behavior giving the triple discontinuity of (4.70)–(4.72) because the pole factors in the denominator are not cancelled in the triple discontinuity

and there would be a conflict with the Steinmann relations. However, the second term (with $n_1 \leftrightarrow n_2$ in (4.76)) resolves the problem. Because of Regge pole factorization this gives essentially the same residue apart from a phase-factor $e^{i\pi(n_1-n_2)}$ (arising from the $n_1 \leftrightarrow n_2$ definition of $d^j_{n_1 n_2}$ and so we obtain

$$\sim \frac{S_{15}^{\alpha_3+\alpha_1-\alpha_2} S_{26}^{\alpha_2-\alpha_3} S_{34}^{\alpha_2-\alpha_1} \beta_{00}^{\alpha_1\alpha_2\alpha_3}}{\sin\pi(\alpha_1+\alpha_3-\alpha_2)\sin\pi(\alpha_1-\alpha_3)} \left[\frac{1}{\sin\pi(\alpha_2-\alpha_1)} - \frac{e^{i\pi(\alpha_1-\alpha_3)}}{\sin\pi(\alpha_2-\alpha_3)}\right] \tag{4.80}$$

$$\equiv \frac{S_{15}^{\alpha_3+\alpha_1-\alpha_2} S_{26}^{\alpha_2-\alpha_3} S_{34}^{\alpha_2-\alpha_1} \tilde{\beta}_{00}^{\alpha_1\alpha_2\alpha_3}}{\sin\pi(\alpha_1+\alpha_3-\alpha_2)\sin\pi(\alpha_2-\alpha_1)\sin\pi(\alpha_2-\alpha_3)}, \tag{4.81}$$

which is now of the form imposed by the Steinmann relations.

The combination of cuts (4.70)–(4.72) is also interesting from another perspective. It was omitted from all the early studies of multi-Regge factorization. It does not occur, for example, in the ladder model of Regge behavior. However, the general formalism certainly allows it to be present and it can, as we have shown, be incorporated with only minor subtleties in our S-W formalism. It has the very interesting property that the Regge pole in the t_2-channel automatically decouples if we continue to particle poles in the t_1 and t_3 channels since there are no poles at $\alpha_1 = 0$ or $\alpha_3 = 0$ in (4.81) (in contrast to (4.56) or (4.63)). Effectively the last constraint in (4.75) implies that the amplitude cannot give an infinite set of partial-waves in the ℓ_2-channel when n_1 and n_2 are fixed at finite integers.

This last property and its generalization will play a fundamental role in our analysis of the Super-Critical Pomeron in Section 7. It also manifests itself in a very different context. Namely the manner that sister Regge trajectories[41] appear in string (or originally) dual models. Such trajectories appear for the first time in the multi-Regge configurations corresponding to Fig. 2.2 and indeed *do not couple* in four-point functions. The property is easily generalized by noting that a triple cut configuration which is to give a four-particle amplitude at particle poles in the t_1 and t_3 channels must have the S_{36} (or z_2) discontinuity which becomes the total energy of the amplitude. In fact only the hexagraphs of Fig. 2.5*b* do have the appropriate discontinuity. The hexagraphs in Figs. 2.5*a*, *c* and *d* have the appropriate discontinuity and pole structure to produce elastic scattering amplitudes in the z_1, z_1 and z_3, and z_3 channels respectively. The cut structure of Fig. 4.9*d* which gives (4.70)–(4.72) is distinct in that it cannot reduce to elastic scattering at particle poles in any combination of t-channels. It is totally a multiparticle amplitude. When we go to more complicated hexagraphs such as, for example, that shown in Fig. 4.11 there will be many multiple dis-

continuities which do not include elastic scattering discontinuities. For example, in Fig. 4.11 there are altogether eight sets of five allowable discontinuities, only four of which contain the M^2 discontinuity which must be present to give a four-particle amplitude at poles in each of the t_1, t_2, t_3 and t_4-channels. We shall return to this example in Section 7.

The above examples should be sufficient to illustrate, in principle at least, how the S-W transform is obtained for the multiple discontinuities in a general hexagraph.

5. REGGE CUTS AND REGGEON UNITARITY FOR HEXAGRAPH AMPLITUDES

In the previous Section we have seen how the analytic structure of many-particle amplitudes is reflected directly in the existence of hexagraph F-G amplitudes and the resultant S-W representations. The most powerful consequences of the formalism will, however, be the results of this Section. We shall see that we can obtain a complete translation of the full multiparticle unitarity equations to the complex angular momentum and helicity planes of a general hexagraph. (The multiparticle unitarity equations referred to here are those applying in the hexagraph cross-channel.) In analogy with previous Sections we begin with an elaborate discussion of elastic unitarity.

5.1 Two-Particle Unitarity

The discontinuity of any amplitude across the two-particle threshold in any channel is well-established. We can write, in standard S-Matrix notation

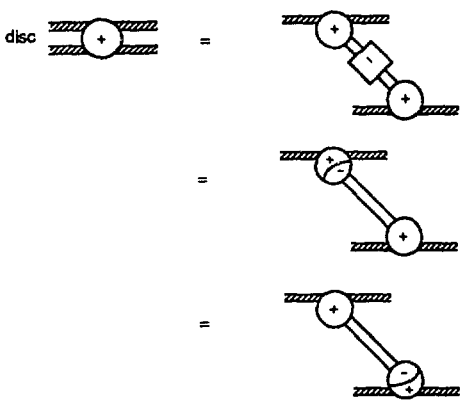

(5.1)

(5.2)

(5.3)

A circle represents the connected part of an S-Matrix element, while a square denotes the full S-Matrix (or its Hermitian conjugate). The channel in which the discontinuity has been taken is clear both from the grouping of the initial and final states shown on the left-hand side and the intermediate states displayed on the right-hand side. In addition a minus sign indicates that an amplitude is evaluated below the cuts associated with the states grouped with this sign.

The hatches in (5.1)–(5.3) indicate an arbitrary number of external lines but if we take single lines in each case we obtain the familiar elastic unitarity equation

(5.4)

The phase-space-space integral involved is the same in all cases, that is if Q is the external 4-momentum,

$$I_2(Q) = i\int d^4P_1 d^4P_2 \delta^4(P_1+P_2-Q)\delta^+(P_1^2-m^2)\delta^+(P_2^2-m^2) \tag{5.5}$$

$$= i\int d^4P_1 \delta^+(P_1^2-m^2)\delta^+\left((Q-P_1)^2-m^2\right), \tag{5.6}$$

where m is the mass of internal state particles. Choosing $Q=(\sqrt{t},0,0,0)$ we can write

$$I_2(t) = i\int \frac{d^3P_1}{2P_{10}}\delta^+(t-2\sqrt{t}P_{10}), \tag{5.7}$$

and using polar coordinates (r,θ,μ) for P_1 gives

$$I_2 = i\int \frac{r^2dr\,\delta^+\left(t-2\sqrt{t}\sqrt{r^2+m^2}\right)}{2\sqrt{r^2+m^2}}\int d(\cos\theta)d\mu \tag{5.8}$$

$$= i\rho(t)\int dg \tag{5.9}$$

where

$$\rho(t) = \frac{\pi}{2}\left[\frac{t-4m^2}{t}\right]^{1/2} \tag{5.10}$$

and

$$\int dg = \frac{1}{8\pi^2}\int_{-1}^{+1} d(\cos\theta)\int_0^{2\pi} d\mu \int_0^{2\pi} d\nu \tag{5.11}$$

is the usual SO(3) group integration in the parameterization (2.13). The additional azimuthal integration over ν that we have introduced is redundant unless the internal state particles carry spin.

It is straightforward to make a partial-wave projection of (5.2) or (5.3). We first introduce a Toller diagram T for the amplitude A whose discontinuity is taken—with the "t-channel" involved chosen as one of the t-channels of the diagram. Cutting the Toller diagram through this particular line defines diagrams T_L and T_R for each of the amplitudes

A_L and A_R appearing on the right-hand side as illustrated in Fig. 5.1. The group integration (5.11) can then be directly written as an integration over g_L, the Lorentz transformation corresponding to the t line of T_L. If g_R and g are respectively transformations associated with the t-line in T_R and T then we have

$$g_R = g_L^{-1} g. \tag{5.12}$$

Consequently if we display the appropriate part of the partial-wave expansion (4.16) for each of A, A_L and A_R by writing

$$A(g) = \sum_{\ell=0}^{\infty} a_\ell D^\ell(g) \tag{5.13}$$

$$A_K(g_K) = \sum_{\ell=0}^{\infty} a_\ell^K D^\ell(g_K) \quad K = L, R \tag{5.14}$$

where we have suppressed all other group-variables and even the helicity-labels indicating the matrix form of both D^ℓ and a_ℓ, we can write (5.2) say, in the form

$$\underset{t}{\text{disc}}\, A(g) = i\rho(t) \int dg_L A_L(g_L) A_R\left(g_L^{-1} g\right). \tag{5.15}$$

We then use the group representation properties of the D^ℓ, that is

$$D^\ell\left(g_L^{-1} g\right) = D^\ell\left(g_L^{-1}\right) D^\ell(g) \tag{5.16}$$

and

$$\int dg_L D^\ell(g_L) D^{\ell'}\left(g_L^{-1}\right) = \delta_{\ell\ell'}/(2\ell+1) \tag{5.17}$$

to obtain the partial-wave projection of (5.15) as

$$\underset{t}{\text{disc}}\, a_\ell = \frac{i\rho(t)}{(2\ell+1)} a_\ell^L a_\ell^R \tag{5.18}$$

The diagonalization of unitarity equations by partial-wave projection is, of course, well-known to be a powerful tool. For us the importance of these equations will be in their continued validity at complex values of the angular momenta (and helicities) involved. An example of this is provided by the elastic unitarity equation obtained from the particular version (5.4) of (5.2). The Carlson condition for uniqueness implies that since (5.18) holds

for all integer ℓ it immediately holds (for each signature) for complex ℓ. Note that in this special case there are no additional helicities involved and $a_\ell \equiv a_\ell^L \equiv a_\ell^\tau(t)$, $\tau = \pm 1$ as defined by (4.9), and $a_\ell^* \equiv a_\ell^R \equiv a_\ell^\tau(t)^*$. Consequently (3.18) gives for complex ℓ (since $a_\ell^\tau(t)$ is real analytic as a function of t)

$$a_\ell^\tau(t) - a_\ell^\tau(t)^* = \frac{i\rho(t)}{(2\ell+1)} a_\ell^\tau(t) a_\ell^\tau(t)^*. \tag{5.19}$$

The power of this equation is most immediately illustrated by supposing that $a_\ell^\tau(t)$ has a "fixed-pole" singularity at $\ell = \alpha$. In this case (5.19) would give

$$\frac{\beta}{\ell - \alpha} - \frac{\beta^*}{\ell - \alpha} = \frac{i\rho(t)}{(2\ell+1)} \frac{\beta\beta^*}{(\ell-\alpha)^2}, \tag{5.20}$$

which is inconsistent unless there is an essential singularity (infinite-order pole) or the residue $\beta = 0$. So fixed-poles are not allowed by elastic unitarity. In contrast a Regge pole at $\ell = \alpha(t)$ gives no problem but (5.19) implies

$$\frac{\beta(t)}{\ell - \alpha(t)} \underset{\ell \to \alpha(t)}{\sim} \frac{i\rho(t)}{(2\ell+1)} \frac{\beta(t)\beta^*(t)}{(\ell - \alpha(t))\,(\alpha(t) - \alpha^*(t))} \tag{5.21}$$

$$\Rightarrow \beta^*(t) = \frac{-i(2\ell+1)}{\rho(t)} [\alpha(t) - \alpha^*(t)] \tag{5.22}$$

Our derivation of (5.18) was actually valid for arbitrary amplitudes involved in (5.2) or (5.3). We simply suppressed all additional variables. Note that since all remaining g_i in the Toller diagram T (besides g) can be identified with the corresponding transformations in T_L or T_R, (5.18) applies directly to the full partial-wave amplitudes obtained by projecting with respect to all g_i.

Unfortunately, perhaps, we cannot continue (5.18) directly to complex ℓ when arbitrary multiparticle amplitudes are involved. As we have demonstrated in previous Sections we must first decompose a multiparticle amplitude into hexagraph amplitudes and then continue to complex angular momenta and helicities in a distinctive manner for each hexagraph. The vital question is therefore whether (5.18) can be broken down into component equations for hexagraph amplitudes?

5.2 Hexagraph Diagonalization of Unitarity Equations

We shall now argue that the unitarity equation is further diagonalized by hexagraph amplitudes. First we note that if we substitute specific hexagraphs H_L and H_R for A_L and A_R in (5.2) we naturally obtain a specific product hexagraph H by contracting out the phase-space lines as illustrated in Fig. 5.2.

The unitarity integral represented by (5.2) (or (5.3)) clearly contains all discontinuities of the product hexagraph. Such cuts correspond to cuts either through just one of the A_L and A_R or to a cut through both amplitudes which avoids the phase-space lines. The combination of cuts in each amplitude with the phase-space integration will certainly give this last form of cut in the complete integral. It follows then that the product of H_L and H_R in the unitarity integral contributes to the product hexagraph H on the left-hand side of (5.2) or (5.3). We now argue that for Regge behavior (in the t-channel) generated in the unitarity integral, the product of H_L and H_R contributes *only* to H.

If we parameterize g as in (2.13) and then consider the Regge limit $z = \cos\theta \to \infty$ it follows from (5.12) that, since we have chosen g_L as integration variables, we must have $z_R = \cos\theta_R \to \infty$ (or possibly $\cos\mu_R \to \infty$) *if* the integration region remains finite in the Regge limit. The form (5.3) for the discontinuity equation implies we can take A_L to be a physical amplitude while A_R is evaluated below its t-channel cut. Consequently if the Regge behavior of A_L is due to singularities at $\ell = \alpha_i(t)$, the Regge behavior of A_R will be due to singularities at $\ell = \alpha_i^*(t)$. Therefore Regge behavior of A associated with singularities at $\ell = \alpha_i(t)$ cannot arise from the Regge behavior of A_R and can only arise if the integration region does not remain finite but is instead pushed out into the Regge region of A_L. That this happens can be seen by considering Fig. 5.3. This shows the $v_L = e^{i\theta_L}$ plane. We can suppose that the integration over μ_L (and ν_L) has been performed with branch-points generated by the cuts of A_L and A_R hitting the end-points at $\cos\mu_L = \pm 1$. At these points (5.12) reduces to

$$\theta = \theta_L \pm \theta_R, \tag{5.23}$$

and so for $\theta \in (0, \pi)$ the physical region $\theta_R \in (0, \pi)$ maps into the v_L-plane as shown in Fig. 5.3. The cuts of A_L (which are independent of θ) and the cuts of A_R (which do depend on θ) are both shown. It is then clear that as $z \to \infty$ (or equivalently $v = e^{i\theta} \to \infty$) the cuts of A_R do indeed move out in the v_L-plane dragging the integration contour into the large v_L

Regge region as shown in Fig. 5.4. Furthermore the *only* singularities (of the integral over v_L) generated out in the Regge region where the Regge behavior of A_L is exposed are those involving pinches (of the integration contour) by a combination of branch-points of both A_L and A_R. But these are just the cuts present in the product hexagraph. Consequently Regge behavior associated with singularities at $\ell = \alpha_i(t)$ contributes only to the product hexagraph. By considering the form (5.2) for the discontinuity formula and by choosing g_R rather than g_L as integration variables we can similarly show that Regge behavior associated with singularities at $\ell = \alpha_i^*(t)$ also contributes only to the product hexagraph.

Once (5.18) is written as an equation for hexagraph amplitudes (with a_ℓ the partial-wave projection for H and a_ℓ^L and a_ℓ^R respectively the partial-wave projections for H_L and H_R) it can immediately be continued to all allowed complex values of the angular momentum and helicity labels on both sides of the equation. This is because the appropriate continuations allowed by the rules of Section 5.5 coincide on both sides of the equation.

We now move onto the technically much more complicated problem of the generation of Regge cuts in multiparticle unitarity integrals. We have elaborated the above argument for hexagraph diagonalization in detail in part because we shall give only an outline of a similar (but much more complicated) argument for the general hexagraph diagonalization of the production of Regge cuts.

5.3 Partial-Wave Diagonalization of Multiparticle Unitarity

We begin with the general discontinuity formula for a multiparticle intermediate state of an arbitrary amplitude. That is we write, similarly to (5.1)–(5.3)

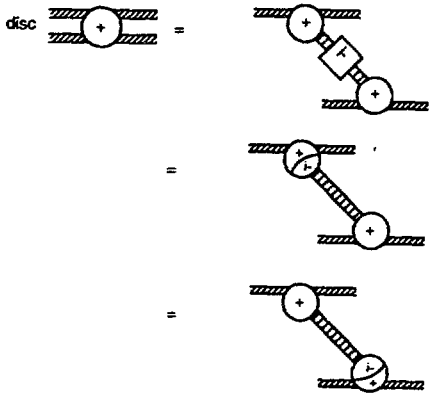

(5.24)

(5.25)

(5.26)

Each set of hatched lines again represents a particular set of particles (and not a sum over such sets). The i in the square-box in (5.24) indicates that the discontinuity is that due to a particular intermediate state i in the discontinuity channel; $\boxed{i-}$ is the inverse of the physical S-Matrix defined with respect to this state (which, of course, defines the internal phase-space integrations). The $i-$ in (5.25) and (5.26)—which will be the formulae we actually use—indicates that an amplitude is evaluated below the i-cut and all sub-channel cuts associated with the phase-space. The complete set of discontinuity formulae of the form (5.24), together with the discontinuity formulae for general Landau singularities, is equivalent to the full set of coupled unitarity equations for all S-Matrix amplitudes. We shall consider only states with an even number of particles since these directly generate multireggeon cuts. The odd number states generate directly reggeon/particle cuts (which do not contribute to high-energy scattering in the cross-channel) or alternatively reggeon cuts involving reggeons which couple only to odd number particle states.

The next step, in analogy with (5.9), is to write the phase-space integration in (5.24)–(5.26) in terms of angular variables. For this purpose we introduce a Toller diagram T_i which directly describes the phase-space integration variables. This new form of Toller diagram is a tree-diagram connecting an initial-line representing the incoming momentum Q to final particles representing the phase-space state as illustrated in Fig. 5.5. Starting from some standard frame s_L for Q we can introduce Lorentz transformations g_j for each of the internal lines of the diagram and a g_L for s_L (just as we did for amplitudes in Section 3). A generalization of (5.5)–(5.11) then gives for the i phase-space integral $I_i(t = Q^2)$

$$I_i(t) = i \int d\rho(t, t_1, \ldots t_j, \ldots) \int dg_L \prod_j dg_j \tag{5.27}$$

where (apart from numerical factors—powers of 2π etc.)

$$\int d\rho(t, t_1, \ldots t_j, \ldots = \int \prod_j dt_j \left[\frac{\lambda^{1/2}(t, t_1, t_2)}{t}\right] \left[\frac{\lambda^{1/2}(t_1, t_3, t_4)}{t_1}\right] \ldots \left[\frac{\lambda^{1/2}(t_j, t_{j+1}, t_{j+2})}{t_j}\right] \ldots . \tag{5.28}$$

There is a λ-function, defined by (2.42), for each internal vertex, including those involving the internal particles—for which the corresponding "t_j" is the mass^2. The integration region is defined by

$$\lambda(t_j, t_{j+1}, t_{j+2}) \geq 0 \qquad \forall j \tag{5.29}$$

$$\Rightarrow \sqrt{t_j} \geq \sqrt{t_{j+1}} + \sqrt{t_{j+2}}, \tag{5.30}$$

if t_j is the largest momentum^2.

As in our discussion of two-particle unitarity we denote the amplitude whose discontinuity we are considering as A and choose a Toller diagram T (in which the i-channel is one of the t-channels) to denote the variables we use to describe A. We denote by A_L and A_R the constituent amplitudes involved in the integrals of (5.25) and (5.26)—the latter being the formula we shall initially discuss. We introduce Toller diagrams T_L and T_R for A_L and A_R by cutting T at the i-line and joining T_i to each of the sub-diagrams formed as illustrated in Fig. 5.6. We can choose the same g_j for T_L and T_R at all internal phase-space lines but at the i line, if the transformations g, g_L and g_R are chosen respectively for T, T_L and T_R, they must again be related by (5.12). By choosing the standard frame s_L for T_i to be the corresponding (external) frame of T_L we can regard the internal phase-space integral (5.27) as expressed directly in terms of the variables of T_L.

Having written the phase-space in the form (5.27) it is straightforward to obtain a partial-wave projection and diagonalization of (5.25) or (5.26) by again utilizing (5.12)–(5.17). However, before giving explicit formulae we first wish to discuss the diagonalization of the equations by hexagraphs. Suppose we consider a Regge (or helicity) limit in which the parameters of g are taken large. If A_L is a physical amplitude with Regge behavior associated with $\ell_k = \alpha_k(t_k)$, where $k = 1, \ldots N$ now labels the internal lines of the Toller diagram attached to particles as illustrated in Fig. 5.6, we can expose Regge behavior associated with all of the $\alpha_k(t_k)$ only if the phase-space integration is pushed out into the corresponding asymptotic regions by the cuts of A_R, in analogy with Fig. 5.4. This means that A_R must have sufficient cuts in (invariant) variables that depend on the parameters of g and also involve the internal particles. If we decompose A_R into hexagraph amplitudes we know that each amplitude has simultaneous cuts in only a limited set of angular variables. We can find hexagraphs with appropriate cuts to distort the contour into helicity-pole limits where all the $\alpha_k(t_k)$ will be exposed but not to distort it into Regge regions. Demanding the appropriate helicity-pole asymptotic behavior determines the internal hexagraph structure of A_L and demanding the appropriate cuts to distort the phase-space determines the internal hexagraph structure of A_R. The external hexagraph structure of both A_L and A_R is determined by requiring that the cut structure of the hexagraph component of A selected be reproduced by the cuts of A_L and A_R.

Following this discussion through in detail shows that A_L and A_R must have the same hexagraph structure as A externally while the internal T_i-lines must all be D-lines as illustrated in Fig. 5.7. Note that A_L and A_R can have distinct D-line structures as illustrated in Fig. 5.8. In general such distinct hexgraphs describe distinct asymptotic cut structures. However, at the phase-space boundary where (as we shall discuss) the Regge cuts are generated, $\lambda = 0 \quad \forall\lambda$ or

$$\sqrt{t_j} = \sqrt{t_{j+1}} + \sqrt{t_{j+2}} \qquad \forall j, \tag{5.31}$$

This implies that all the Q_j (of T_i) are parallel and the asymptotic cut structures associated with the various possible D-line structures cannot be distinguished. The distinct hexagraphs are then distinguished only by the t-channels in which their Regge singularities appear and not by their cut structure.

The hexagraph projection of (5.3) (or (5.2)) therefore has the form

$$\text{disc } H = i \int d\rho \int dg_L \prod_j dg_j \, H_L(g_L, \ldots, g_j, \ldots) H_R\left(g_L^{-1} g, \ldots, g_j, \ldots\right), \tag{5.32}$$

and the partial-wave projection takes the form

$$\text{disc } a_\ell^H = i \int d\rho \sum_{\underset{\sim}{N}, \underset{\sim}{n}} a^{H_L}_{\ell \underset{\sim}{N} \underset{\sim}{n}} a^{H_R}_{\ell \underset{\sim}{N} \underset{\sim}{n}}. \tag{5.33}$$

We have suppressed all the external hexagraph partial-wave labels (angular momenta and helicities) and formally indicated the sums over the internal helicity labels $\underset{\sim}{n}$ and angular momenta $\underset{\sim}{N} = \underset{\sim}{\ell} - \underset{\sim}{n}$ of all the D-graphs in T_i. (Note that we must choose a particular hexagraph for T_i and use it for both H_L and H_R to carry through the following analysis.)

The continuation of (5.33) to complex ℓ is achieved by an adaptation of the S-W transform procedure of the last Section. The sums over $\underset{\sim}{N}$ converge for complex ℓ (in analogy with the corresponding S-W sums). The first D-graph in T_i contributes a sum of the form

$$\sum_{\underset{\sim}{n}} \equiv \left(\sum_{n_1} \sum_{n_2} \right)_{|n_1 + n_2| \leq \ell}, \tag{5.34}$$

which, in the particular case that there are no additional D-graphs in T_i, we can define for complex ℓ as

$$\sum_{\underset{\sim}{n}} = \sum_{\tau_1,\tau_2} \frac{\sin\frac{\pi}{2}(\ell-\tau')}{-16} \int \frac{dn_1 dn_2}{\sin\frac{\pi}{2}(n_1-\tau_1')\sin\frac{\pi}{2}(n_2-\tau_2')\sin\frac{\pi}{2}(\ell-n_1-n_2-(\tau'-(\tau_1'+\tau_2')))}$$

$$+\{n_1\to -n_1\}+\{n_2\to -n_2\}+\{n_1,n_2\to -n_1,-n_2\}, \tag{5.35}$$

where $\tau' = \frac{1}{2}(1-\tau)$, $\tau_i' = \frac{1}{2}(1-\tau_i)$. Inserting (5.35) into (5.33) defines a signatured continuation to complex ℓ, using the appropriate continuations of $a^{H_L}_{\ell \underset{\sim}{N} \underset{\sim}{n}}$ and $a^{H_R}_{\ell \underset{\sim}{N} \underset{\sim}{n}}$. If n_1 is coupled to an additional D-graph, as illustrated in Fig. 5.9, then the factor $\left[\sin\frac{\pi}{2}(n_1-\tau_1')\right]^{-1}$ in (5.35) is replaced by an analogous expression to (5.35) that is

$$\sum_{n_3,n_4} \to \sum_{\tau_3,\tau_4} \frac{-1}{16} \int \frac{dn_3 dn_4}{\sin\frac{\pi}{2}(n_3-\tau_3')\sin\frac{\pi}{2}(n_4-\tau_4')\sin\frac{\pi}{2}(n_1-n_3-n_4-(\tau_1'-(\tau_3'+\tau_4')))}. \tag{5.36}$$

Similarly if n_2 is coupled to an additional D-graph the factor $\left[\sin\frac{\pi}{2}(n_2-\tau_2')\right]^{-1}$ is replaced by an analogous expression. This process is repeated until the complete sum over $\underset{\sim}{n}$ in (5.33) is similarly represented.

Regge cuts are generated in the continuation of (5.33) by the combination of internal Regge poles with the nonsense singularities (4.44) and the helicity integrals (5.35) and (5.36). From (4.41) and (4.42) it follows that each of $a^{H_L}_{\ell \underset{\sim}{N} \underset{\sim}{n}}$ and $a^{H_R}_{\ell \underset{\sim}{N} \underset{\sim}{n}}$ will have square root nonsense wrong-signature singularities in their complex (angular momentum and helicity) continuations, which combine to give poles to be inserted in the integrals (5.35) and (5.36). Therefore we insert such a fixed-pole into (5.33) for each vertex of T_i *not involving particles* and use such poles to perform as many helicity integrations of the form (5.36) as possible. This will leave only the helicity integrals for hexagraph lines attached directly to the internal particles. If we also keep only the $\underset{\sim}{N} = \underset{\sim}{Q}$ part of (5.33) we then obtain the "fixed-pole"

contribution due to a $2M$ particle state, that is

$$\text{disc}\, a^\tau(\ell) \sim \sin\frac{\pi}{2}(\ell-\tau') \sum_{\tau_1,\tau_2,\ldots} \int_{\lambda>0,\forall\lambda} d\tilde{\rho} \frac{dm_1 dm_2 \ldots \xi_M N^{L\tau\tau_1\tau_2\ldots} N^{R\tau\tau_1\tau_2\ldots}}{\sin\frac{\pi}{2}(m_1-\tau_1')\sin\frac{\pi}{2}(m_2-\tau_2')\ldots(\ell-m_1-m_2\ldots+M-1)}, \tag{5.37}$$

where $m_1, \ldots m_M$ now label the helicities coupled to internal particles and N^L and N^R are fixed-pole residues of $a^{H_L}(\ell)$ and $a^{H_R}(\ell)$ respectively. If we extract an appropriate Jacobian factor (cf. D of (4.45)) in defining N^L and N^R we can write

$$\int d\tilde{\rho} \equiv \int d\hat{\rho} \prod_{k=1}^{m} \rho_k \equiv \frac{\int \prod_j dt_j \prod_{k=1}^{M} \rho_k}{[\lambda^{1/2}(t,t_1,t_2)\ldots\lambda^{1/2}(t_j,t_{j+1},t_{j+2})]^{1/2}}, \tag{5.38}$$

where each ρ_k is a two-particle phase-space factor (5.10) and there is a $\lambda^{1/2}$ factor for each non-particle vertex of T_i. The ξ_M factor in (5.37) originates from the denominator factor $\sin\frac{\pi}{2}(\ell-n_1-n_2-\tau'+\tau_1'+\tau_2')$ in (5.35) or $\sin\frac{\pi}{2}(n_1-n_3-n_4-\tau_1'+\tau_3'+\tau_4')$ in (5.36). When evaluated at a nonsense, wrong-signature, point such a factor gives (-1) for two even-signature Regge poles, $(+1)$ for two odd-signature Regge poles and (-1) for an even/odd-signature combination.

If we also perform the m_k integrations in (5.37) by picking up the Regge poles of N^L at $m_k = \alpha_k(t_k)$ $k = 1,\ldots,M$ (the corresponding poles of N^R will be at $m_k = \alpha_k^*(t_k)$) we can use the factorization property

$$N^L(\underset{\sim}{\ell}, \underset{\sim}{m}, \ldots) \underset{m_k\to\alpha_k}{\sim} \frac{N^L_{\alpha_k}\beta_k}{m_k-\alpha_k}, \tag{5.39}$$

and exploit the unitarity equation (5.18) to eliminate both ρ_k and β_k. We then obtain

$$\text{disc}\, a^\tau(\ell) \sim \sin\frac{\pi}{2}(\ell-\tau')\xi_M \int d\hat{\rho} \frac{N^{L\tau\underset{\sim}{\tau}}_{\underset{\sim}{\alpha}} N^{R\tau\underset{\sim}{\tau}}_{\underset{\sim}{\alpha}}}{\left[\ell-1-\sum_{k=1}^{M}(\alpha_k-1)\right]\prod_{k=1}^{M}\sin\frac{\pi}{2}(\alpha_k-\tau_k')}. \tag{5.40}$$

The M-reggeon cut is generated in (5.40) by the nonsense-pole factor hitting the boundary of the phase-space (5.31). This implies that

$$\sqrt{t_k} = \frac{\sqrt{t}}{M} \qquad \forall k \Rightarrow t_k = t/M^2. \tag{5.41}$$

and at $t = 0$ the branch-point is located at

$$\ell = \alpha_M(0) = \alpha_1(0) + \cdots \alpha_M(0) - M + 1. \tag{5.42}$$

In the simple case $\alpha_k(t_k) = \alpha(t_k),\ \ k = 1, \ldots M$ the location is given for all t by

$$\ell = \alpha_M(t) = M\alpha\left(\frac{t}{M^2}\right) - M + 1. \tag{5.43}$$

To derive a complete discontinuity formula from (5.40) we write it in the general "matrix" form

$$a(\ell) - a^i(\ell) = \Gamma(\ell)a(\ell)a^i(\ell), \tag{5.44}$$

where $\Gamma(\ell)$ denotes the phase-space which generates the cut. Since $a^i(\ell)$ does not contain the reggeon cut generated by $\Gamma(\ell)$ but $a(\ell)$ does, (5.44) implies (if δ_ℓ is the ℓ-plane discontinuity)

$$\delta_\ell a(\ell) = [\delta_\ell \Gamma(\ell)]\, a(\ell^+)a(\ell^-), \tag{5.45}$$

where $\pm$ implies the amplitude is evaluated above or below the reggeon cut involved. From the formal structure of (5.45) we can now derive a general discontinuity formula for an M-reggeon cut in *any* t-channel of *any* hexagraph F-G amplitude in the form

$$\underset{\ell=\alpha_M(t)}{\text{disc}}\, a^{H\tau}(\ell) = \sin\frac{\pi}{2}(\ell - \tau')\xi_M \int d\hat{\rho} N_{\underset{\sim}{\alpha}}^{H_{L}\tau\underset{\sim}{\tau}}(\ell^+) N_{\alpha}^{H_{R}\tau\underset{\sim}{\tau}}(\ell^-) \frac{\delta\left(\ell - 1 - \sum_{k=1}^{M}(\alpha_k - 1)\right)}{\sin\frac{\pi}{2}(\alpha_1 - \tau_1')\ldots\sin\frac{\pi}{2}(\alpha_m - \tau_M')}. \tag{5.46}$$

This formula, that is *reggeon unitarity*, has been known[7] (apart from signature factor details) for over twenty years and it has also been understood for a long time that it provides a general, model-independent basis for the Reggeon Field Theory. This will be the subject of the next Section. However, for the purposes of this article, it is vital that (5.46) holds for a general hexagraph and so controls far more than just elastic scattering and the RFT. As we shall see it is the consequences of (5.46) for the formation of bound-states whose scattering is also controlled by (5.46) that will enable us to study the Pomeron phase-transition and also analyze infra-red divergences in QCD.

It is important to emphasise that although our discussion has been specific to singularities generated by Regge poles it could clearly be carried through to at least locate the trajectory of "multi-Reggeon" singularities generated by any initial "reggeon" singularity.

In particular if the initial singularity is due to an Expanding Disc, the two-particle unitarity equation (5.18) continued to complex ℓ implies that this singularity occurs in all (vacuum) channels. "Multi/Expanding Disc" singularities will then be generated by the foregoing analysis. The difficulty is that the phase-space integration in the analog of (5.40) will involve additional integrations over the full branch-cuts of all the contributing "discs". Since these branch-cuts will overlap in the discontinuity formula analagous to (5.46) the result is ambiguous and there is no well-defined discontinuity.

The ambiguity of (5.46) when the basic singularities are branch-points can be viewed as resulting from the lack of sufficient locality for such states in rapidity and impact parameter space. In contrast Regge pole states are well- localised and so a multi-Regge pole state is well defined. Although it would be difficult to prove conclusively it seems very unlikely that (5.46) is actually a well-defined equation if the contributing singularities are anything other than Regge poles or Regge cuts generated from Regge poles. Certainly we can say that Regge poles and their multi-Reggeon cuts (or "thresholds") are the only form of angular plane singularity structure known to satisfy full multiparticle unitarity in the cross-channel.

6. REGGEON FIELD THEORY AND THE CRITICAL POMERON

Reggeon Field Theory (RFT) has been derived and formulated from many different starting points since Gribov's seminal paper,[14] and we shall describe some of them in this Section. First we want to emphasize the viewpoint that RFT is a technical device for obtaining a scaling solution of the reggeon unitarity equations for the particular case of an even-signature Pomeron regge pole, with trajectory $j = \alpha_{I\!P}(t)$, where the intercept is

$$\alpha_{I\!P}(0) = 1. \tag{6.1}$$

Note that when (6.1) holds we also have, from (5.43), that

$$\alpha_{M I\!P}(0) = 1, \tag{6.2}$$

where $j = \alpha_{M I\!P}(t)$ is the trajectory of the M-Pomeron cut. Therefore all the Pomeron singularities accumulate at one point as illustrated in Fig. 6.1 and we must look for a simultaneous solution of all the corresponding discontinuity formulae.

The idea that high-energy diffraction scattering is described by a Pomeron with unit intercept has a lengthy phenomenological history. Here we shall be emphasizing the theoretical virtues and attractions of this idea. Most immediately we shall concentrate on the existence of a renormalization group solution of the reggeon unitarity equations in terms of infra-red fixed-point behavior.

6.1 Reggeon Unitarity Phase-Space for Pomerons

The initial significance of considering an even signature Regge pole satisfying (6.1) is that we can neglect the signature factors in (5.46), that is for small values of all t_i'

$$\xi_M \sim (-1)^{M-1}, \quad \sin\frac{\pi}{2}(\alpha_1 - \tau_1') \sim \cdots \sim \sin\frac{\pi}{2}(\alpha_M - \tau_M') \sim \sin\frac{\pi}{2}(\ell - \tau') \sim 1. \tag{6.3}$$

In this case (5.46) can be conveniently rewritten by introducing the usual RFT variables, that is energies E_i and two-dimensional ("transverse") momenta k_i where

$$\ell_i = 1 - E_i \quad \text{and} \quad t_i = k_i^2 \qquad \forall i \tag{6.4}.$$

We can then write (with $\Delta_k = 1 - \alpha_k(t_k)$)

$$\delta\left(\ell - 1 - \sum_{k=1}^{M} \Delta_k\right) \leftrightarrow \int \prod_k dE_k \delta(E_k - \Delta_k) \delta(E - \sum_{k=1}^{M} E_k)$$

$$\Rightarrow \text{energy conservation + energy-shell} \tag{6.5}$$

$$\int \frac{dt_j dt_k}{\lambda^{1/2}(t_i, t_j, t_k)} \leftrightarrow \int d^2\underline{k}_j d^2\underline{k}_k \delta^2\left(\underline{k}_i - \underline{k}_j - \underline{k}_k\right)$$

$$\Rightarrow \text{momentum conservation + phase-space integration.} \tag{6.6}$$

Consequently the even-signature elastic amplitude $a^\tau(\ell, t)$ will satisfy the corresponding reggeon unitarity equation (5.46) if it can be written in the form

$$a^\tau(\ell, t) \equiv F\left(E, \underline{k}^2\right) = \sum_{n,m=1}^{\infty} F_{nm}(E, \underline{k}^2), \tag{6.7}$$

where

$$\begin{aligned} F_{nm}\left(E, \underline{k}^2\right) = & \int \left[\prod_i dE_i d^2\underline{k}_i \delta\left(E - \sum_{i=1}^{n} E_i\right) \delta^2\left(\underline{k} - \sum_{i=1}^{n} \underline{k}_i\right)\right] g_n\left(\underline{k}_1, \ldots \underline{k}_n\right) \\ & \times \int \left[\prod_j dE'_j d^2\underline{k}'_j \delta\left(E - \sum_{j=1}^{n} E'_j\right) \delta^2\left(\underline{k} - \sum_{i=1}^{n} \underline{k}'_i\right)\right] g_m\left(\underline{k}'_1, \ldots \underline{k}'_m\right) \\ & \times G_{nm}\left(E_1, \ldots E_n, E'_1, \ldots, E'_m, \underline{k}_1, \ldots \underline{k}_n, \underline{k}'_1, \ldots \underline{k}'_m\right), \end{aligned} \tag{6.8}$$

and the G_{nm} are Pomeron "Greens functions" satisfying the unitarity equation

$$\begin{aligned} G_{nm}(E + i\epsilon, \underline{k}) - G_{nm}(E - i\epsilon, \underline{k}) = & \sum_r (-1)^r \int \left[\prod_s dE_s d^2\underline{k}_s \delta\left(E_s - \Delta_s\left(\underline{k}_s^2\right)\right)\right] \delta\left(E - \sum_{s=1}^{r} E_s\right) \\ & \times \delta\left(\underline{k} - \sum_{s=1}^{r} \underline{k}_s\right) G_{nr}(E + i\epsilon, \underline{k}) G_{rm}(E - i\epsilon, \underline{k}). \end{aligned} \tag{6.9}$$

The g_n are general couplings of n-Pomerons to the external particles. Equations (6.8) and (6.9) are illustrated in Figs. 6.2 and 6.3.

6.2 The RFT Graphical Expansion

It is straightforward to write a general solution to (6.9) in terms of a (non-relativistic)

Feynman graph expansion involving arbitrary non-singular (but momentum dependent) vertices. That is we take as inverse propagator

$$\Gamma^0_{1,1} = \left[E - \Delta(k^2)\right] = \left[E - \Delta_0 + \alpha'_0 \underline{k}^2 + \alpha''_0 \underline{k}^4 + \cdots\right], \tag{6.10}$$

where now $\Delta_0 = 1 - \alpha_{I\!P}(0)$. Therefore for $\Delta_0 > 0$, single Pomeron exchange gives total cross-sections going to zero (as $S^{-\Delta_0}$) and so gives a trivial high-energy S-Matrix (in the sense discussed in the introduction).

As three-point function (with the notation of Fig. 6.4) we take

$$\Gamma^0_{1,2} = i\left(r_0 + r_{01}\underline{k}_1^2 + r_{02}\underline{k}_2^2 + \tilde{r}_{01}E_1 + \cdots\right). \tag{6.11}$$

As four-point functions

$$\Gamma^0_{1,3} = \left(\lambda_0 + \lambda_{01}\underline{k}_1^2 + \lambda_{02}\underline{k}_2^2 + \tilde{\lambda}_{01}E_1 + \cdots\right) \tag{6.12}$$

$$\Gamma^0_{2,2} = \left(\lambda'_0 + \lambda'_{01}\underline{k}_1^2 + \cdots\right), \tag{6.13}$$

and so on. We write down the complete set of topologically distinct diagrams with a loop integration $\int dE\, d^2\underline{k}$ for each loop, together with momentum and energy conservation imposed at each vertex. The $\underline{k}$-integration is over the whole plane, while the E-integration can be taken to be down the imaginary axis. The factor of i in (6.11) (and all vertices for odd numbers of Pomerons) reproduces the $(-1)^r$ factor in (6.9) when the usual Feynman graph cutting rules are applied.

A lagrangian can be written in terms of fields which are functions of conjugate variables to E and $\underline{k}$. $\bar{\psi}(\underset{\sim}{x}, y)$ and $\psi(\underset{\sim}{x}, y)$ are respectively Pomeron creation and destruction operators with $\underset{\sim}{x}$ the impact parameter conjugate to $\underline{k}$ and y the rapidity ($\sim \ln s \sim \ln z$) conjugate to E. In this case

$$\begin{aligned}\mathcal{L}(\bar{\psi}, \psi) = {} & \frac{1}{2} i \bar{\psi} \overleftrightarrow{\frac{\partial}{\partial y}} \psi - \alpha'_0 \nabla\bar{\psi} \cdot \nabla\psi - \Delta_0 \bar{\psi}\psi - \alpha''_0 \nabla^2\bar{\psi} \cdot \nabla^2\psi \\ & \cdots + \frac{-i}{2}\left[r_0\bar{\psi}^2\psi + r_0\bar{\psi}\psi^2 + r_{01}\bar{\psi}\psi\nabla^2\psi + \cdots\right] \\ & + \frac{1}{6}\left[\lambda_0\bar{\psi}^3\psi + \lambda_0\bar{\psi}\psi^3 + \cdots\right] + \cdots.\end{aligned} \tag{6.14}$$

6.3 The Renormalization Group

Next we discuss the implementation of a Wilson renormalization group transformation on the effective Lagrangian (6.14). This transformation can be formulated in a variety of ways. The most direct, in our opinion, is to integrate out regions of energy and momenta in the Feynman graphs generated by (6.10)-(6.13). (For this purpose it will be preferable to bend the E-contours away from the imaginary axis as illustrated in Fig. 6.5). The most sophisticated view of the RFT that we have written for the Pomeron is perhaps to suppose that we can write a complete effective lagrangian involving all hadronic Regge poles such that all reggeon unitarity equations are satisfied. In the neighborhood of $j = 1$, $t = 0$ (i.e. $E \sim \underline{k}^2 \sim 0$) only the Pomeron trajectory is *relevant* and so integrating out all $|E| \geq \mu$, say, and also all $|k^2| \geq \mu$ will (for μ sufficiently small) lead to an effective field theory for Pomerons only, with a cut-off μ in the Feynman graphs.

We can specifically illustrate the renormalization group transformation $\mu \to \mu/2$ by considering the three-Pomeron graphs of Fig. 6.6. Integrating over E and $\underline{k}$ in the region $\mu > |E|$, $|\underline{k}^2| > \mu/2$ and expanding the result as a Taylor series in E_1, $\underline{k}_1$, E_2, $\underline{k}_2$ gives $r_0(\mu) \to r_0(\mu/2)$ through

$$\begin{aligned} r_0(\mu) - r_0^3(\mu) \int_{\substack{\mu > |E|, \\ |\underline{k}^2| \geq \mu/2}} dE\, d^2\underline{k} \frac{1}{[E - \Delta(\underline{k}^2)]} \frac{1}{[E + E_1 - \Delta((\underline{k} + \underline{k}_1)^2)]} \\ \frac{1}{\left[E_2 - E - \Delta\left((\underline{k}_2 - \underline{k})^2\right)\right]} + \cdots \\ = r_0\left(\frac{\mu}{2}\right) + r_{01}\left(\frac{\mu}{2}\right) k_1^2 + \cdots . \end{aligned} \tag{6.15}$$

The complete transformation is defined by carrying out this procedure on all graphs.

If we carry out a general transformation $\mu \to \mu/\zeta$ and then rescale E and $\underline{k}$ by

$$E \to \zeta E, \quad \underline{k}^2 \to \zeta \underline{k}^2, \tag{6.16}$$

the cut-off in the Feynman graph expansion remains formally unchanged. However, each parameter g in the lagrangian (6.14) will change by

$$g \to \zeta^{\nu_g} g + g', \tag{6.17}$$

where ν_g is the canonical dimension of g and g' depends on all the other parameters of the lagrangian. The original values of parameters with $\nu_g < 0$ will be completely suppressed after a sequence of such transformations. Therefore if a *fixed-point* in parameter space is approached by such a process the bare parameters with $\nu_g < 0$ must be "irrelevant" (in Wilson's terminology) to the existence of the fixed-point. Consequently we can look for a fixed-point by keeping only those parameters with positive canonical dimension. In our case we have

$$\nu_{\Delta_0} = 1, \quad \nu_{r_0} = \frac{1}{2} \quad \nu_{\alpha'_0} = 0, \ldots . \tag{6.18}$$

6.4 The Critical Pomeron

By expanding the theory in powers of $\epsilon = 4 - D$, where D is the number of transverse dimensions, we can show that there is indeed a fixed-point at finite values of r and Δ (the renormalized values of r_0 and Δ_0), that is at

$$r^2 = \frac{4\pi^2}{3}\epsilon, \quad \Delta = 0 \, (\equiv \alpha_{I\!P}(0) = 1) \, . \tag{6.19}$$

Assuming this fixed-point persists to $\epsilon = 2$, the corresponding theory describes an interacting Pomeron satisfying (6.1) and so potentially gives the *non-trivial* theory that we are looking for. The theory has the "universality" property familiar from critical phenomenon behavior in phase-transition theory and thus is referred to as the *Critical Pomeron.* In this case universality implies that the asymptotic predictions of the theory can be calculated without knowledge of the initial bare parameters of the lagrangian (6.14), *except that* $\Delta = 0$ *must be satisfied.* Δ is analogous to temperature (or renormalized mass) in this context. Given that $\Delta = 0$ the β-function for r can be calculated and this shows that the fixed-point is indeed "infra-red stable" as illustrated in Fig. 6.7, so that the theory is driven to this point in the "infra-red" region $E \sim \underline{k}^2 \sim 0$. To calculate specific properties of the resulting critical theory it is simpler to use the Gellmann-Low form of the renormalization group applied to the theory containing only the relevant parameters.

6.5 Renormalization Group Analysis

We study the triple Pomeron theory with bare lagrangian

$$\mathcal{L}_R = \frac{1}{2}\bar{\psi} \overleftrightarrow{\frac{\partial}{\partial y}} \psi - \alpha'_0 \nabla\bar{\psi}\nabla\psi - \Delta_0\bar{\psi}\psi - \frac{1}{2} i r_0 \left[\bar{\psi}\psi^2 + \bar{\psi}^2\psi\right], \tag{6.20}$$

and renormalized lagrangian

$$\mathcal{L}_R = \frac{1}{2} z_3 \bar{\psi} \overleftrightarrow{\frac{\partial}{\partial y}} \psi - z_3 z_2 \alpha' \nabla\bar{\psi}\nabla\psi - z_3 \Delta\bar{\psi}\psi - \frac{1}{2} i z_1 r \left[\bar{\psi}\psi^2 + \bar{\psi}^2\psi\right], \tag{6.21}$$

corresponding to the renormalizations

$$\psi = z_3^{-1/2}\psi_0 \tag{6.22}$$

$$\alpha' = z_2^{-1}\alpha_0' \tag{6.23}$$

and

$$r = z_3^{3/2} z_1^{-1} r_0. \tag{6.24}$$

The renormalization constants are determined by normalization conditions,the most straightforward being

$$\left.\frac{\partial i\Gamma^R_{(1,1)}}{\partial E}\right|_{E=-E_{t'},\underline{k}^2=0} = 1 \tag{6.25}$$

$$\left.\frac{\partial i\Gamma^R_{(1,1)}}{\partial \underline{k}^2}\right|_{E=-E_N,\underline{k}^2=0} = -\alpha' \tag{6.26}$$

$$\Gamma^R_{(1,2)}\Big|_{E_1=2E_2=2E_3=-E_N,\ \underline{k}_i=0} = \frac{r}{(2\pi)^{\frac{5-\epsilon}{2}}}. \tag{6.27}$$

In general we should also impose $\Delta = 0$, which is equivalent to

$$\Gamma^R_{(1,1)}\Big|_{E=\underline{k}^2=0} = 0. \tag{6.28}$$

In practice, however, computations are made by combining the ϵ-expansion with perturbation theory. Within the ϵ-expansion setting $\Delta_0 = 0$ is sufficient to impose $\Delta = 0$ and so satisfy (6.28) automatically. (6.25)–(6.27) are then simply equations for z_1, z_2 and z_3. Note that a general Green's function satisfies

$$\Gamma^R_{(n,m)}\left(E_i, \underline{k}_i, r, \alpha'\right) = z_3^{(n+m)/2}\Gamma_{(n,m)}\left(E_i, \underline{k}_i, r_0, \alpha_0'\right). \tag{6.29}$$

The independence of E_N of the bare Greens functions leads to the renormalization group equation

$$\left[E_N\frac{\partial}{\partial E_N} + \beta(g)\frac{\partial}{\partial g} + \zeta(g,\alpha')\frac{\partial}{\partial \alpha'} - \frac{1}{2}(n+m)\gamma(g)\right]\Gamma^R_{(m,n)}\left(E_i, \underline{k}_i, g, \alpha', E_N\right) = 0, \tag{6.30}$$

where g is the dimensionless coupling

$$g(E_N) = \frac{r(E_N)}{[\alpha'(E_N)]^{1-\frac{\epsilon}{4}}} E_N^{-\frac{\epsilon}{4}}, \tag{6.31}$$

with γ, β and ζ defined by

$$\gamma(g) = E_N \frac{\partial}{\partial E_N} \ln z_3(\alpha_0', r_0, E_N)\Big|_{\alpha_0', r_0 \text{ fixed}} \tag{6.32}$$

$$\beta(g) = E_N \frac{\partial g}{\partial E_N}\Big|_{\alpha_0', r_0 \text{ fixed}} \tag{6.33}$$

$$\zeta(g) = E_N \frac{\partial \alpha'(E_N)}{\partial E_N}\Big|_{\alpha_0', r_0 \text{ fixed}}. \tag{6.34}$$

The well-known solution to Eq. (6.30) is

$$\begin{aligned}\Gamma^R_{(n,m)}(\xi E_i, \underline{k}_i, g, \alpha', E_N) = \Gamma^R_{(n,m)}(E_i, \underline{k}_i, \bar{g}(-t), \bar{\alpha}'(-t), E_N) \\ \times \exp \int_{-t'}^{0} dt' \left[1 - \frac{1}{2}(n+m)\gamma(\bar{g}(t'))\right],\end{aligned} \tag{6.35}$$

where $t = \ln \xi$

$$\frac{d\bar{g}}{dt} = -\beta(\bar{g}(t)), \qquad \bar{g}(0) = g, \tag{6.36}$$

$$\frac{d\bar{\alpha}'(t)}{dt} = \bar{\alpha}'(t) - \zeta(\bar{\alpha}'(t), g(t)), \quad \bar{\alpha}'(0) = \alpha'. \tag{6.37}$$

(6.35) provides the most simple scaling laws for the Critical Pomeron. Within the ϵ-expansion

$$\beta = -\frac{\epsilon g}{4} + \frac{6g^3}{4(8\pi)^2} + \cdots \tag{6.38}$$

$$\zeta = -\frac{\alpha' g^2}{4(8\pi)^2} + \cdots \tag{6.39}$$

$$\gamma = -\frac{g^2}{2(8\pi)^2} + \cdots, \tag{6.40}$$

and so we find the fixed-point (6.19) of β. For $\Gamma^R_{(1,1)}$, (6.35) implies that

$$\Gamma^R_{1,1}(\xi E, \underline{k}, g_1 \alpha', E_N) = \xi^{1-\gamma(g_1)} \Gamma^R_{(1,1)}\left(E, \underline{k}, g, \alpha \xi^{-z(g_q)}, E_N\right), \tag{6.41}$$

where $g = g_1$ is the fixed-point zero of β and $z = 1 - \zeta/\bar{\alpha}'$. Setting $k^2 = 0$ gives directly

$$\Gamma^R_{(1,1)}(E, \underline{k}^2 = 0) \underset{E \to 0}{\sim} E^{1-\gamma(g_1)}, \tag{6.42}$$

giving the well-known Critical Pomeron result[15,16] for the total cross-section

$$\sigma_T \underset{s \to \infty}{\sim} [\ln s]^\eta, \tag{6.43}$$

where

$$\eta = -\gamma\left(g_1^2\right) = \frac{\epsilon}{12} + O(\epsilon^2). \tag{6.44}$$

Since $\eta > 0$ the Critical Pomeron theory is indeed *non-trivial.* Much more elaborate scaling properties can be derived by adopting more general renormalization conditions than (6.25)–(6.27) so that a transverse momentum scale $\underline{k}_N$ is introduced in addition to the energy scale E_N. A line-integral representation of $\Gamma_{(1,1)}$ of the form[42]

$$\Gamma_{(1,1)}(E, \underline{k}^2) = \int d\sigma \left[\partial\Gamma_{(1,1)} \frac{\partial E}{\partial \sigma} + \frac{\partial \Gamma_{(1,1)}}{\partial \underline{k}^2} \frac{\partial \underline{k}^2}{\partial E}\right] \tag{6.45}$$

can be combined with the more general scaling forms obtained and the ϵ-expansion to give[43] (to lowest order in ϵ)

$$\begin{aligned} \Gamma_{(1,1)}\left(E, \underline{k}^2\right) = \frac{i}{1+\epsilon/12} (-E)^{1+\epsilon/12} \left[\frac{(8\pi)^2\epsilon}{24}\right] \left[\frac{2\left(\alpha_0'\right)^{1-\epsilon/4}}{r_0}\right]^{1/3} \\ \times \left[1 + \eta\left(1 + \frac{\epsilon}{24}\right)\right] \left[1 + \frac{\eta}{2}\right]^{\epsilon/12}, \end{aligned} \tag{6.46}$$

where η is given implicitly by

$$\frac{\alpha_0' \underline{k}^2}{(-E)^{1+\epsilon/24}} = \left[\frac{(8\pi)^2\epsilon}{24}\right]^{1/12} \left[\frac{2(\alpha_0')^{1-\epsilon/4}}{r_0}\right]^{1/6} \eta\,(1 + \eta/2)^{\epsilon/24}. \tag{6.47}$$

The general scaling law

$$\frac{d\sigma}{dt} \sim (\ln s)^{\epsilon/6} F^2\left(-\frac{\alpha_0' t [\ln s]^{1+\epsilon/24}}{K}\right) \tag{6.48}$$

is then obtained with F given explicitly by

$$F(x) = x^{(-\epsilon/12)/(1+\epsilon/24)}\Gamma(1+\epsilon/12)$$
$$\times \int_{-i\infty}^{+i\infty} \frac{dw\, e^{-wx^{1/(1+\epsilon/24)}}\,[1+\bar{\eta}/2]^{-\epsilon/12}}{(-w)^{1+\epsilon/12}\,[1+\bar{\eta}(1+\epsilon/24)]^2\,\pi i}, \tag{6.49}$$

with

$$\bar{\eta}(1+\bar{\eta}/2)^{\epsilon/24} = (-w)^{-1-\epsilon/24}, \tag{6.50}$$

and

$$K = \left[\frac{(8\pi)^2\epsilon(\alpha_0')^{(2-\epsilon/2)}}{6r_0^2}\right]^{1/12}.$$

(6.48) gives the diffraction peak shown in Fig. 6.8, which is not that far from the data[44] at ISR energies. Unfortunately the $O(\epsilon^2)$ calculations do not improve the agreement.[45] At the higher collider energies of the CERN $S\bar{p}pS$ and the Fermilab Tevatron collider there are apparently far greater deviations from Critical Pomeron behavior.[46]

Apart from the rising total cross-section and diffraction peak scaling given by (6.43) and (6.48) respectively, other well-known scaling properties of the Critical Pomeron are the rising and peaking of the central plateau

$$\frac{d\sigma}{dy} \sim \left(\frac{1}{2}\ln s - y\right)^{\eta}\left(\frac{1}{2}\ln s + y\right)^{\eta}, \tag{6.51}$$

and also central region KNO scaling of the multiplicity moments

$$\langle n^p\rangle \sim C_p\langle n\rangle^{\eta p}. \tag{6.52}$$

We shall not, however, attempt a comprehensive review of Critical Pomeron scaling properties here, even though a suitable review does not exist in the literature. Further references can be found in Refs. 47 and 48.

In a sense the Critical Pomeron is the summit of Multi-Regge theory and abstract Pomeron theory. The Reggeon Unitarity equations derived in the last Section are essentially sufficient to determine the Reggeon Field Theory rules for all multi-Regge regions directly related to measurable physical cross-sections. This is illustrated for high-mass diffractive production in Ref. 49 where the triple-Regge RFT rules are derived. The same rules are

directly derived from "hybrid" Feynman graphs in Ref. 43 and the triple Pomeron analogue of (6.48) is calculated. In general we anticipate that the RFT formulation of the Critical Pomeron, when combined with Reggeon Unitarity, provides a complete *non-trivial* high-energy S-Matrix as we claimed in the Introduction.

Although all Critical Pomeron Greens Functions have scaling behavior at (or close to) zero momentum transfer, it is straightforward to show that a simple Pomeron pole and multi-Pomeron cuts emerge for positive momentum transfer[42]. This ensures that Reggeon Unitarity, and therefore full multiparticle cross-channel unitarity, is satisfied by the Critical theory. It has also been shown[50,51] that the Critical Pomeron satisfies all known direct channel unitarity constraints. From the above analysis it might appear that theory can only be calculated in the $\epsilon-$ expansion (which is presumably not a very good approximation at $\epsilon = 2$). However, while this is true as a matter of practise at present, it certainly is not true in principle. In particular it has been shown[52] that a phase-transition is indeed present in the physical number of dimensions.

Since the Critical Pomeron is completely formulated and is (in principle) absolutely calculable without reference to any underlying theory it clearly provides a uniquely attractive possibility for the high-energy behavior of hadron amplitudes. At present it is also the *only* known unitary possibility. As we emphasised in the last Section it is very likely that Reggeon Unitarity requires that high-energy behavior be built up from Regge poles. That it involve a single Pomeron pole only might (as we discuss in Part 2) be a deeper requirement of QCD and the strong interaction.

In determining the significance of the Critical Pomeron phase- transition within QCD an important part of our understanding will come from the properties of the Critical Pomeron interaction with secondary Regge trajectories.

6.6 The Critical Pomeron and Secondary Regge Trajectories

From (5.42) we note that the Regge cut $\alpha_{R\mathbb{M}^{\mathbb{P}}}(t)$ due to one distinct reggeon and M-Pomerons has the intercept

$$\alpha_{R\mathbb{M}^{\mathbb{P}}}(0) = \alpha_R(0) + M\left(\alpha_{\mathbb{P}}(0) - 1\right) \tag{6.53}$$

and so when $\alpha_{\mathbb{P}}(0) = 1$ we have also

$$\alpha_{R\mathbb{M}^{\mathbb{P}}}(0) = \alpha_R(0). \tag{6.54}$$

That is the RMIPcuts all collide with the R trajectory at $t = 0$ in close similarity to the collision of IPcuts and pole illustrated in Fig. 6.1.

The renormalization group has been used to study the RMIPcollision with both a "boson" Regge pole with "bare" trajectory[53]

$$j = \alpha_0 + \alpha' t + \cdots, \tag{6.55}$$

and[54] with a "fermion" with "bare" trajectory

$$j = \alpha_0 + \beta' \sqrt{t} + \alpha' t + \cdots. \tag{6.56}$$

In both cases fixed-points were found giving scaling behavior similar to (6.42) (or (6.46)) for the reggeon propagator. In the case of the fermion (6.56) the inverse propagator is argued to have the form

$$\Gamma^F_{(1,1)}(\mathcal{E}, \underline{k}^2) \sim \mathcal{E}^{-1-\eta} \left[\phi_1(z) + \sqrt{z}\phi_2(z)\right], \tag{6.57}$$

where $z = k^2/\mathcal{E}^{1+\nu}$ and $\mathcal{E} = E - \left(1 - \alpha_0^F\right)$, with α_0^F the renormalized fermion intercept. The form (6.57) arises only if an appropriate fixed-point exists. Such a fixed-point does exist in the ϵ-expansion but it is only partially infra-red stable.

The inverse propagator (6.57) has some very interesting properties. First the renormalized trajectory has the form

$$\mathcal{E} = C(k^2)^{1/\nu} + \cdots, \tag{6.58}$$

where C is determined by a zero of $[\phi_1(z) + \sqrt{z}\phi_2(z)]$. This is the same analytic form as the Pomeron trajectory (although the coefficient C is not the same) and, since $\nu \sim 1$ in the ϵ-expansion, can be expected to give an almost linear trajectory. Secondly, since the sign of $\sqrt{z}$ in (6.57) is determined by the parity of the fermion trajectory, it can be shown[54] that (6.57) actually describes a parity doublet of trajectories for $t = -k^2 < 0$ while for $t > 0$ only one parity trajectory is present on the physical sheet of the $\mathcal{E}$-plane.

Although (6.57) has been developed to describe fermion trajectories it could also describe parity-doublet boson trajectories with only one parity present for positive t (where particles are generated). There have in fact been phenomenological arguments[55] that the pion trajectory should be parity-doubled for negative t. Note that for a pion with $m_\pi^2 = 0$,

the RMIPpile-up described by (6.54) actually takes place at the particle pole, i.e. $t = m_\pi^2 = 0$. Consequently the $t = 0$ singularities, of Regge residue functions etc., related to the Critical Pomeron behavior are very likely to be inter-related with the (Adler) zeroes of pion scattering amplitudes. In fact before the advent of QCD there was much discussion[56] of how the $t = 0$ behavior of Regge amplitudes might be deeply connected to the PCAC structure of pion amplitudes. We are here adding the extra suggestion that the Critical Pomeron should also be part of the physical solution. Of course, the whole subject has been barely discussed in the context of QCD. We shall return to the inter-relation of chiral symmetry breaking and the Critical Pomeron in QCD in the second part of this article.

For the next Section the most important result of the secondary trajectory analysis is that the Critical Pomeron interactions dominate the "bare" reggeon so completely that even the nature (parity in particular) of the particle states on the trajectory is basically modified. In attempting to define a Super-Critical Pomeron, as we shall do, it will be vital to take into account the Pomeron component of the particle states.

6.7 RFT From Hexagraph Products

The above construction of RFT was completely abstract with no physical properties ascribed to the individual graphs. We shall now outline two further constructions—the first making contact with the multiple discontinuity hexagraph structure of amplitudes discussed in previous Sections. The final construction will be completely phenomenological.

Our purpose now is to view the RFT perturbation theory graphs as built up by a process of "sewing" hexagraph amplitudes together. For this it is necessary to rewrite all graphs in the time-ordered (that is rapidity-ordered in this context) Rayleigh-Schrodinger form. This is achieved by performing all energy loop integrations. The resulting expansion can be represented by the set of distinct hexagraph loops which are obtained by joining all hexagraph tree diagrams together in all possible ways. If the rapidity-ordering of the vertices in any graph is ambiguous (the rapidity-axis is thought of as increasing along the horizontal lines of the hexagraph) distinct orderings define distinct graphs. The g_n must also be represented by generalized hexagraph vertices as illustrated in Fig. 6.9 and if vertices other than the triple Pomeron vertex are to be present corresponding new hexagraph vertices must also be introduced. The hexagraph loop expansion for the elastic scattering amplitude involving only triple Pomeron vertices is illustrated in Fig. 6.10.

The amplitude for a particular hexagraph loop diagram is obtained by first allowing

transverse momenta to flow along all internal lines (with momentum conservation at each vertex) and writing $\int d^2\underline{k}$ for each loop. A propagator is then written for each intermediate state, which in this case is each distinct set of horizontal lines cut by a single vertical line—as illustrated in Fig. 6.11. The corresponding propagator is

$$\left[E - \sum_i \Delta\left(\underline{k}_i^2\right)\right]^{-1}, \tag{6.59}$$

where the sum is over the horizontal lines involved. The vertices are now functions of the transverse momenta only.

In the rapidity-ordered formulation the propagators (6.59) correspond directly to the nonsense fixed-pole factor $[\ell - 1 - \sum(\alpha_k - 1)]^{-1}$ appearing in the discontinuity formula (5.40). Consequently the RFT expansion can be thought of as resulting from the iteration of (5.40) beginning with a Regge-pole approximation for the $N_{\underset{\sim}{\alpha}}^{\tau\tau}$. Since we know precisely how "s-channel" discontinuities of hexagraph amplitudes are taken it is clear that building up graphs in this manner, in principal at least, allows us to explicitly discuss the s-channel discontinuity content of general RFT graphs. For the even signature Pomeron the dropping of signature factors through (6.2) implies that taking discontinuities involves only the removal (or changing sign) of factors of i in vertices. Before giving the *rules for "cut RFT"* which make this explicit we first discuss a very simple physical motivation for RFT in terms of multiparticle production processes. This physical picture underlay most physicists' understanding of RFT during the years of its development.[57,58]

6.8 RFT as an Effective Field Theory of Multiplicity Fluctuations

We suppose that in first approximation all hadrons are produced by an elementary process. That is the particles of an average multiplicity event are uniformly spread across the rapidity axis (apart from short-range fluctuations) and with a sharp cut-off (exponential) in transverse momentum. A multiperiphal model for pion production, or ladder diagrams in $\lambda\phi^3$ scalar field theory, would be good realizations of such a production process. In fact the representation of the production process as in Fig. 6.12 can be thought of either as representing the actual (multiperipheral) amplitude or as representing the distribution of particles on the rapidity-axis. When elastic scattering is calculated through unitarity as indicated in Fig. 6.13 the output will be a shrinking diffraction peak—that is a Regge pole,

with trajectory $\alpha_{I\!P}(t)$ say. We shall assume that events with close to the average multiplicity are well-reproduced by this production process.

We next assume that events with close to twice the average multiplicity can similarly be represented by the same production process doubled up on the rapidity axis as illustrated in Fig. 6.14. If the basic process produces Regge pole behavior

$$A(s,t) \sim S^{\alpha_{I\!P}(t)}, \tag{6.60}$$

then the "doubled-up" process will give two Pomeron Regge cut behavior, that is

$$A(s,t) \sim \frac{S^{2\alpha_{I\!P}(t)-1}}{\ln s}. \tag{6.61}$$

Similarly we assume that events with three times the average multiplicity are well represented by three Pomerons and so on. (These assumptions are realized in suitably transverse-momentum cut-off field-theoretic models.)

If we move on to discuss events with distinct multiplicity densities on distinct portions of the rapidity-axis we will generate more complicated RFT graphs as illustrated in Fig. 6.15. In general then each N-Pomeron intermediate state corresponds to a multiplicity density of N-times the average multiplicity on the corresponding portion of the rapidity-axis. However, because of the different possibilities for taking discontinuities in underlying Feynman graphs (or because of the possible discontinuities through a hexagraph—in the hexagraph construction discussed above) each RFT graph also represents a variety of processes besides the basic multiplicity fluctuation that we have so far associated with it.

The complete set of physical processes associated with a particular RFT graph corresponds to the possible discontinuities of the graph. These are the allowable cuts through the associated hexagraph loop diagram—with the *additional possibility* that a cut entering a vertex through a horizontal line can *exit simultaneously* through both slanting lines as illustrated in Fig. 6.16 *if these lines are part of a hexagraph loop.* This is because the formation of loops allows *distinct cuts in a hexagraph tree diagram to coincide as a single cut of a loop amplitude.* The basic multiplicity fluctuation interpretation of an RFT graph described above corresponds to cutting all Pomerons in the graph. In general uncut Pomerons represent the absorption of some basic production process as illustrated in Fig. 6.17.

The complete set of cut RFT graphs, with the AGK cutting rules[57] incorporated, is described[59] by the "cut Reggeon Field Theory" (CRFT). This involves both cut and uncut

propagators, with the uncut propagators given both $+i\epsilon$ and $-i\epsilon$ prescription. That is we have propagators

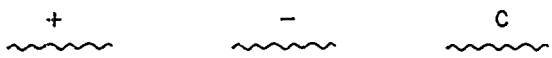

(6.62)

and vertices

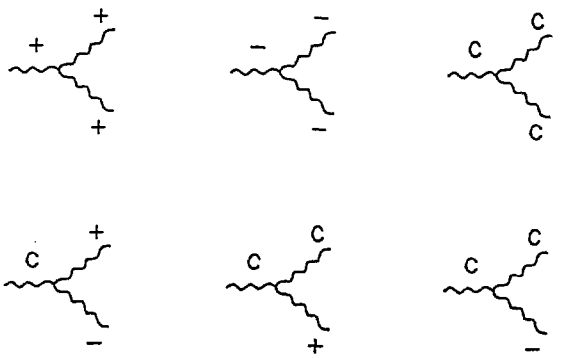

(6.63)

The corresponding lagrangian involves three Pomeron creation operators $\bar{\psi}_+$, $\bar{\psi}_-$, $\bar{\psi}_c$ and three destruction operators ψ_+, ψ_-, ψ_c and has the form

$$\begin{aligned}\mathcal{L} =& \mathcal{L}_+^0 + \mathcal{L}_-^0 + \mathcal{L}_c^0 + \frac{ir_0}{2}\left(\bar{\psi}_+\psi_+^2 + \bar{\psi}_+^2\psi_+\right) - \frac{ir_0}{2}\left(\bar{\psi}_-\psi_-^2 + \bar{\psi}_-^2\psi_-\right) \\ &+ \frac{r_0}{\sqrt{2}}\left(\bar{\psi}_c\psi_c^2 + \bar{\psi}_c^2\psi_c\right) + \frac{r_0}{\sqrt{2}}\left(\bar{\psi}_c\psi_+\psi_- + \psi_c\bar{\psi}_+\bar{\psi}_-\right) \\ &+ \frac{ir_0}{2}\left(\bar{\psi}_c\psi_c\psi_+ + \psi_c\bar{\psi}_c\bar{\psi}_+\right) - \frac{ir_0}{2}\left(\bar{\psi}_c\psi_c\psi_- + \psi_c\bar{\psi}_c\bar{\psi}_-\right),\end{aligned} \tag{6.64}$$

with each of the free terms $\mathcal{L}_+^0$, $\mathcal{L}_-^0$ and $\mathcal{L}_c^0$ the same as in (6.14) or (6.20). The lagrangian $\mathcal{L}_c$ generates the full set of discontinuities of all RFT graphs and allows at least the formal s-channel unitarity properties of the theory to be discussed.

If $\alpha_{I\!P}(0) < 1$, that is $\Delta_0 > 0$, the interaction graphs will not significantly disturb the multiplicity distribution given by the "non-enhanced" graphs of the form Fig. 6.13, Fig. 6.14 etc. and the full multiplicity distribution will look as illustrated in Fig. 6.18 with peaks at the average multiplicity, twice the average multiplicity etc. As Δ_0 approaches Δ_{0c}, the bare-value giving the $\Delta = 0$ Critical Pomeron, the peaks in the multiplicity distribution

merge to give a KNO distribution satisfying (6.52). Consequently the Critical Pomeron can be understood as a critical phenomenom of multiplicity fluctuations producing KNO scaling. We shall come back to this interpretation in the second part of this article.

7. THE SUPER-CRITICAL POMERON

In this Section, we address the question of what could be the new phase approached as the Pomeron becomes Critical. This question was first asked before QCD was accepted as the underlying strong interaction theory and so at that time it was very unclear that a Pomeron with $\Delta_0 \ll 0$ could or should make any sense, since this corresponds to (a first approximation with) total cross-sections *increasing* like $S^{-\Delta_0}$. At the time there was no conception of a new hadronic phase that might be reached in a Pomeron phase transition. Now, of course, we understand that QCD has more than one distinct phase and it is clearly plausible that the Critical Pomeron is related to one of the anticipated phase-transitions. In this case we should be able to identify a Super-Critical phase with distinct properties.

7.1 Classical Vacua for $\Delta_0 < \Delta_{0C}$

The effective RFT lagrangian near the Critical Pomeron fixed-point is the simple triple Pomeron theory with the lagrangian (6.20). For $\Delta_0 \gg 0$, the perturbation expansion described in the last Section defines the theory. It is a super-renormalizable theory and so the perturbation expansion is expected to be Borel summable. The critical behavior occurs at some $\Delta_0 = \Delta_{0C}$ and it can be shown that without a transverse momentum cut-off $\Delta_{0C} = -\infty$. With a cut-off we have[42]

$$\Delta_{0C} = \frac{r_0^2}{\alpha_0'} \ln \frac{r_0^2}{\alpha_0' \Lambda_\perp} + 0(r_0^2) \quad < 0. \tag{7.1}$$

To define a (cut-off) theory with $\Delta_0 \ll \Delta_{0C}$, we can look for a classical field configuration minimizing the "potential"

$$V(\bar{\psi}, \psi) = \Delta_0 \bar{\psi}\psi + \frac{ir_0}{2}(\bar{\psi}^2\psi + \bar{\psi}\psi^2). \tag{7.2}$$

Imposing

$$\frac{\partial V}{\partial \bar{\psi}} = \frac{\partial V}{\partial \psi} = 0, \tag{7.3}$$

we immediately find four stationary points, that is

$$\text{I} \qquad \psi = \bar{\psi} = 0 \tag{7.4}$$

$$\text{II} \qquad \psi = 0, \bar{\psi} = \frac{2i\Delta_0}{r_0} \tag{7.5}$$

$$\text{III} \qquad \psi = \frac{2i\Delta_0}{r_0}, \bar{\psi} = 0 \tag{7.6}$$

$$\text{IV} \qquad \psi = \bar{\psi} = \frac{2i\Delta_0}{3r_0}. \tag{7.7}$$

I is, of course, the "vacuum" used to define the original perturbation expansion giving the subcritical theory. The asymmetry of II and III with respect to $\bar{\psi} \leftrightarrow \psi$ implies that the perturbative theory developed around either of these points breaks Lorentz invariance and so does not give an acceptable theory. IV seems therefore to be the obvious choice to use to define a new theory. Shifting each of ψ and $\bar{\psi}$ by (7.7) and dropping a constant leads to

$$\tilde{V}(\bar{\psi}, \psi) = \frac{-\Delta_0}{3}\bar{\psi}\psi - \frac{\Delta_0}{3}\bar{\psi}^2 - \frac{\Delta_0}{3}\psi^2 + \frac{ir_0}{2}(\bar{\psi}^2\psi + \bar{\psi}\psi^2) \tag{7.8}$$

This has reversed the sign of the intercept (or "mass") term and so potentially gives a sensible theory for $\Delta_0 \ll 0$. However, (7.8) also contains the two source terms $\frac{-\Delta_0}{3}\bar{\psi}^2$ and $-\frac{\Delta_0}{3}\psi^2$, and previously this has always led[30] to the rejection of this theory. The path-integral which, formally at least, represents the theory defined by (7.8) is not well-defined because of the source terms. The problem can be seen to arise diagrammatically if we consider the perturbation expansion in powers of r_0. This requires the summation of an infinite series involving the source terms at each order. Consider in particular the series of Fig. 7.1 in zero transverse dimensions. We obtain

$$\sum_{n=0}^{\infty} \frac{1}{(E + \frac{\Delta_0}{3})} \left[\frac{-\Delta_0^2}{(3E - \Delta_0)(3E + \Delta_0)}\right]^n = \left[\frac{E - \frac{\Delta_0}{3}}{E^2}\right] \tag{7.9}$$

and so instead of having a Pomeron pole with intercept less than one, we have a *double-pole with intercept one.* This problems persists in two transverse momentum dimensions *if the diagrams of Fig. 7.1 are indeed present in the theory.*

In fact all previous attempts to define a Super-Critical Pomeron theory have been based on trying to combine II and III in some manner or utilizing classical "instanton" solutions linking I, II, and III. The expanding disc solution[19–21] , which certainly saturates the Froissart bound and may even violate it, is obtained by keeping I as the vacuum and

letting transitions to II and from III back to I contribute to scattering amplitudes. All of our previous efforts[24] to define a Super-Critical theory have been based on utilizing II as the vacuum on one half of the rapidity axis and III as the vacuum on the other half. We now believe that when the Super-Critical problem is properly formulated, it is clear that IV provides the correct answer and that the problematic graphs of Fig. 7.1 (and many others of a related form) do not in fact appear in the theory. The key to understanding this resolution of the problem is the multiparticle hexagraph formalism of previous Sections.

7.2 The Physical Significance of the Pomeron Vacuum

Our introduction of RFT in the last Section was as a diagrammatic solution of the reggeon unitarity equations. This provides a well-defined formulation which is effectively what emerges from all field-theoretic or string models generating the RFT directly. However, when we consider changing the "vacuum" in the formalism, we at first sight lose all control of the physical significance of the diagrams we are manipulating. It is particularly difficult to determine what the physical significance of the Pomeron source diagrams might be. Since it is these diagrams that cause the problems in our attempt to define a Super-Critical theory, understanding their physical significance is clearly crucial. In fact since the Pomeron is only defined by the scattering of hadrons, it would seem that the "Pomeron vacuum" can only be redefined by some underlying redefinition of hadron states. But this apparently takes us into the full problem of the hadronic vacuum which surely can not be discussed solely within the RFT formalism.

Fortunately, there is a sense in which we can bring the redefinition of a hadron, as the Pomeron becomes Critical, into our formalism and this will ultimately be sufficient to resolve the vacuum problems. We noted in Sect. 6.6 that all secondary (hadron) trajectories are significantly modified by Pomeron Regge cuts as the Pomeron becomes Critical. We shall now argue that it is this redefinition which gives a well-defined meaning to the set of Super-Critical Pomeron graphs associated with the new vacuum IV above.

We shall assume that as the Pomeron becomes Super-Critical, it is a good initial approximation to consider the new hadron reggeons as differing from the old simply by the presence of an infinite sum of Pomerons with zero energy and momentum as illustrated in Fig. 7.2 The relative weighting of the terms with different number of Pomerons is actually determined by the vacuum expectation value (VEV) IV. That is in terms of diagrams, the choice of a classical stationary point for the Pomeron VEV can be thought of as simply

achieving the cancellation of the vacuum production processes illustrated in Fig. 7.3. Requiring this cancellation determines therefore the relative weighting of $(N+1)$ to N Pomerons in a reggeon for all N and directly fixes the value of the VEV.

We now need to consider the scattering of the new reggeons via Pomeron graphs with the additional requirement that the *reggeons are forming bound-state particles.* This means that we must necessarily consider the complicated scattering process illustrated in Fig. 7.4 and to discuss bound-state formation by the reggeon we must consider the hexagraph structure of the amplitudes involved.

7.3 Hexagraph Analysis of the Scattering of Bound-States Formed by Regge Cuts

As discussed in Section 4 we can isolate a single partial-wave which satisfies straightforward Reggeon Unitarity equations by exploiting helicity-pole limits. Therefore we define each of the reggeon + Pomeron sum configurations in Fig. 7.4 by (physical) helicity-pole limits of the hexagraph amplitude defined by Fig. 4.11. From our description of the S-W representations of hexagraph amplitudes in Section 4 we also know that particle poles appear accompanying Regge pole behavior only for the appropriate multiple discontinuity structure. Consequently, if the scattering illustrated in Fig. 7.4 is to contain dynamically generated particle poles in each reggeon channel (by the reggeon plus zero-energy Pomeron sum), not only must it correspond to the hexagraph of Fig. 4.11, but in addition the *amplitude must contain a multiple discontinuity set which is consistent with* the presence of *particle poles* in each channel. The possible five-fold discontinuities are illustrated in Fig. 7.5. There are also discontinuity sets, analogous to those of Fig. 4.9d in the hexagraph of Fig. 2.5b, which are inconsistent with the presence of the desired particle poles and these are illustrated in Fig. 7.6.

Since we are considering the contribution of Pomeron Regge cuts in each hexagraph channel, we also know from Section 5 that the *Regge cut* discontinuities in each individual contribution to the sums of Fig. 7.4 can be described in terms of the fixed-pole residues of hexagraph amplitudes of the form shown in Fig. 7.7. Consequently, our task is to construct the general set of "RFT graphs" with Regge cut discontinuities of the form illustrated in Fig. 7.7, which also have momentum space discontinuities of the form of Fig. 7.5. This will give us the desired bound-state amplitudes of the form of Fig. 7.4.

To study the Super-Critical Pomeron therefore we are apparently faced with the major theoretical problem of constructing RFT graphs for a general multiparticle hexagraph. (This

goes beyond the problem of constructing RFT for physical cross-sections discussed in the last Section—for which we asserted Reggeon Unitarity is sufficient.) There is clearly no problem in formulating rules for the RFT graphs in which all Pomeron or reggeon/Pomeron interactions are confined to one hexagraph t-channel, that is graphs of the form of Fig. 7.8 which correspond directly to hexagraphs of the form of Fig. 7.7. The rules developed for a single t-channel, as described in the last Section, just apply ("multiplicatively") to each of the channels involved. In general, however, we can expect to have RFT graphs involving arbitrary numbers of Pomeron interactions and connecting the different t-channels. A simple graph of this form is shown in Fig. 7.9. New problems necessarily arise in formulating RFT rules for such graphs, as we now discuss.

An apparent problem occurs if we consider the Regge cuts corresponding to the dashed lines in Fig. 7.9. According to the above discussion each discontinuity should be expressible in the form given by (5.46) in terms of nonsense, fixed-pole, hexagraph amplitudes of the form illustrated in Fig. 7.7. The component amplitudes of Fig. 7.9 correspond to the hexagraphs shown in Fig. 7.10 which do not have the appropriate form. However, the multiple discontinuities of the graphs in Fig. 7.10 do actually coincide with particular sets contained in the appropriate hexagraphs, as illustrated in Fig. 7.11. Consequently, the graphs of Fig. 7.10 do indeed contain the necessary fixed-pole residues to give the Regge cuts picked out in Fig. 7.9 and in this particular case there is no problem. In other graphs discussed below, this problem will result in their elimination.

The second problem we encounter with Fig. 7.9 is that although we expect such a configuration to contribute to the Regge cuts shown, we can not find a natural way to express the graph in terms of transverse momentum integrals. We can not simultaneously replace all three Regge cut discontinuities by transverse momentum integrals, as we did for the complete single-channel reggeon unitarity equation in (6.8) and (6.9). The transverse momentum planes involved are distinct and so there is no natural way to let transverse momentum flow through Fig. 7.9. Fortunately we can determine the contribution of this graph to the reggeon scattering amplitude of Fig. 7.4 (involving zero energy and momentum Pomerons) by studying the forward amplitude related to the "Di-Triple Regge" inclusive cross-section[60,61], since this involves only a single transverse momentum plane, and the RFT rules for this cross-section are determined by straightforward extension of the arguments of Ref. 49. Indeed it is clear that if the Pomerons involved in the outer discontinuities of Fig. 7.9 carry zero energy and transverse momentum so that there is *no outer loop integrations*

then the graph has an unambiguous form as a single transverse momentum integral with the propagators illustrated in Fig. 7.12. Placing each of the external reggeon propagators $[E_1 - \Delta_R(t_1)]^{-1}$, $[E_2 - \Delta_R(t_2)]^{-1}$ on shell and summing over the rapidity orderings of the internal vertices gives an amplitude

$$\sim [E - \Delta_{I\!P}(t)]^{-2} \int d^2\underline{k}\, \frac{r_0^4}{[2\Delta_{I\!P}(\underline{k}^2)]^2} \frac{1}{[E - \Delta_{I\!P}(\underline{k}^2) - \Delta_{I\!P}(\underline{k} - \underline{q})^2]} \tag{7.10}$$

where $t = q^2$ and we have factored off Pomeron/reggeon and external particle vertices. If each of the zero energy Pomerons is weighted by the VEV of IV above, then we obtain exactly the Super-Critical graph of Fig. 7.13.

We can effectively construct the complete set of hexagraph loops contributing to the reggeon scattering of Fig. 7.4 in the same manner as for Fig. 7.12. A very important element of the procedure is that we are to construct amplitudes with the discontinuity structure of Fig. 7.5 only and reject those with discontinuities corresponding to Fig. 7.6. We must also ensure that all Regge cut contributions involve amplitudes with discontinuities consistent with the hexagraph structure of Fig. 7.7. These requirements make a very interesting selection of potential graphs if we construct discontinuities according to the CRFT rules of the last Section. For example, consider the graph of Fig. 7.14 which potentially generates a Super-Critical graph of the form of Fig. 7.1. Applying the cutting rules shows this contains only the cuts of Fig. 7.15, which are in fact of the form of Fig. 7.6, and so *this graph is rejected* since it does not contribute to an amplitude with the necessary bound-state poles.

Following the above analysis through in detail for a general graph, we find that all "desirable" graphs of the Super-Critical theory of IV above contribute to the relevant multiple discontinuities. The intercept is shifted by the set of graphs shown in Fig. 7.16 and the cancellation of Fig. 7.3 will take place if the reggeon states contain appropriately weighted numbers of Pomerons as discussed above. None of the graphs of Fig. 7.1 contributes, or graphs of the form Fig. 7.17, for example, which would produce similar problems if they did contribute. The full reggeon graphs generating the Super-Critical graphs of Fig. 7.17 (and all graphs with a related structure) are actually eliminated because the amplitudes that would give the necessary Regge cut discontinuities in the reggeon channels do not have the right (momentum-space) cut structure to contribute to the hexagraphs of Fig. 7.7. (Therefore such graphs do not generate the Regge cuts that they appear to and so are essentially meaningless.) We conclude that if we take the Super-Critical Pomeron to be defined by

reggeon scattering, then a consistent set of graphs is generated corresponding to the "new vacuum" of IV above. The vital point being that the actual source diagrams contributing are *only a subset of those naively generated* by the potential (7.8).

The lowest order Super-Critical graphs generated by reggeon scattering are shown in Fig. 7.18. Note that the graph of Fig. 7.19 is absent because the corresponding reggeon graph has only the discontinuity structure of Fig. 7.6. This last graph has always been present in our previous (unsuccessful) attempts at formulating the Super-Critical theory. There is no immediate problem (from the RFT viewpoint) caused by the presence of graphs of this form, but its absence follows straightforwardly from the present procedure. In fact the *absence* of this graph is the *key* to understanding the *reggeon unitarity*, that is intermediate reggeon state properties, of the Super-Critical theory. A problem we were never able to resolve satisfactorily in our previous approaches.

The one-loop graphs of Fig. 7.18 at first sight give a two-Pomeron discontinuity of the form illustrated in Fig. 7.20 with a new triple Pomeron vertex

$$-i\Gamma_{1,2}(k_1,k_2) = r_0 - \frac{\Delta_0 r_0}{2(\Delta_0 + 3\alpha_0' k_1^2)} - \frac{\Delta_0 r_0}{2(\Delta_0 + 3\alpha_0' k_2^2)} \tag{7.11}$$

$$= \frac{3\alpha_0' r_0}{2\Delta_0}(k_1^2 + k_2^2) + \cdots . \tag{7.12}$$

which therefore *vanishes* at zero transverse momentum. However, the unitarity product of Fig. 7.20 will include a "cross-product" of the form generated by Fig. 7.19 which is absent from Fig. 7.18. Therefore, this contribution must be subtracted from Fig. 7.20. But Fig. 7.19 can be written directly in the form

$$[E - \Delta_{\mathbb{P}}(t)]^{-2} \int d^2\underline{k}\, \frac{-r_0^4}{4\Delta(\underline{k}^2)\Delta\left((\underline{k}-\underline{q})^2\right)\left[E - \Delta(\underline{k}^2) - \Delta\left((\underline{k}-\underline{q})^2\right)\right]} \tag{7.13}$$

which is exactly the contribution to the Pomeron propagator of a two *vector* Regge pole state with propagator

$$\Gamma^V_{(1,1)}(E,\underline{k}^2) = \frac{1}{[E - \Delta(\underline{k}^2)]}\frac{1}{\Delta(\underline{k}^2)}. \tag{7.14}$$

The second factor is the particle-pole which is the small Δ approximation to the "signature factor" $[\sin\frac{\pi}{2}\Delta]^{-1}$ associated with an odd-signature reggeon in the discontinuity formula (5.46). Furthermore, since we must subtract the discontinuity due to (7.13) and it already

has a negative sign, we must add a *positive* two vector contribution to the reggeon unitarity equation. From (5.46) this is the *correct sign* for a two-reggeon cut contribution due to odd-signature reggeons. The full one-loop reggeon unitarity equation can therefore be represented as in Fig. 7.21.

If we consider arbitrary high-order graphs in the Super-Critical expansion, we also find new one/many Pomeron vertices having the form illustrated in Fig. 8.22. Again not all of the graphs necessary for reggeon unitarity, involving only Pomeron intermediate states, will be generated. It will therefore be necessary to add appropriate odd-signature contributions with the propagator (7.14). Although we have not demonstrated that this can be done completely consistently, to all orders, there are no obvious problems. (It is clearly important that only even numbers of odd-signature reggeons can contribute to an even-signature Pomeron amplitude.) In effect all of the divergences of the theory in rapidity (due to $\alpha_{I\!P}(0) > 1$) are absorbed into the momentum transfer dependent singularities of the vertices and the signature factor poles of the odd-signature reggeon.

We conclude that the Super-Critical Pomeron is characterized by the existence of a Pomeron condensate and the existence of a single odd-signature trajectory degenerate with that of the Pomeron. The odd-signature trajectory produces a vector particle with a mass given by

$$\Delta(\underline{k}^2) = 0 \quad \Rightarrow \quad \underline{k}^2 = M^2 = \Delta/\alpha' \tag{7.15}$$

Of course, if we wish to confirm that a candidate high-energy theory is in the Super-Critical Pomeron phase we should also confirm the structure of the triple Pomeron vertex (7.12) and the full structure of the vertices illustrated in Fig. 7.22. As we emphasized in the Introduction the intercept of the Pomeron is again below one in the Super-Critical phase and so as in the Sub-Critical phase the high-energy S-Matrix is "trivial" in the sense discussed in the Introduction—that is all cross-sections go asymptotically to zero. Note that the analysis of Ref. 30 should be readily adaptable to show that the Critical Scaling Laws develop consistently as the Critical Point is approached from either the Sub-Critical or the Super-Critical Phase.

8. SUMMARY

We have provided a general basis for the development of multi-Regge theory and the formulation of the Critical Pomeron as giving the only known *non-trivial* unitary high-energy S-Matrix. We emphasised the solution of angular momentum plane unitarity but noted that the Critical Pomeron has also been shown to satisfy all other derived unitarity constraints. The Critical point arises as cross-sections are increased to the maximum consistent with unitarity. Beyond this point the resultant high-energy divergences are absorbed into the particle singularities associated with the vector particle which emerges in the Super-Critical Phase. Therefore we have shown, in the abstract and without any reference to gauge theories, that when a theory (with equal particle and anti-particle cross-sections) is pushed beyond the unitarity limit the result is the "deconfinement" of a Reggeised vector particle. Our ultimate aim is to be able to claim that we have directly discovered the gluon and QCD within the Pomeron by studying the structure of the interactions of this vector particle. We shall have made some progress towards this goal by the end of Part 2.

It is clear that the abstract and general nature of the formalism developed in this article makes it very difficult to tie up the loose ends that would be involved in any claim for uniqueness of the Critical Pomeron. However, although we shall not attempt a proof, we do believe that Regge behavior is intimately correlated with the analyticity properties of many-particle amplitudes and that Reggeon Unitarity *requires* that high-energy behavior be formulated in terms of interacting Regge poles if it is to be consistent with cross-channel unitarity. That the Pomeron must be a *single* Regge pole is ultimately understood[25] in the context of QCD as being a requirement of the factorisation properties needed for "Wee Partons" when the parton model is combined with a confining and symmetry-breaking vacuum. Since this combination is probably necessary to get a theory which is both ultra-violet finite and unitary, we believe the Critical Pomeron is the unique possibility for a strongly-interacting, confining, theory of the kind that we anticipate is given by QCD. There may, however, be a more complicated high-energy S-Matrix which involves some partial deconfinement in the form of the photon (and the weak-interaction vector bosons). In relation to this we suspect that a unitary symmetry any bigger than SU(3) is necessarily broken spontaneously *because of* (high-energy) unitarity and that a generalised version of the Super-Critical Pomeron may describe the symmetry-breaking.

REFERENCES

1. H. P. Stapp and A. R. White, in proceedings of the Les Houches Institute "Structural Analysis of Collision Amplitudes", published by North Holland (1976).

2. H. P. Stapp and A. R. White, Phys. Rev. **D26**, 2145 (1982).

3. J.H. Weis, Phys. Rev. **D6**, 2823 (1972).

4. R. C. Brower, C. E. DeTar and J. H. Weis, Phys. Reports **14**, 257 (1974).

5. C. E. DeTar and J. H. Weis, Phys. Rev. **D4**, 3141 (1971).

6. G. F. Chew and S. C. Frautschi, Phys. Rev. Lett. **7**, 394 (1961).

7. V. N. Gribov, I. Ya. Pomeranchuk and K. A. Ter-Martirosyan, Phys. Rev. **139B**, 184 (1965).

8. V. N. Gribov and A. A. Migdal, Sov. J. Nucl. Phys. **8**, 583 (1968).

9. J. Finkelstein and K. Kajantie, Phys. Lett. **26B**, 305 (1968).

10. H. D. I. Abarbanel, G. F. Chew, M. L. Goldberger and L. M. Sanders, Phys. Rev. Lett. **26**, 937 (1971).

11. R. C. Brower, A. H. Mueller, A. Sen and J. H. Weis, Phys. Lett. **46B**, 105 (1973).

12. C. E. Jones, F. E. Low, S.-H. Tye, G. Veneziano and J. E. Young, Phys. Rev. Lett. **26**, 675 (1971).

13. R. C. Brower and J. H. Weis, Phys. Lett. **41B**, 631 (1972).

14. V. N. Gribov, Sov. Phys. JETP **26**, 414 (1968).

15. H. D. I. Abarbanel, J. B. Bronzan, R. L. Sugar and A. R. White, Phys. Repts. **21C**, 119 (1975).

16. A. A. Migdal, A. M. Polyakov and K. A. Ter-Martirosyan, Zh. Eksp. Teor. Fiz. **67**, 84 (1974).

17. H. D. I. Abarbanel and J. B. Bronzan, Phys. Rev. **D9**, 2397 (1974).

18. M. Ciafaloni, G. Marchesini and G. Veneziano, Nucl. Phys. **B98**, 472 (1975).

19. D. Amati, M. Ciafaloni, M. LeBellac and G. Marchesini, Nucl. Phys. **B112**, 107 (1976).

20. J. L. Cardy, Nucl. Phys. **B115**, 141 (1976).

21. J. B. Bronzan and R. L. Sugar, Phys. Rev. **D16**, 466 (1977).

22. A. R. White, Proceedings of the third Blois workshop on "Elastic and Diffractive Scattering—the Interface of Soft and Hard Processes in QCD"—Nucl. Phys. (Proc. Suppl.) **B12**, (1990).

23. W. Nahm, Comm. Math. Phys. **105**, 1 (1986).

24. A. R. White, proceedings of "Hadron Physics at High Energies", Marseilles (1978) and Proceedings of XIXth International Conference on High Energy Physics, Tokyo (1978).

25. A. R. White, Phys. Rev. **D29**, 1435 (1984).

26. A. R. White, in Hadronic Multiparticle Production—Advanced Series on Directions in High Energy Physics (World Scientific Publishing Co. 1988).

27. A. R. White, in Proceedings of Hadronic Matter in Collision, Tucson (1988), published by World Scientific Publishing Co.

28. M. Toller, Riv. Nuovo Cimento **1**, 403 (1969); Nuovo Cimento **62A**, 341 (1969).

29. N. Bali, G. F. Chew and A. Pignotti, Phys. Rev. **163**, 1572 (1967).

30. H. D. I. Abarbanel, J. B. Bronzan, R. L. Sugar and A. Schwimmer, Phys. Rev. **D14**, 632 (1976).

31. P. Goddard and A. R. White, Nucl. Phys. **B17**, 45 (1970).

32. J. Bros, H. Epstein and V. Glaser, Comm. Math. Phys. **1**, 240 (1965).

33. A. Martin, Scattering Theory: Unitarity, Analyticity and Crossing, Lecture Notes in Physics (Springer, Berlin, 1969).

34. H. Epstein, in proceedings of the Brandeis Summer Institute "Axiomatic Field Theory", published by Gordon and Breach (1965).

35. H. Epstein, V. Glaser and R. Stora, in proceedings of the Les Houches Institute "Structural Analysis of Collision Amplitudes", published by North Holland (1976).

36. K. Cahill and H. P. Stapp, Ann. of Physics **90**, 438 (1975). This paper contains a comprehensive description of the Bros, Epstein and Glaser formalism.

37. D. Iagolnitzer and H. P. Stapp, in proceedings of the Les Houches Institute "Structural Analysis of Collision Amplitudes", published by North Holland (1976).

38. J. Coster and H. P. Stapp, J. Math. Phys. **16**, 1288 (1975).

39. M. Sato, Recent Developments in Hyperfunction Theory and its Applications to Physics, Lecture Notes in Physics **39**, Springer-Verlag (1975).

40. P. Goddard and A. R. White, Nuovo Cimento **1A**, 645 (1971).

41. P. Hoyer, N. A. Tornqvist and B. R. Webber, Nucl. Phys. **B115**, 429 (1976).

42. R. L. Sugar and A. R. White, Phys. Rev. **D10**, 4074 (1974).

43. H. D. I. Abarbanel, J. Bartels, J. B. Bronzan and D. Sidhu, Phys. Rev. **D12**, 2459,2798 (1978).

44. E. Nagy *et al.*, Nucl. Phys. **B150**, 221 (1979).

45. M. Baig, J. Bartels and J. W. Dash, Nucl. Phys. **B237**, 502 (1984).

46. K. Kang and A. R. White, Argonne/Brown preprint ANL-HEP-PR-90-12, BROWN-HET-743 (1990).

47. M. Moshe, Phys. Repts. **37C**, 255 (1978).

48. A. R. White, Proceedings of Proton-Antiproton Collider Physics—1981, Madison, Wisconsin. AIP Conf. Proc. No.85, Particle and Fields Subseries No.26.

49. J. L. Cardy, R. L. Sugar and A. R. White, Phys. Lett. **55B**, 384 (1975).

50. J. Bartels and E. Rabinovici, Phys. Lett. **58B**, 171 (1975).

51. J. L. Cardy, Phys. Rev. **D12**, 3346 (1975).

52. J. L. Cardy, Nucl. Phys. **B109**, 255 (1976).

53. H. D. I. Abarbanel and R. L. Sugar, Phys. Rev. **D10**, 721 (1974).

54. J. Bartels and R. Savit, Phys. Rev. **D11**, 2300 (1975).

55. C. Bromberg *et al.*, Nucl. Phys. **B232**, 189 (1983).

56. S. Mandelstam, Phys. Rev. **168**, 1884 (1968).

57. V. A. Abramovskii, V. N. Gribov and O. V. Kancheli, Sov. J. Nucl. Phys. **18**, 308 (1974).

58. A. H. Mueller, Proceedings of the European Physical Society Conference, Aix-en-Provence (1973).

59. J. L. Cardy and P. Suryani, Phys. Rev. **D13**, 1064 (1976).

60. D. Z. Freedman, C. E. Jones, F. E. Low and J. E. Young, Phys. Rev. Lett. **26**, 1197 (1971).

61. C. Jen, K. Kang, P. Shen and C. I. Tan, Phys. Rev. Lett. **27**, 458 (1971), Ann. Phys. **72**, 548 (1971).

FIGURE CAPTIONS

Fig. 2.1 A General Toller Diagram.

Fig. 2.2 Examples of Toller diagrams generating Planar Toller diagrams.

Fig. 2.3 The generation of hexagraph vertices.

Fig. 2.4 A planar Toller diagram generating two hexagraphs.

Fig. 2.5 The thirty-two hexagraphs generated by the eight Toller diagrams of Fig. 2.2(a).

Fig. 2.6 Twisting a hexagraph.

Fig. 3.1 The integration contour for (3.2).

Fig. 3.2 Branch-points emerging from the unphysical side of normal thresholds.

Fig. 3.3 "Infinitesimal" analyticity domains surrounding the normal threshold branch cuts.

Fig. 3.4 A 2–4 amplitude with a "bad" boundary-value.

Fig. 3.5 An allowable cut (discontinuity) through a hexagraph.

Fig. 4.1 The contour C for (4.3).

Fig. 4.2 A T-graph.

Fig. 4.3 A D-graph.

Fig. 4.4 A V-graph.

Fig. 4.5 Cut-plane analyticity in the u-plane.

Fig. 4.6 A hexagraph containing a single V-graph.

Fig. 4.7 The two hexagraphs joined by the V-graph in Fig. 4.6.

Fig. 4.8 A single T-graph with D-graph structures attached.

Fig. 4.9 Allowable cuts of the hexagraphs of Fig. 2.5 and the conjugate Toller diagrams.

Fig. 6.11 Intermediate states are each represented by a propagator Γ_i of the form of (6.59).

Fig. 6.12 The production process is uniformly spread on the rapidity axis.

Fig. 6.13 Elastic scattering, as the shadow of the production process, is a Pomeron Regge pole.

Fig. 6.14 The production process for events with twice the average multiplicity.

Fig. 6.15 Varying multiplicity densities on the rapidity axis generate higher-order Pomeron graphs.

Fig. 6.16 Uncut Pomerons correspond to absorption of the basic production process.

Fig. 6.17 A further cut allowed in hexagraph loops.

Fig. 6.18 The multiplicity distribution for $\alpha_{I\!P}(0) < 1$.

Fig. 7.1 Diagrams involving vacuum production but no triple Pomeron coupling.

Fig. 7.2 The first approximation to the modification of hadron reggeons as the Pomeron becomes Super-Critical.

Fig. 7.3 The cancellation of vacuum production at a "classical" stationary point.

Fig. 7.4 The scattering of Super-Critical hadron reggeons.

Fig. 7.5 Five-fold discontinuities consistent with particle poles in each reggion leg.

Fig. 7.6 Five-fold discontinuities inconsistent with particle poles in each reggeon leg.

Fig. 7.7 The form of hexagraphs which contribute to Regge Cut discontinuities in both the Pomeron and Reggeon channels of Fig. 7.4.

Fig. 7.8 Multi-channel Pomeron and Reggeon-Pomeron Interactions described by "multiplicative" Reggeon Field Theory rules.

Fig. 7.9 An example of a Pomeron graph with different channels connected.

Fig. 7.10 Hexagraphs corresponding to the component graphs of Fig. 7.9.

Fig. 7.11 The same set of cuts in two distinct hexagraphs.

Fig. 7.12 A graph that contributes to the Super-Critical Theory.

Fig. 7.13 A Super-Critical Pomeron graph.

Fig. 7.14 Generation of a Super-Critical graph of the form of Fig. 7.1.

Fig. 7.15 Five-fold discontinuity of the graph of Fig. 7.14.

Fig. 7.16 Generation of the Super-Critical graphs which shift the intercept.

Fig. 7.17 Further graphs which do not contribute to the Super-Critical theory.

Fig. 7.18 The perturbative expansion of the Super-Critical Pomeron propagator.

Fig. 7.19 Another graph with the wrong discontinuity structure.

Fig. 7.20 Reggeon unitarity with the new vertices included.

Fig. 7.21 The full reggeon unitarity equation involving the Super-Critical odd-signature partner to the Pomeron.

Fig. 7.22 The structure of higher-order vertices in the Super-Critical expansion.

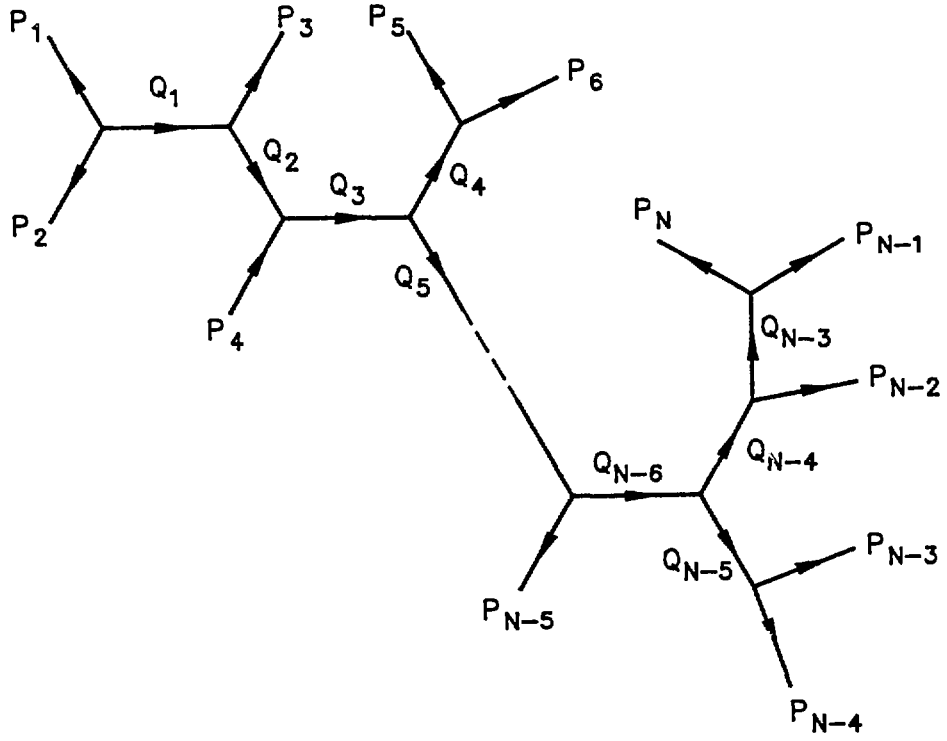
P1
P2
P3
P4
P5
P6
PN
PN-1
PN-2
PN-3
PN-4
PN-5
Q1
Q2
Q3
Q4
Q5
QN-3
QN-4
QN-5
QN-6

Fig. 2.1

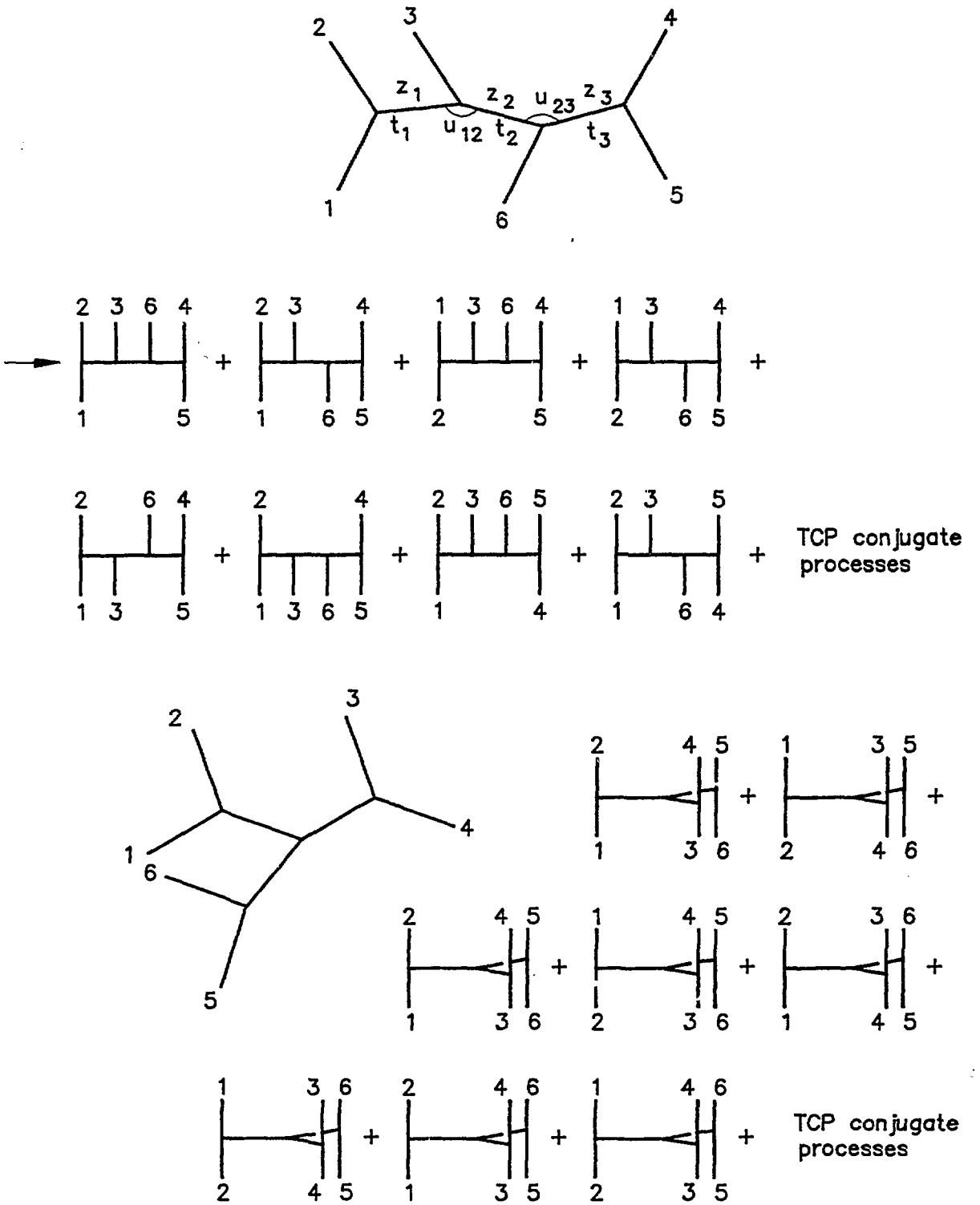
2
3
4
z_1
z_2
u_{23}
z_3
t_1
u_{12}
t_2
t_3
1
6
5
2 3 6 4
1 5
2 3 4
1 6 5
1 3 6 4
2 5
1 3 4
2 6 5
2 6 4
1 3 5
2 4
1 3 6 5
2 3 6 5
1 4
2 3 5
1 6 4
TCP conjugate processes
2
3
4
1
6
5
2 4 5
1 3 6
1 3 5
2 4 6
2 4 5
1 3 6
1 4 5
2 3 6
2 3 6
1 4 5
1 3 6
2 4 5
1 4 6
2 3 5
TCP conjugate processes

Fig. 2.2

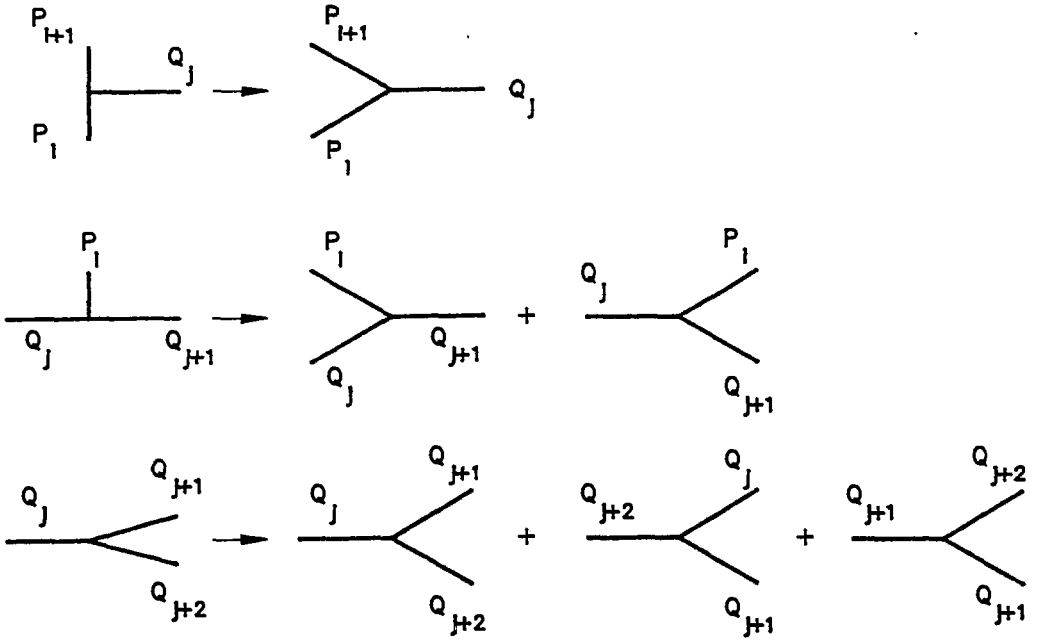

Fig. 2.3

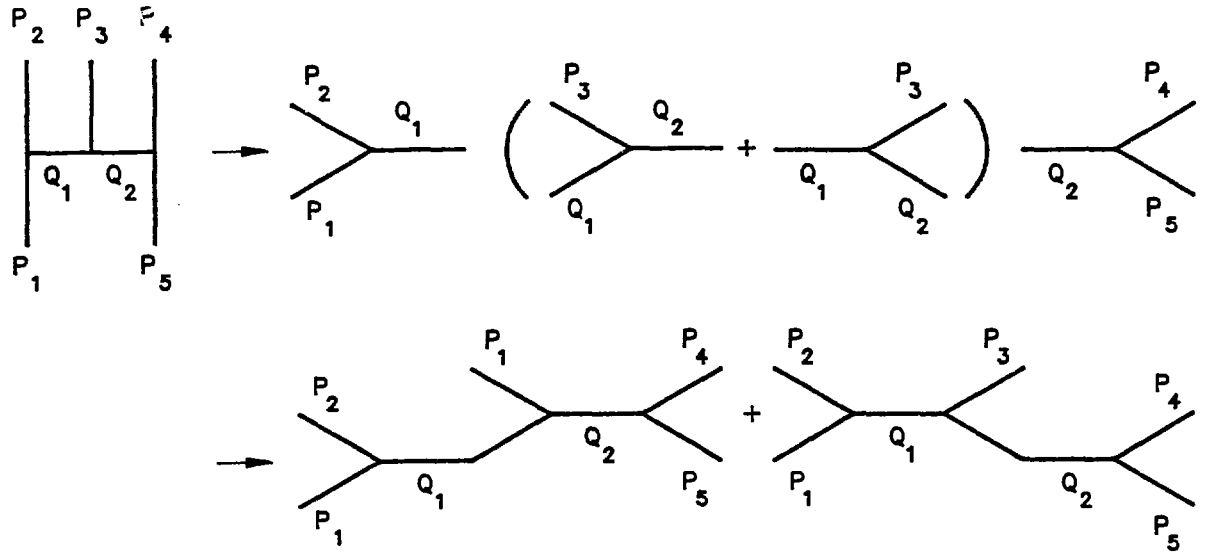

Fig. 2.4

03643

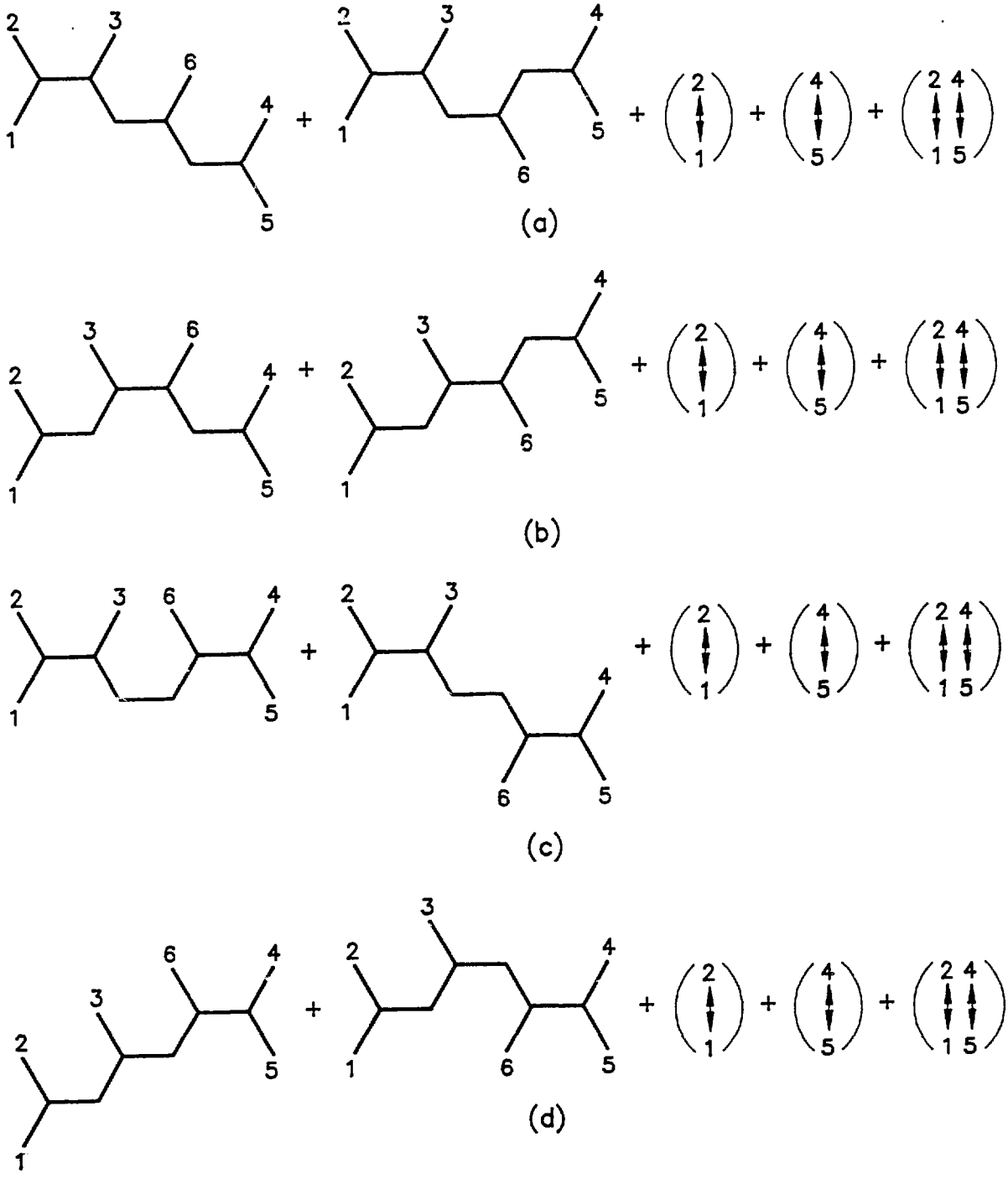

Fig. 2.5

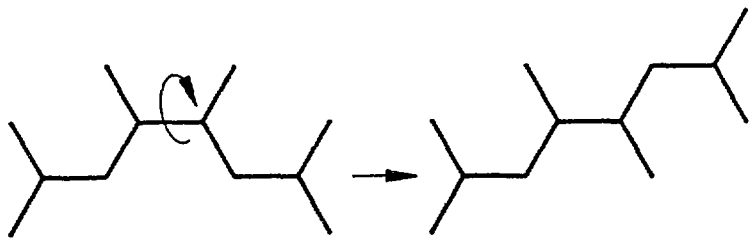

Fig. 2.6

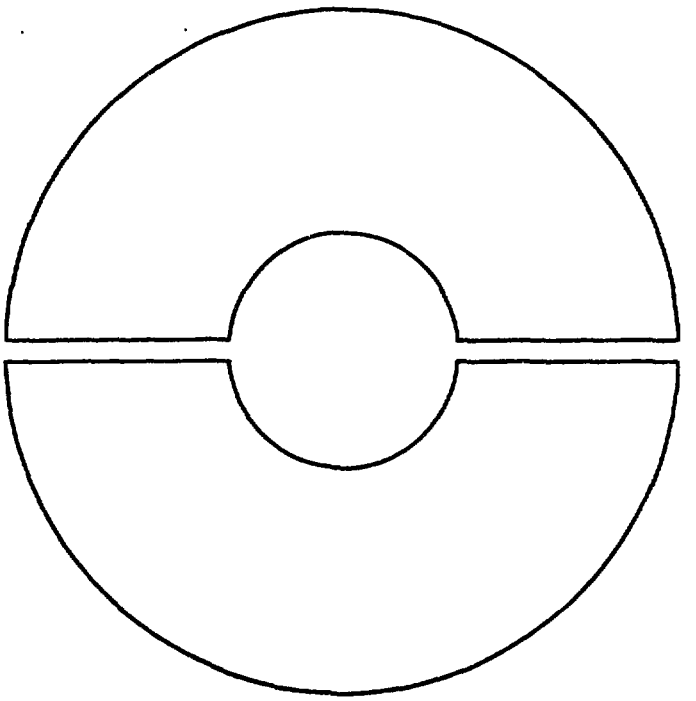

Fig. 3.1

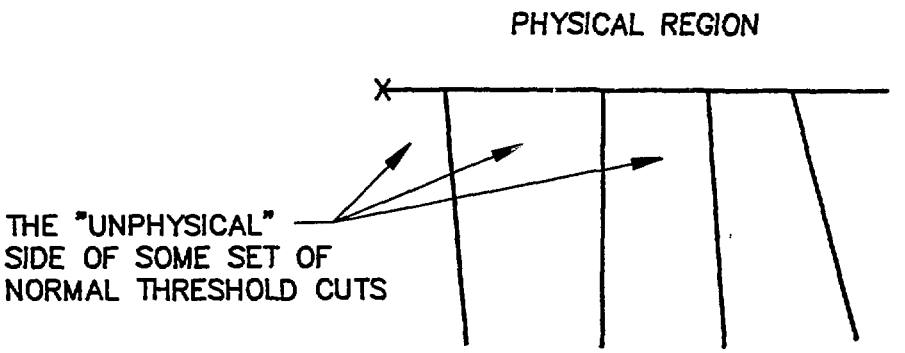
PHYSICAL REGION
THE "UNPHYSICAL"
SIDE OF SOME SET OF
NORMAL THRESHOLD CUTS

Fig. 3.2

Fig. 3.3

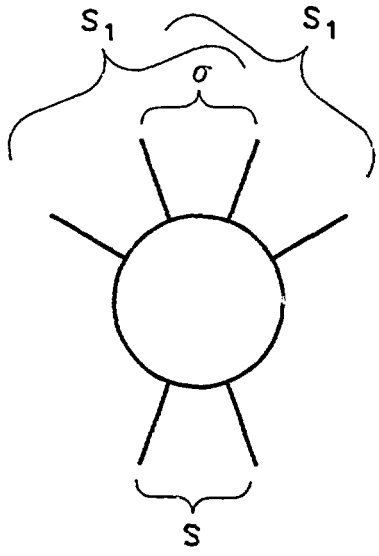

Fig. 3.4

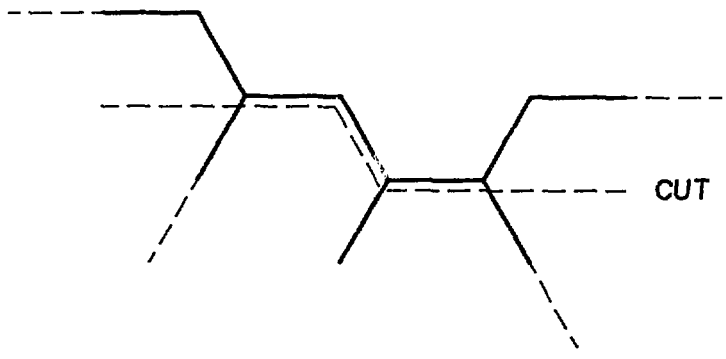

Fig. 3.5

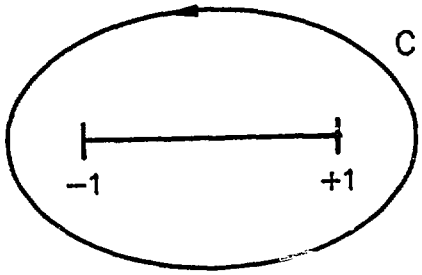

Fig. 4.1

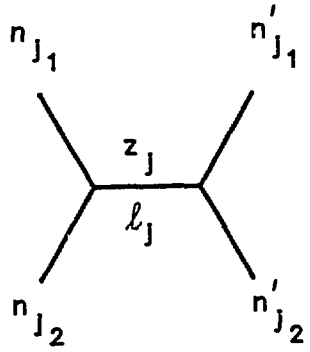

Fig. 4.2

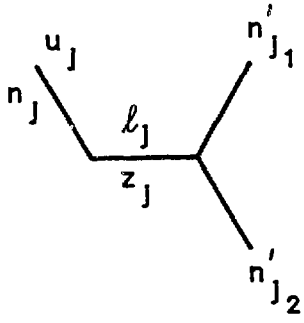

Fig. 4.3

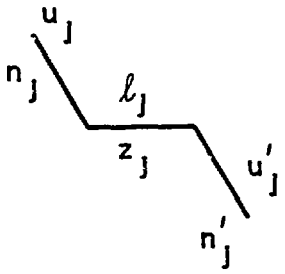

Fig. 4.4

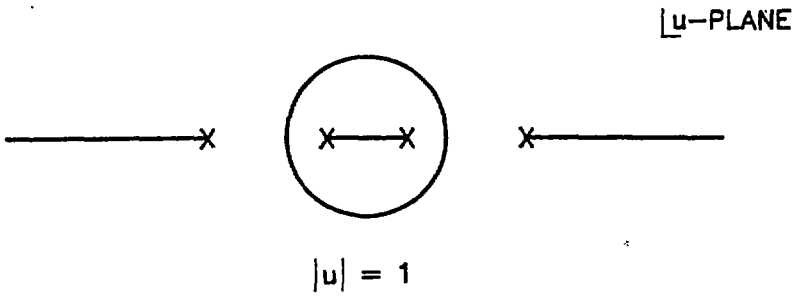

Fig. 4.5

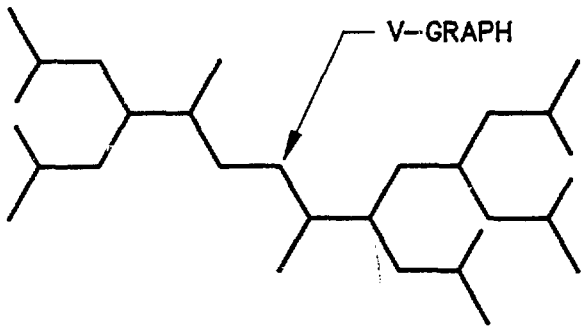

Fig. 4.6

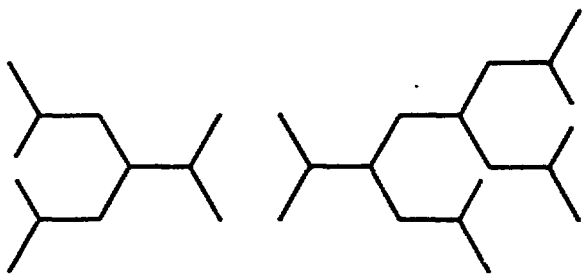

Fig. 4.7

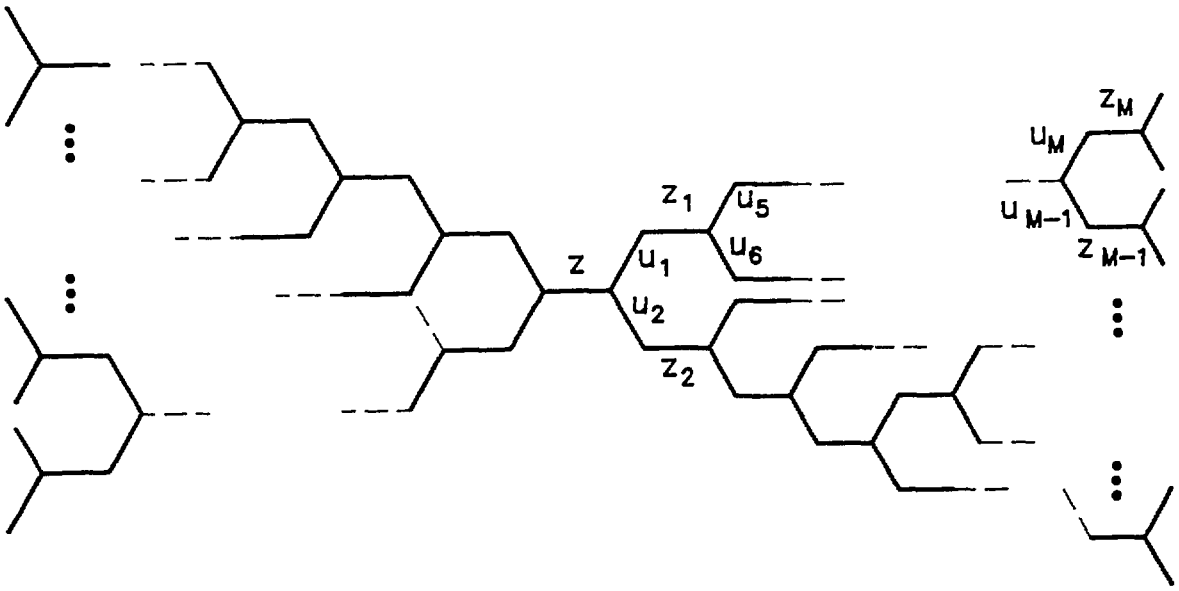

Fig. 4.8

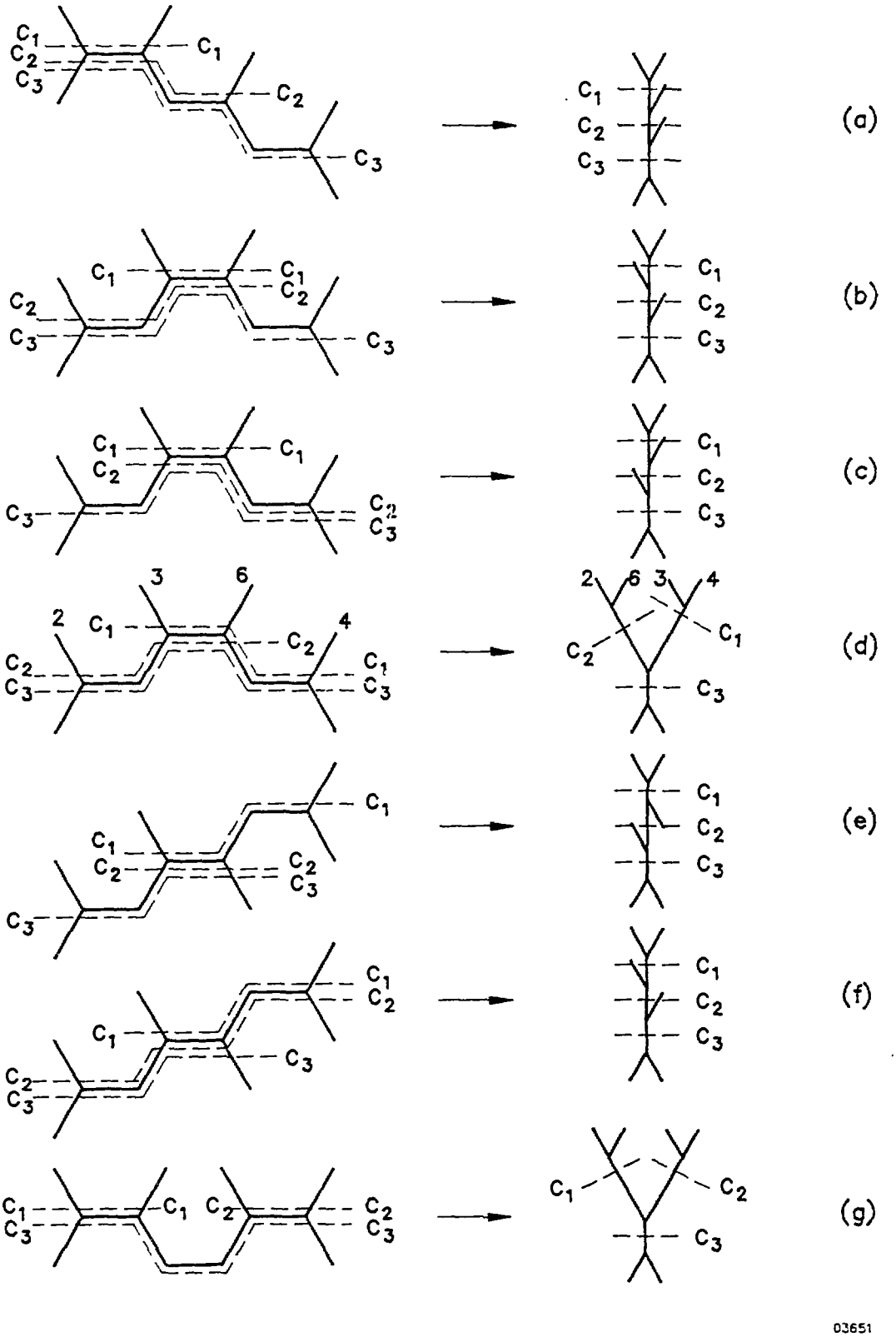

Fig. 4.9

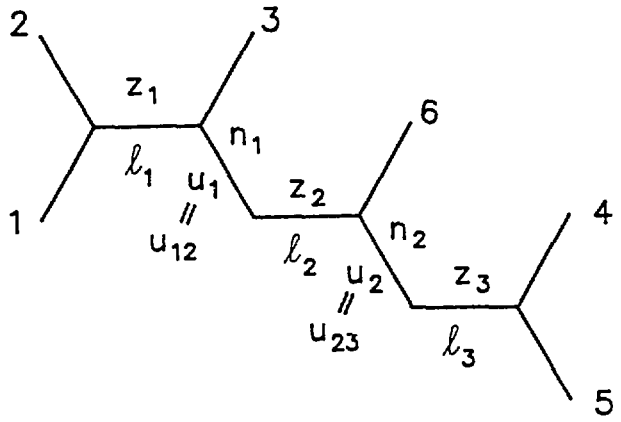

Fig. 4.10

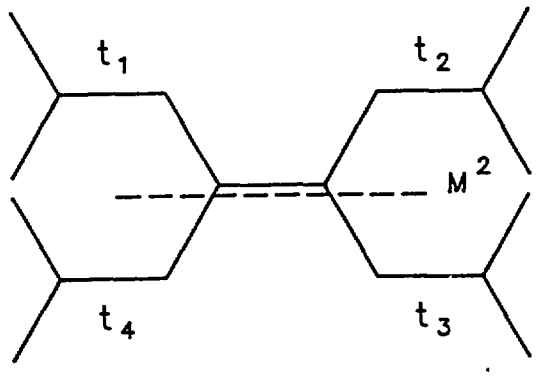

Fig. 4.11

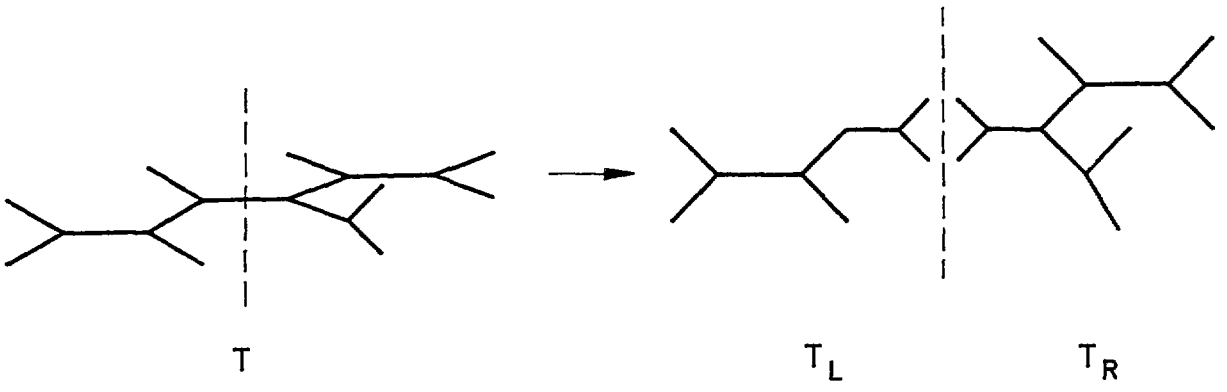

Fig. 5.1

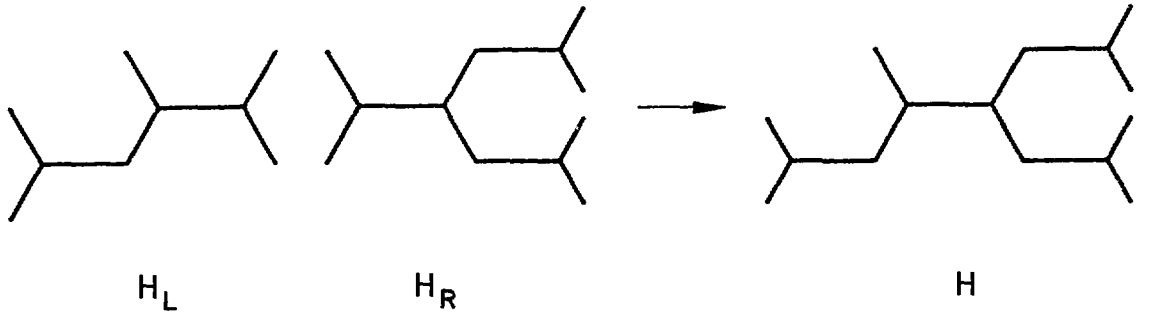

Fig. 5.2

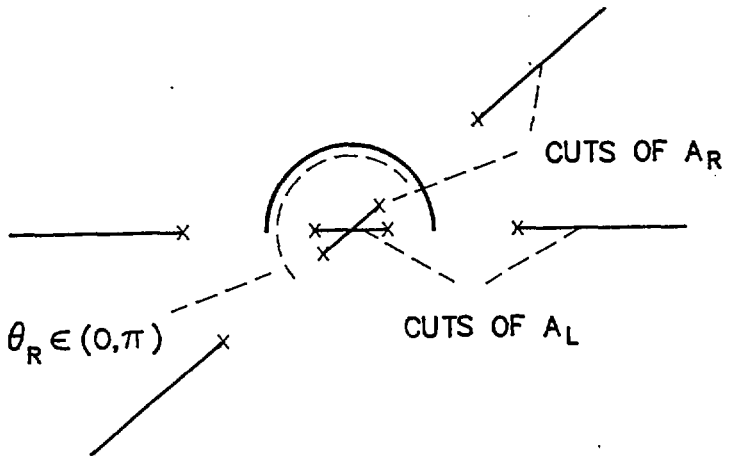

Fig. 5.3

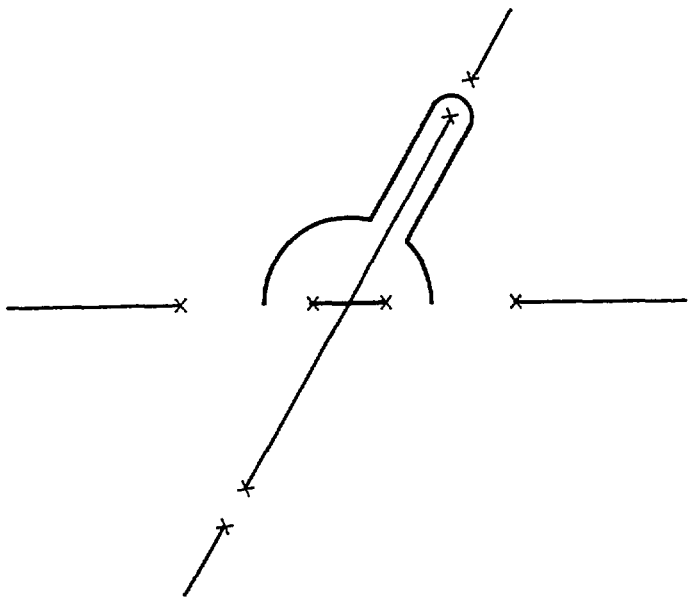

Fig. 5.4

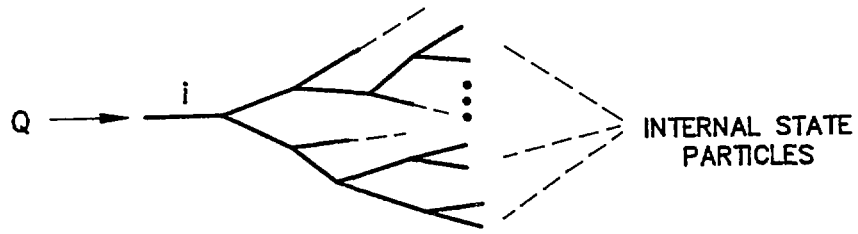

Fig. 5.5

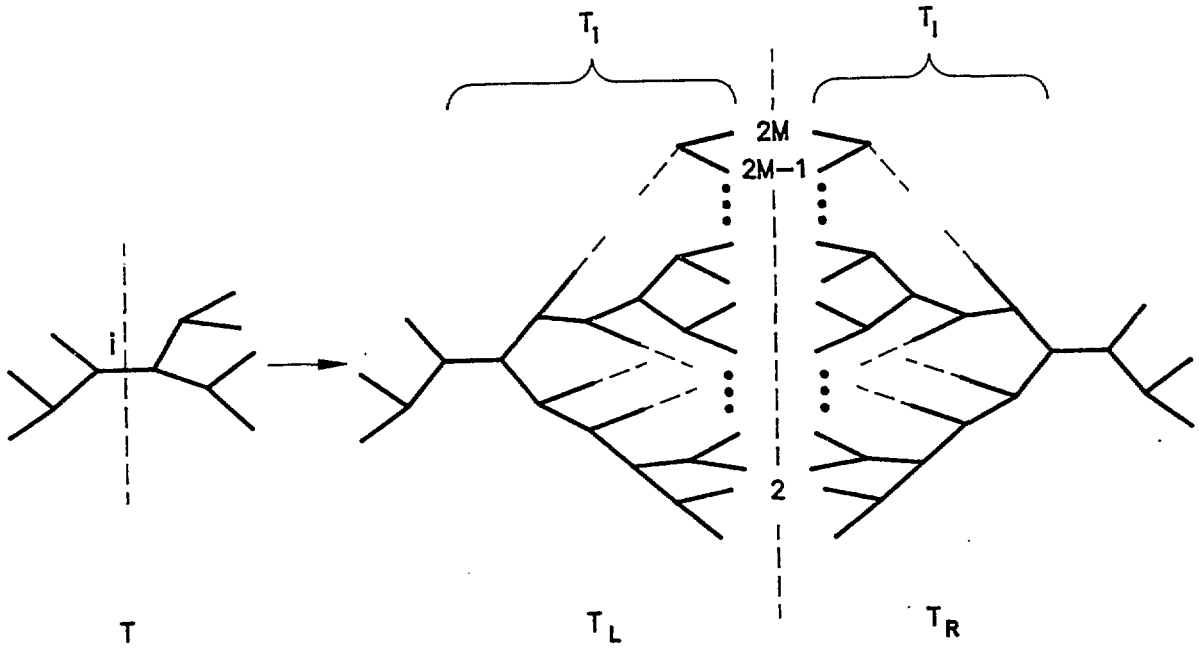

Fig. 5.6

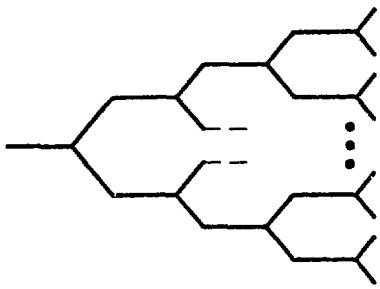

Fig. 5.7

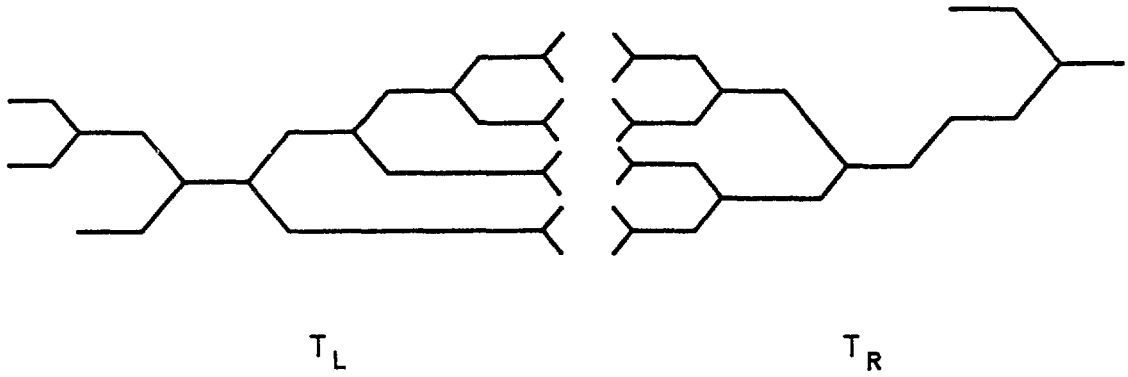

Fig. 5.8

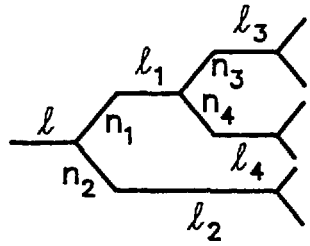

Fig. 5.9

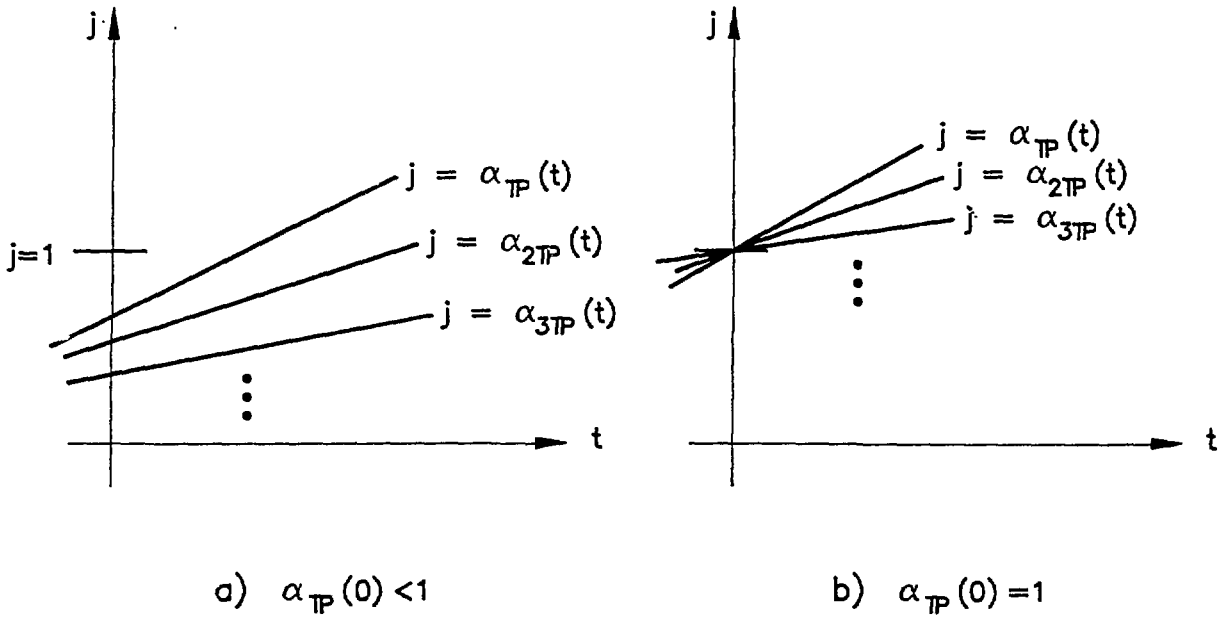
j
j = α_IP (t)
j = α_2IP (t)
j = α_3IP (t)
j=1
t
a) α_IP (0) <1
j
j = α_IP (t)
j = α_2IP (t)
j = α_3IP (t)
t
b) α_IP (0) =1

Fig. 6.1

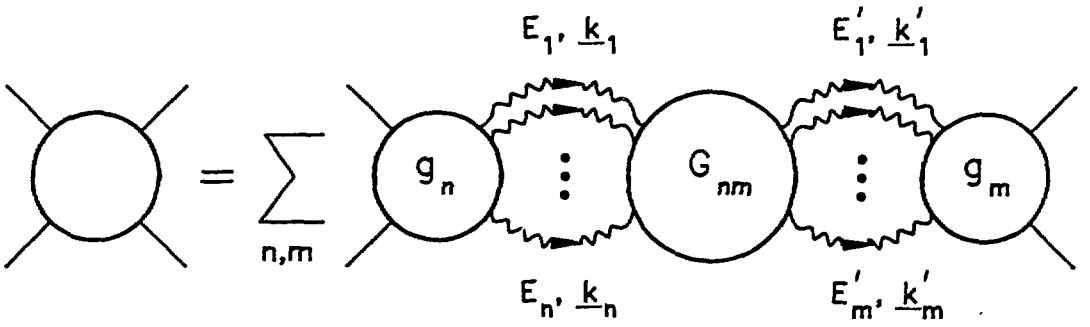
E_1, k_1
E'_1, k'_1
g_n
G_nm
g_m
n,m
E_n, k_n
E'_m, k'_m

Fig. 6.2

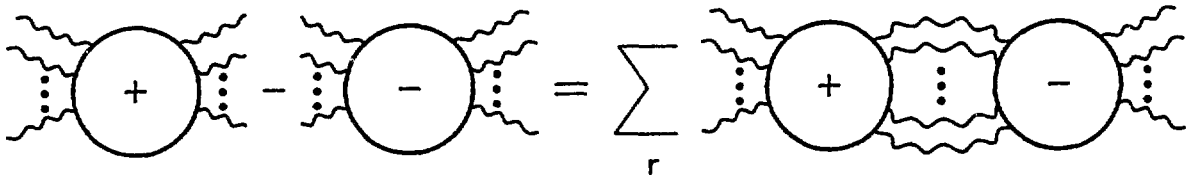
+
−
=
r
+
−

Fig. 6.3

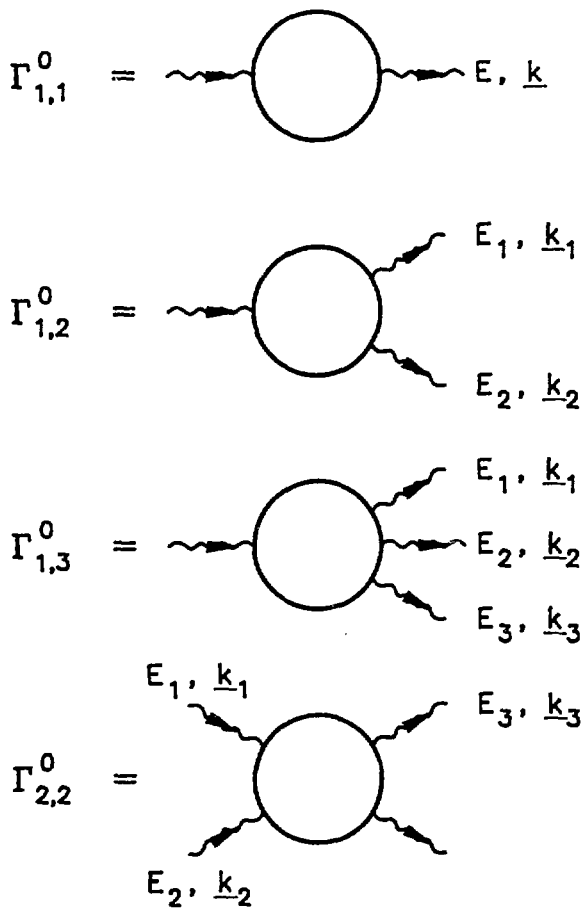
$\Gamma^0_{1,1}$ = E, k
$\Gamma^0_{1,2}$ = E_1, k_1 E_2, k_2
$\Gamma^0_{1,3}$ = E_1, k_1 E_2, k_2 E_3, k_3
$\Gamma^0_{2,2}$ = E_1, k_1 E_3, k_3 E_2, k_2

Fig. 6.4

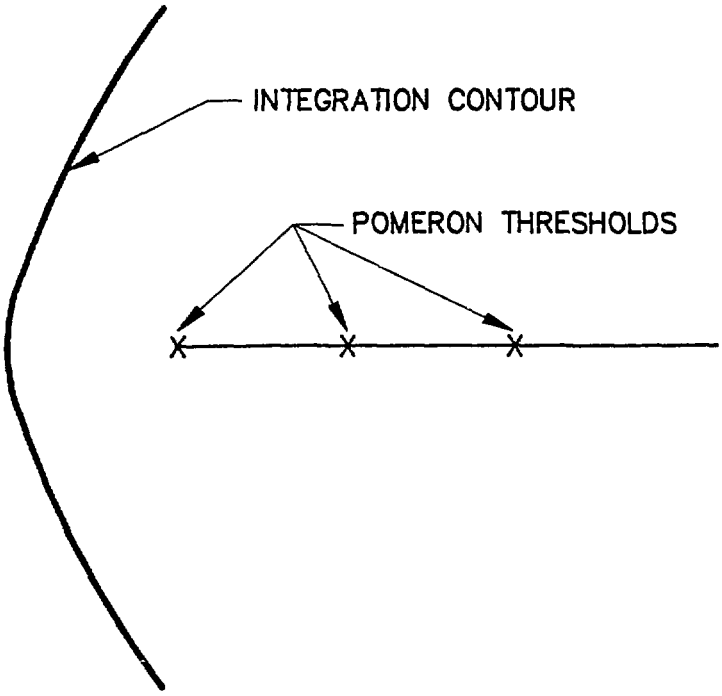
INTEGRATION CONTOUR
POMERON THRESHOLDS

Fig. 6.5

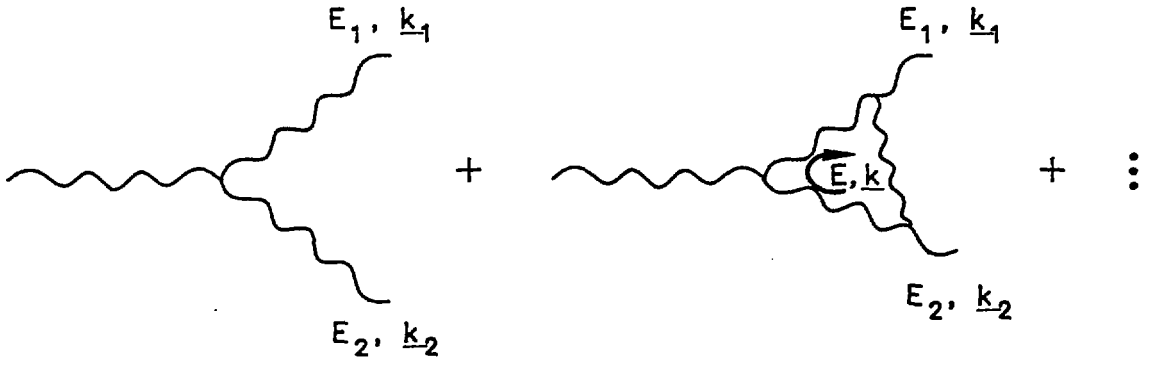
E1, k1
E2, k2
+
E1, k1
E, k
E2, k2
+

Fig. 6.6

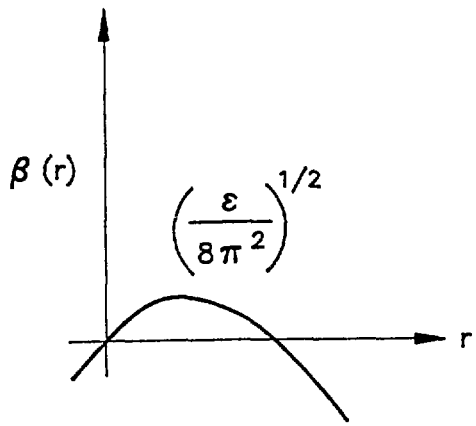

Fig. 6.7

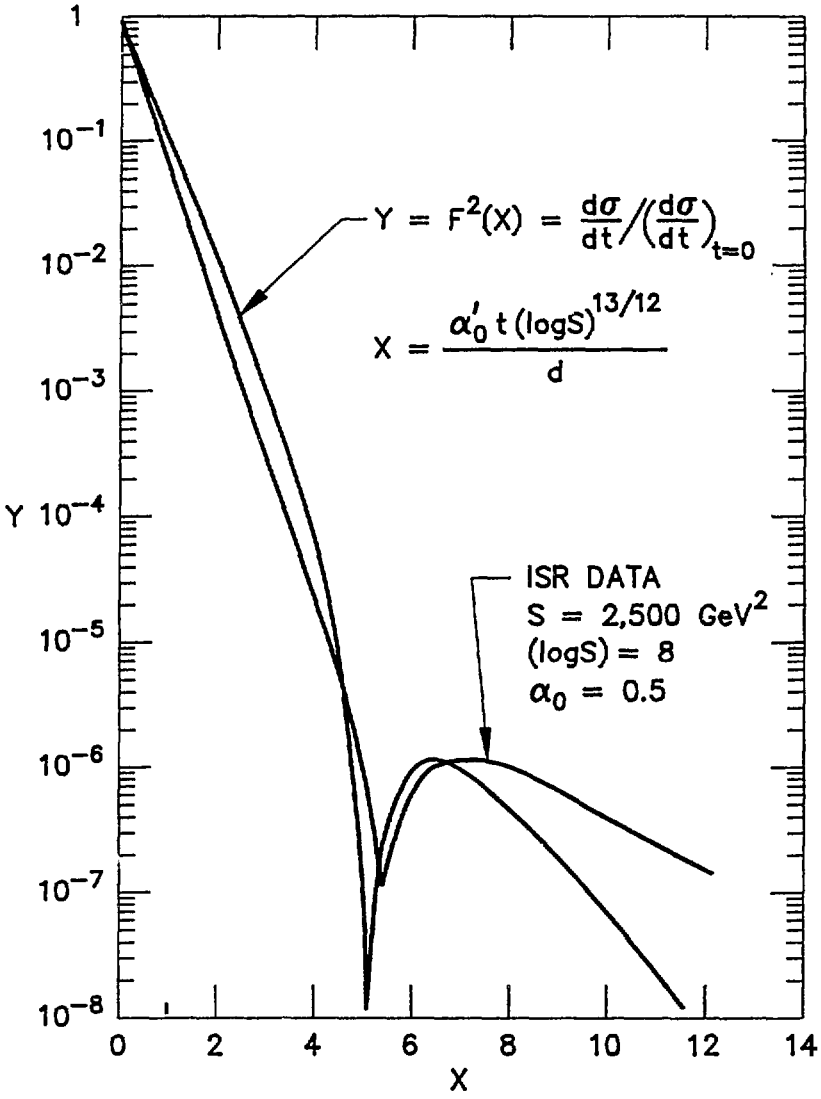
1
10^{-1}
10^{-2}
10^{-3}
Y 10^{-4}
10^{-5}
10^{-6}
10^{-7}
10^{-8}
0
2
4
6
8
10
12
14
X
$Y = F^2(X) = \frac{d\sigma}{dt} / \left(\frac{d\sigma}{dt}\right)_{t=0}$
$X = \frac{\alpha_0' t (\log S)^{13/12}}{d}$
ISR DATA
S = 2,500 GeV^2
(logS) = 8
α_0 = 0.5

Fig. 6.8

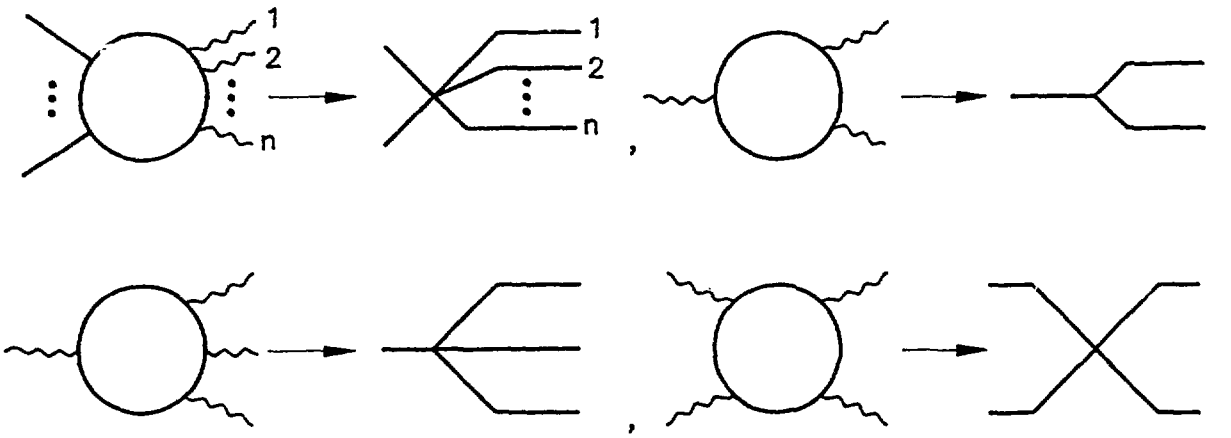

Fig. 6.9

03660

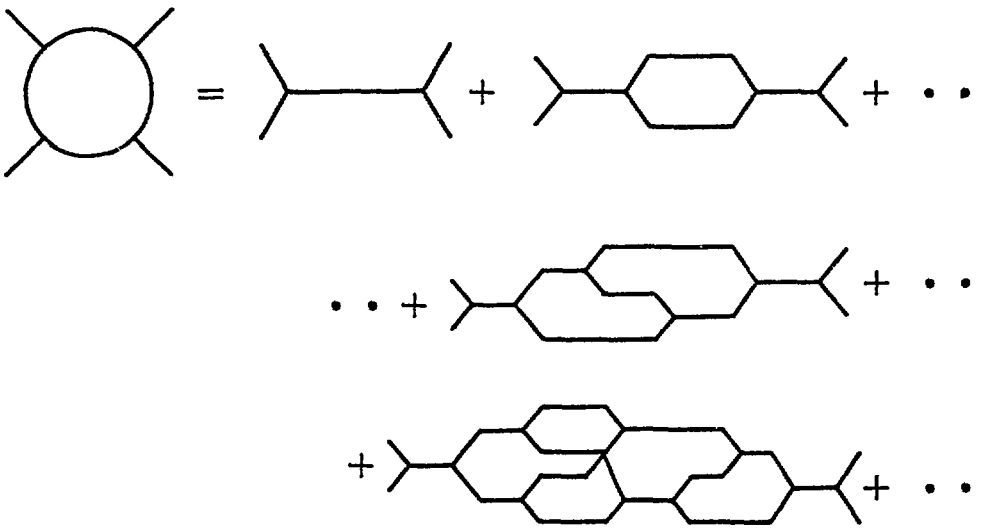

Fig. 6.10

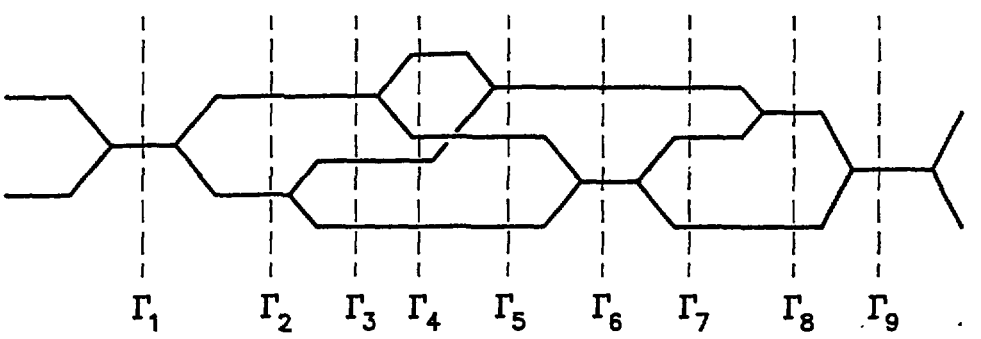

Fig. 6.11

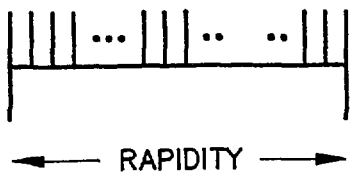

Fig. 6.12

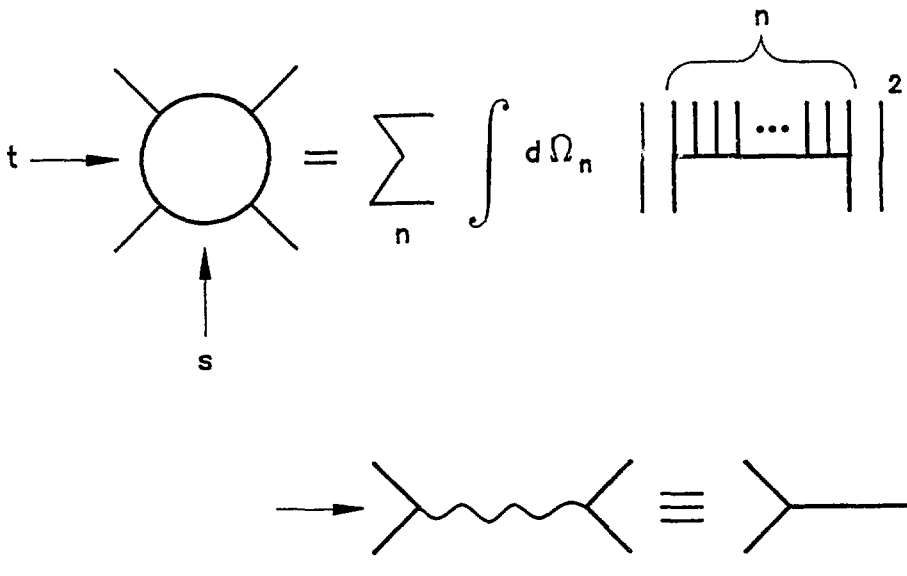

Fig. 6.13

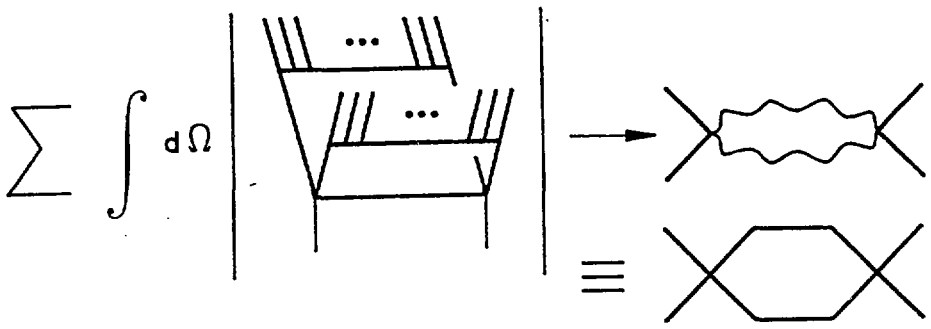

Fig. 6.14

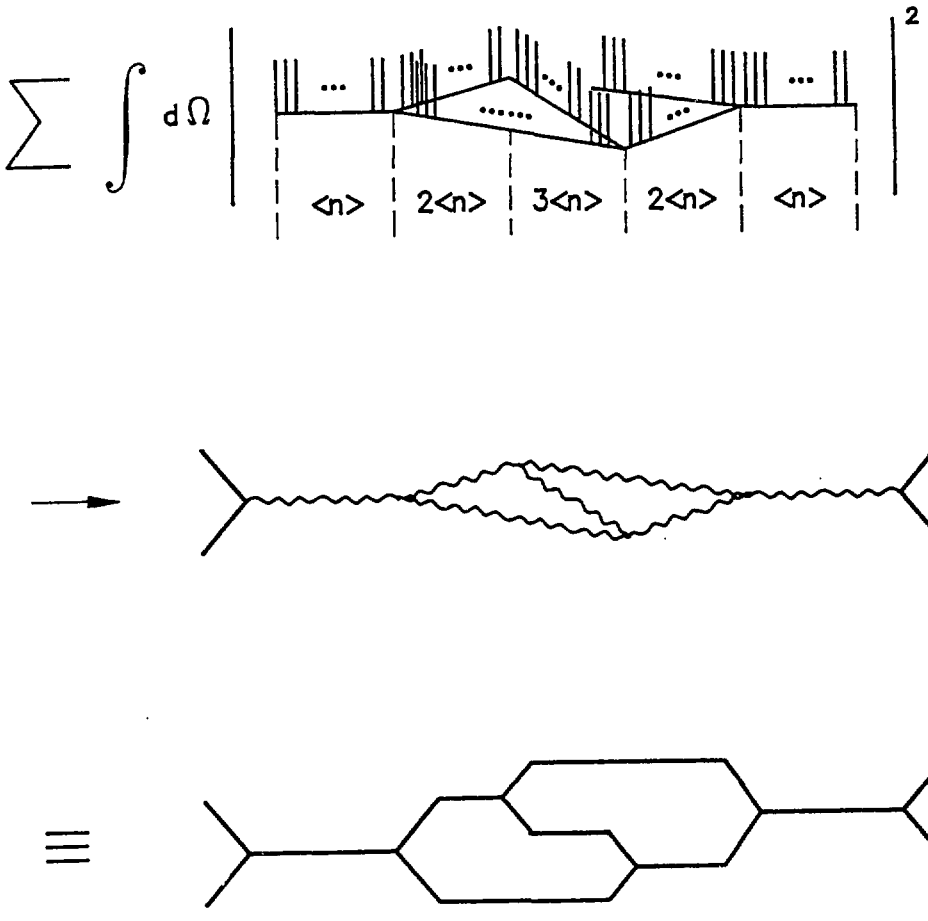

Fig. 6.15

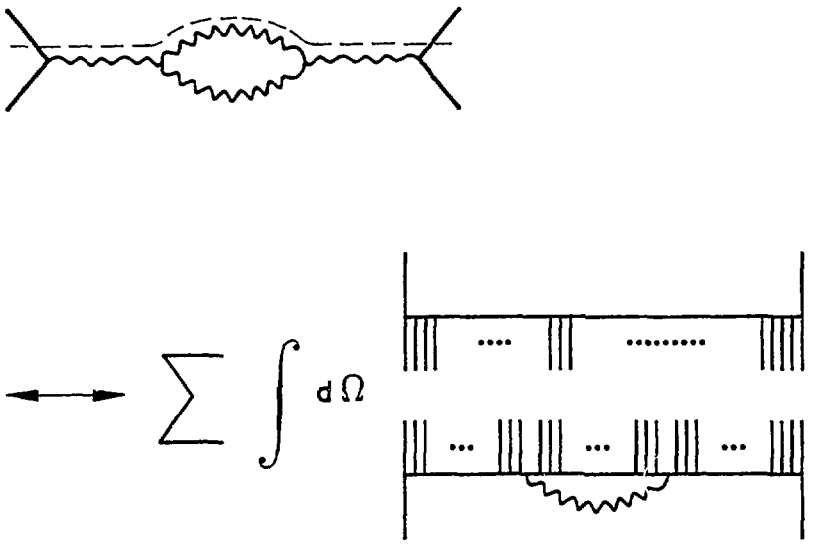

Fig. 6.16

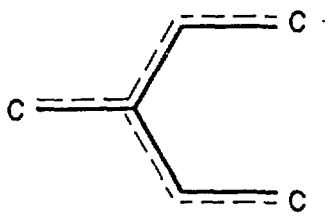

Fig. 6.17

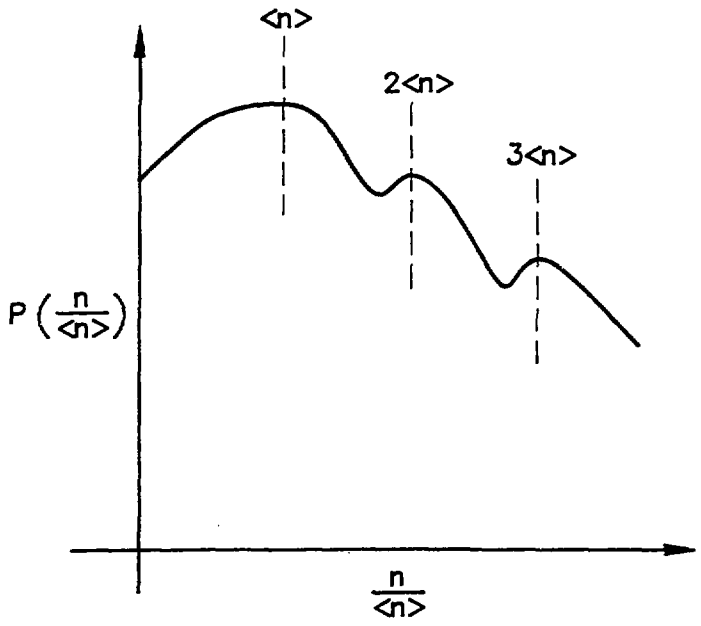

Fig. 6.18

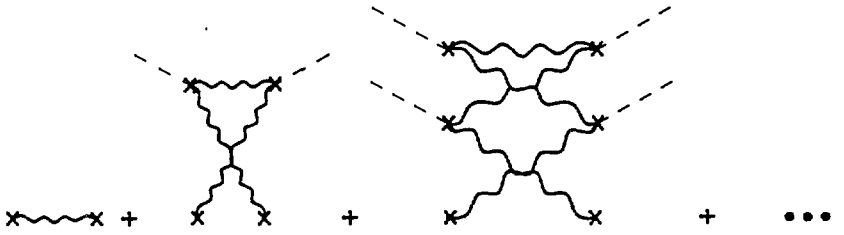

Fig. 7.1

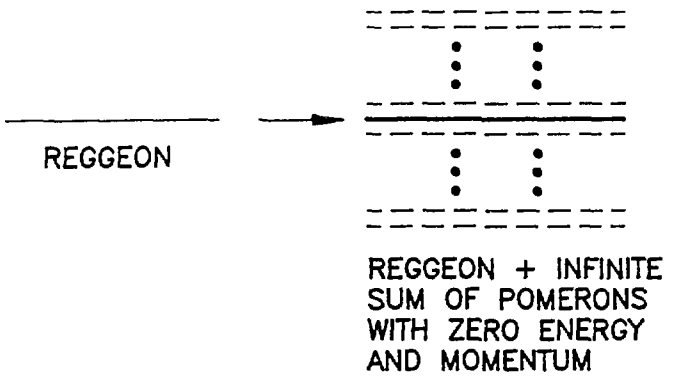

Fig. 7.2

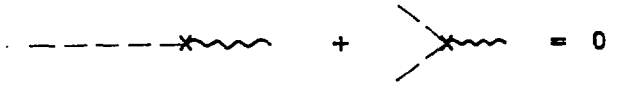

Fig. 7.3

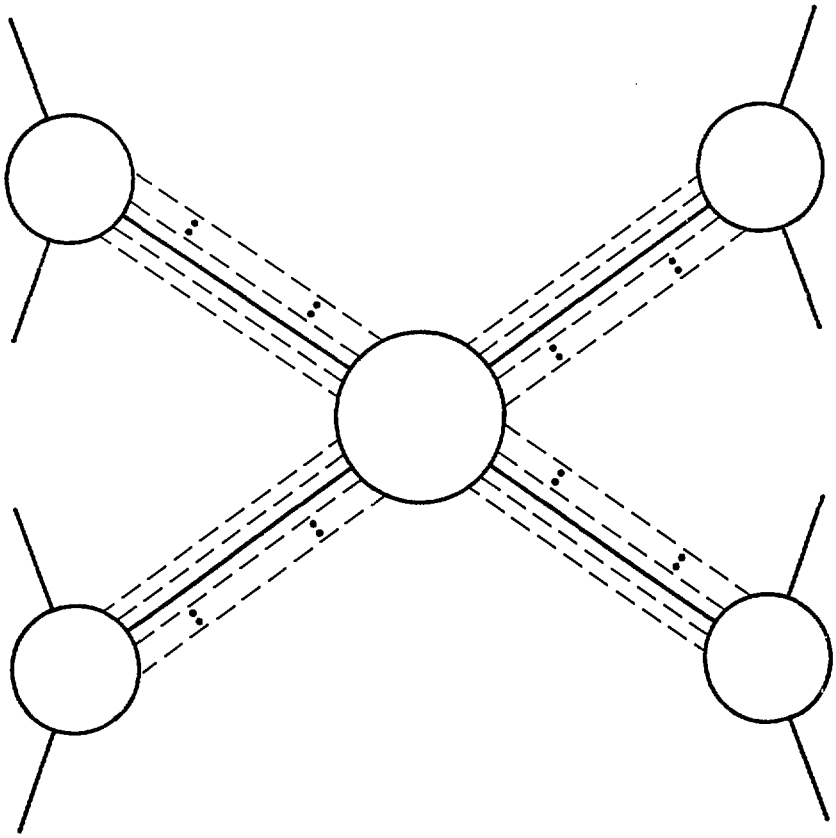

Fig. 7.4

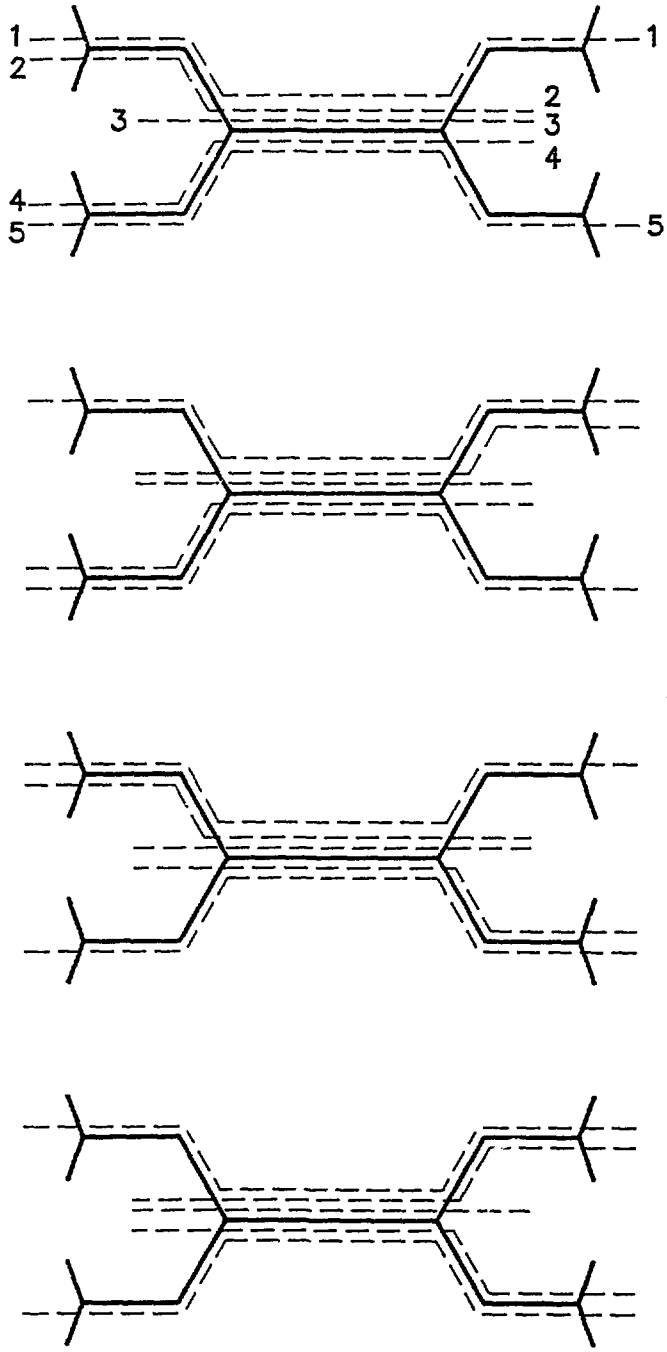

Fig. 7.5

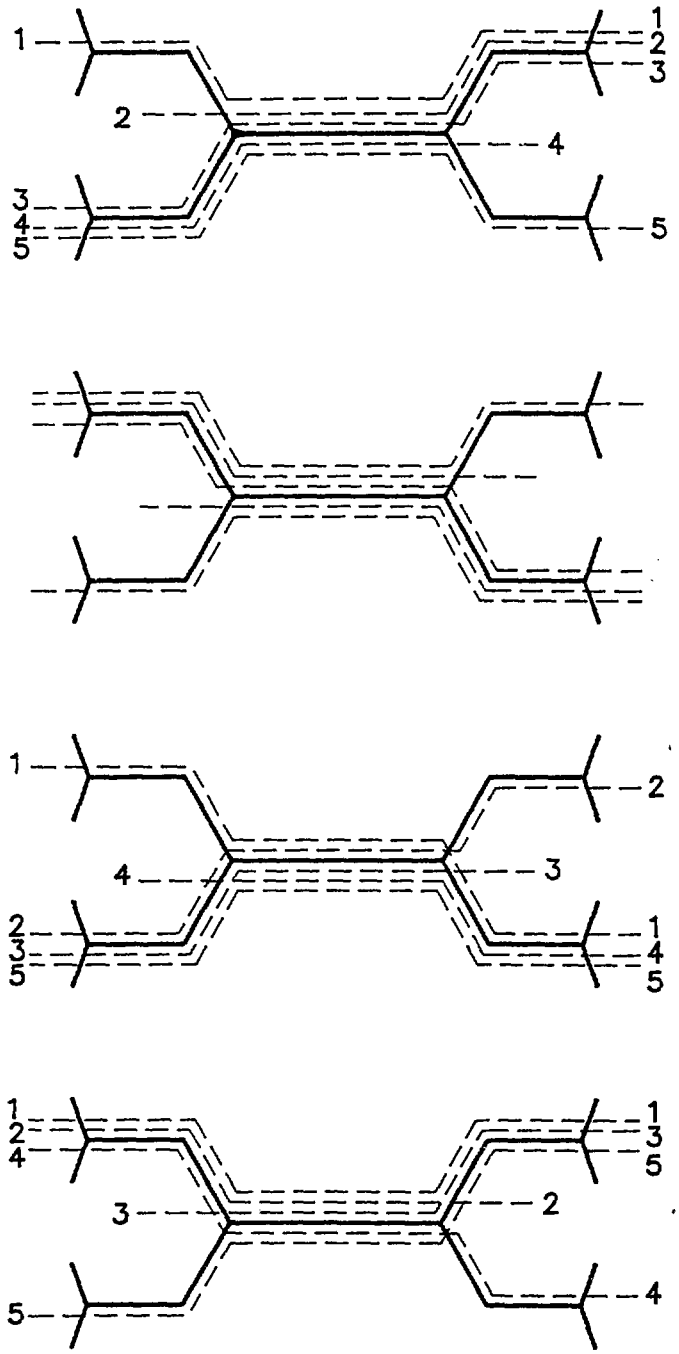

Fig. 7.6

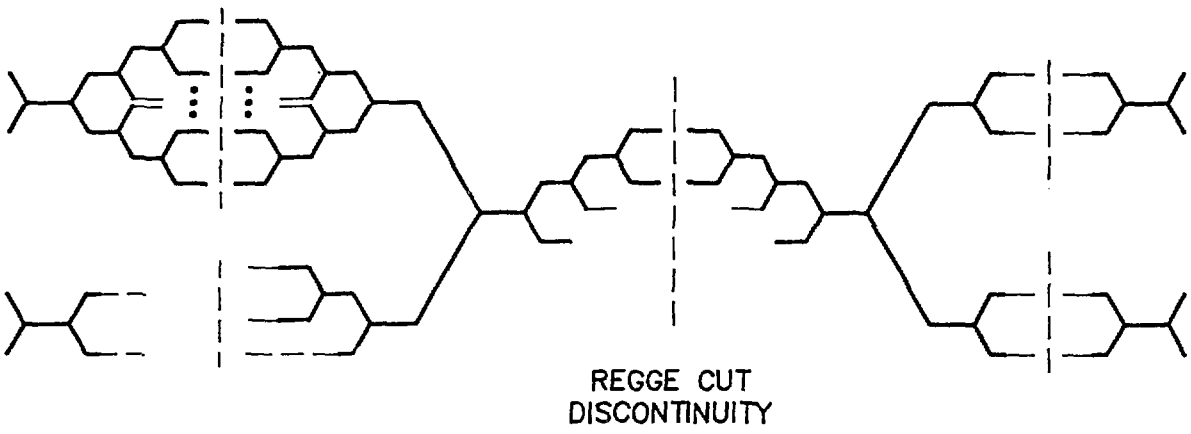
REGGE CUT
DISCONTINUITY

Fig. 7.7

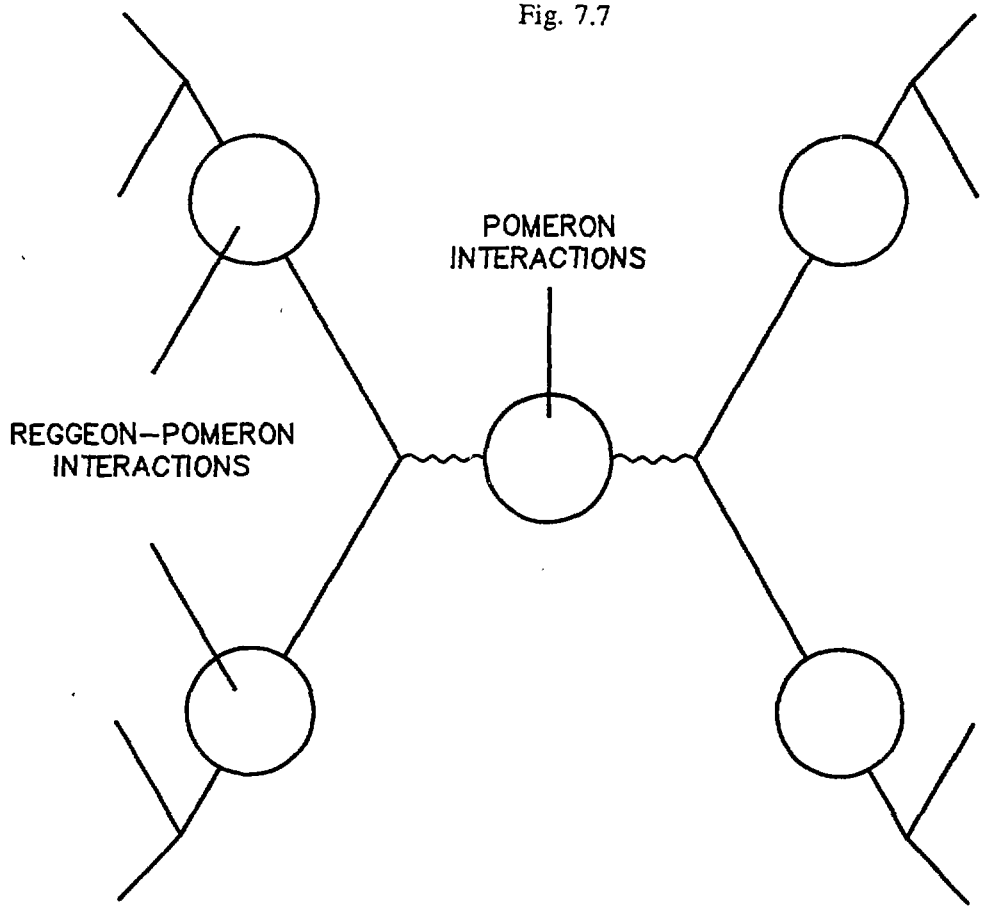
POMERON
INTERACTIONS
REGGEON–POMERON
INTERACTIONS

Fig. 7.8

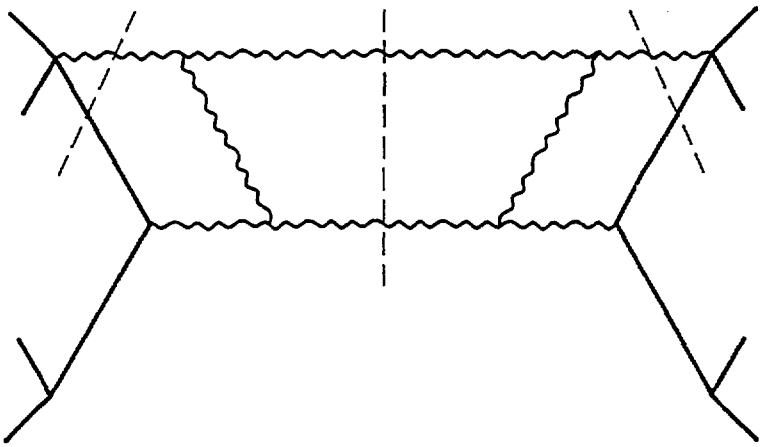

Fig. 7.9

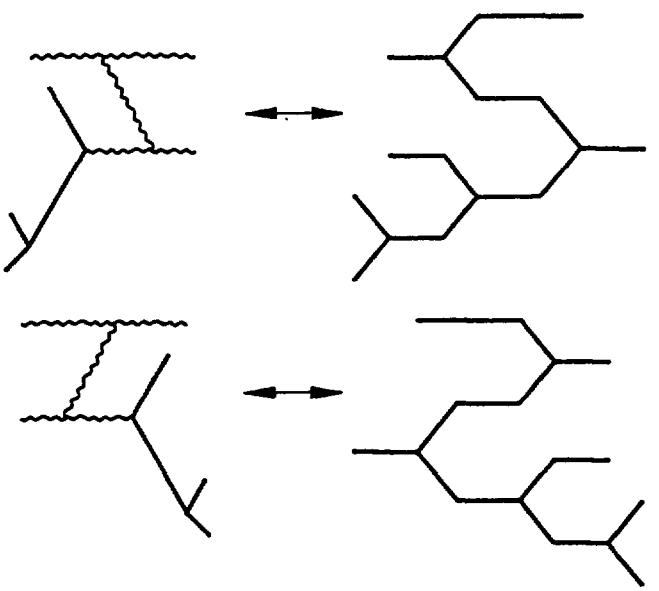

Fig. 7.10

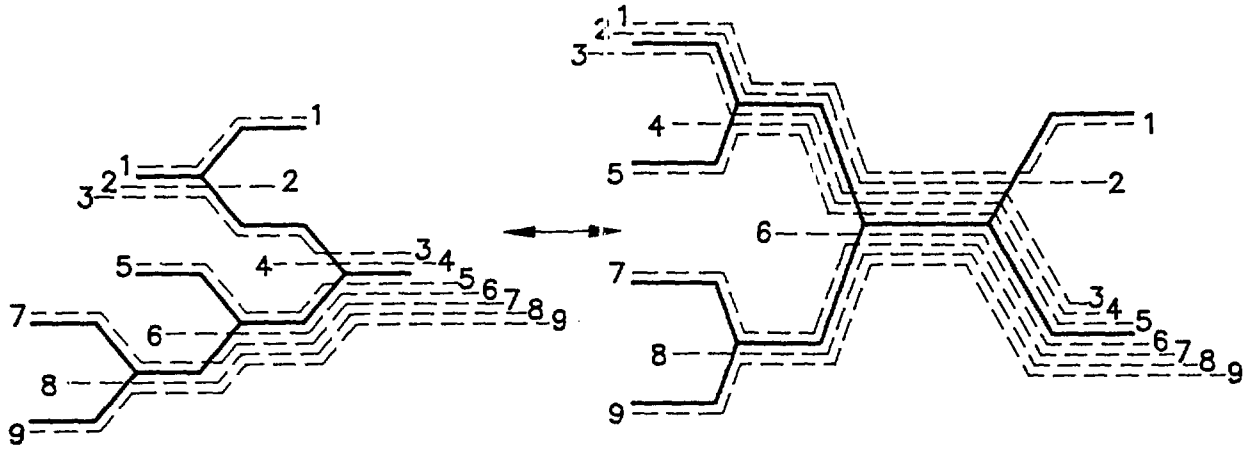

Fig. 7.11

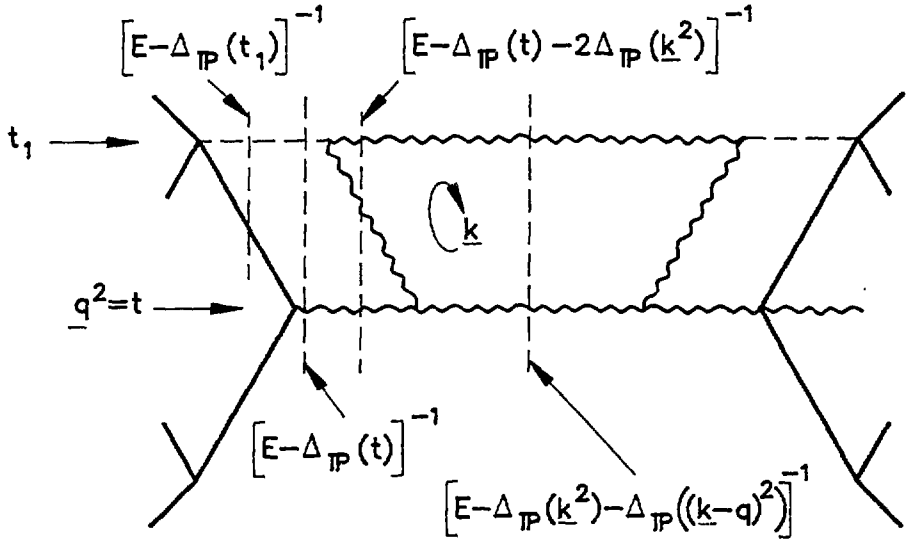

Fig. 7.12

Fig. 7.13

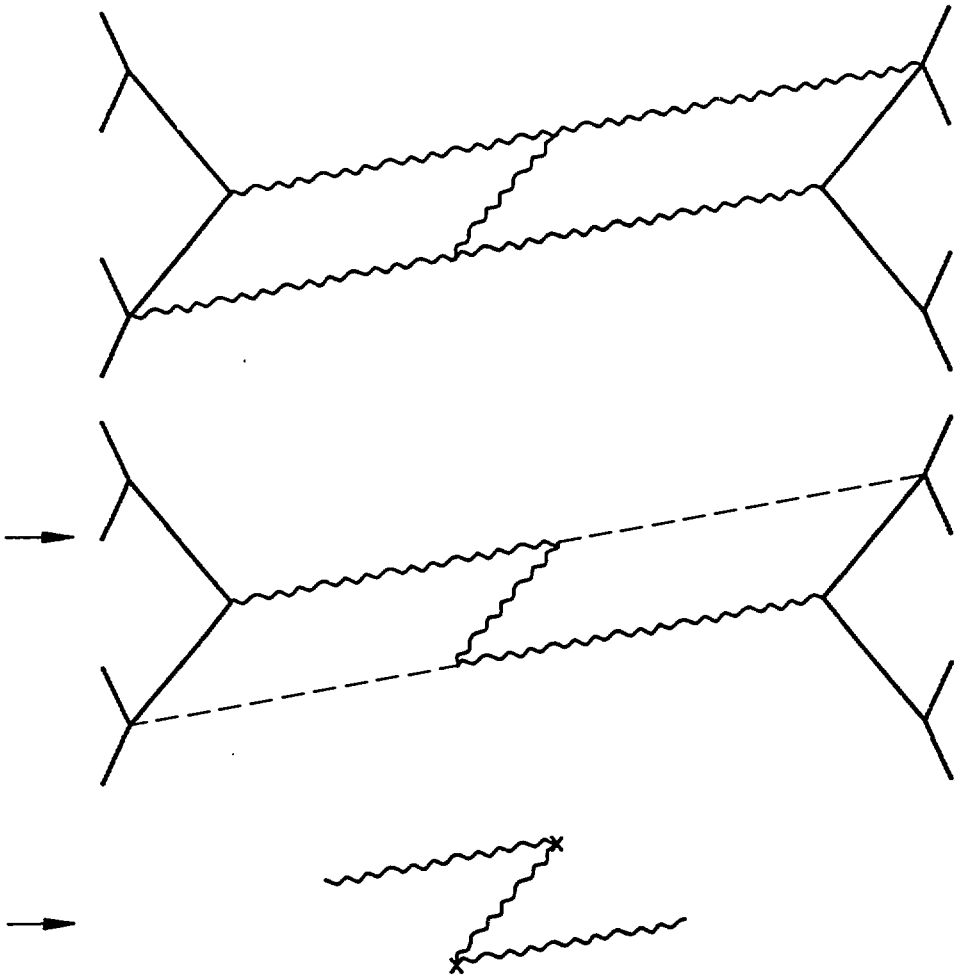

Fig. 7.14

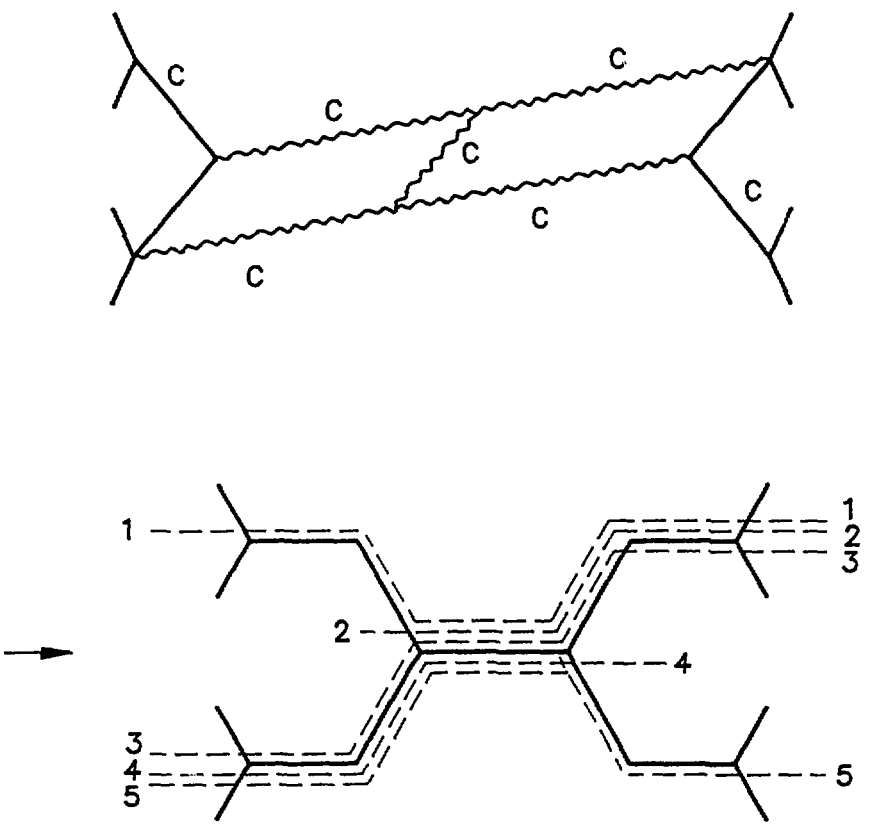

Fig. 7.15

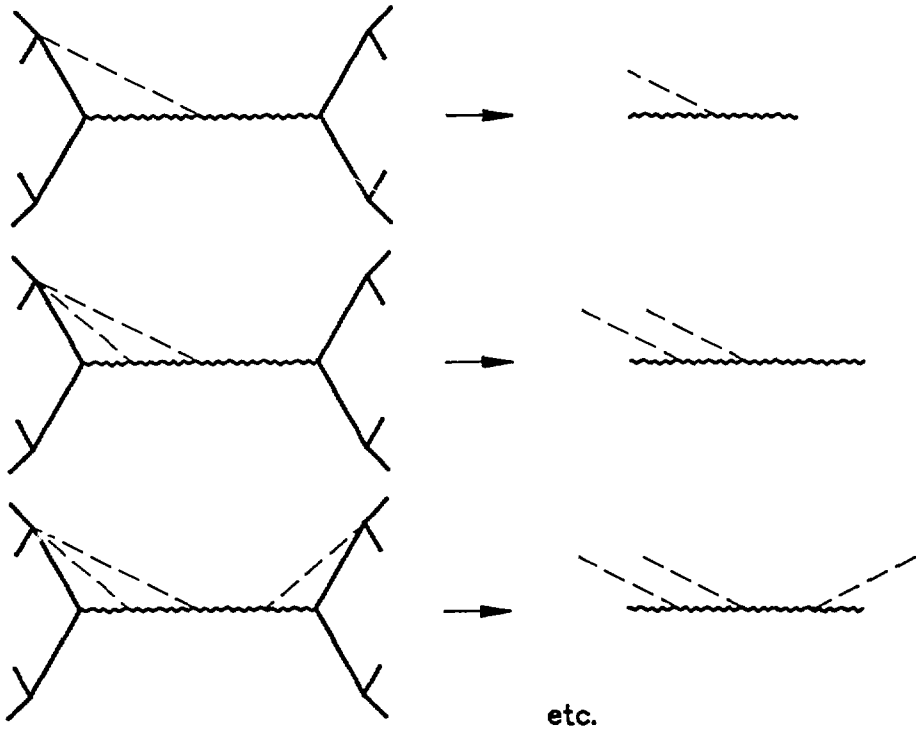

Fig. 7.16

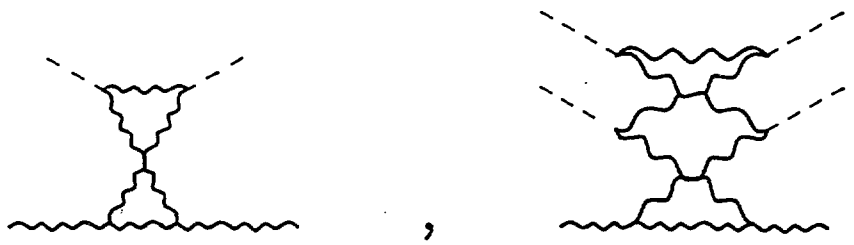

Fig. 7.17

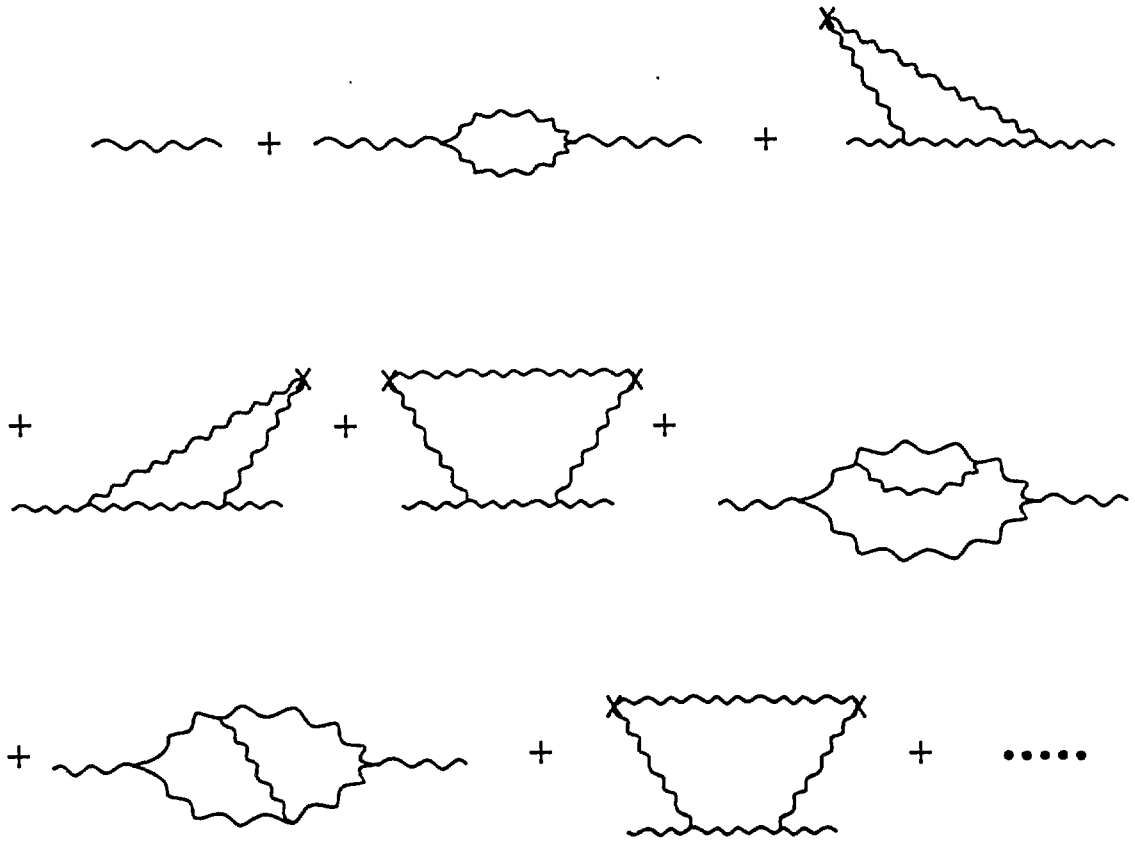

Fig. 7.18

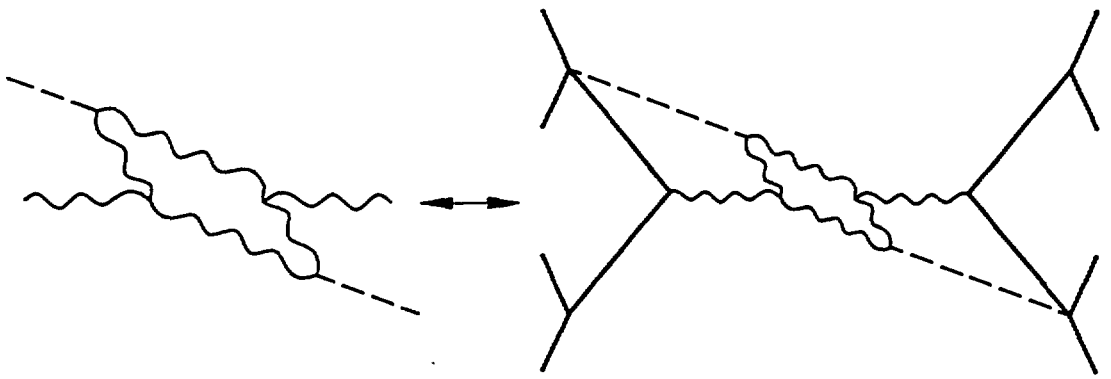

Fig. 7.19

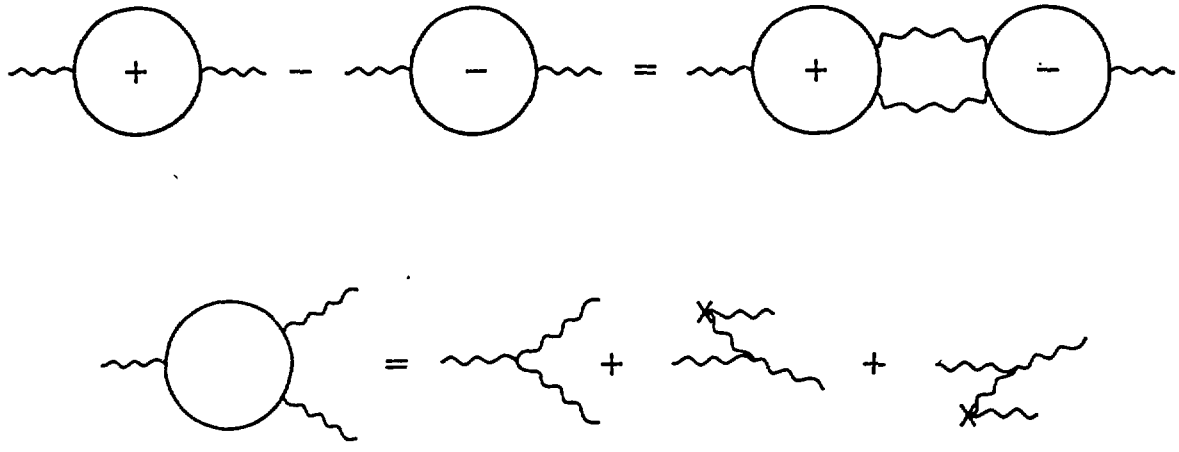

Fig. 7.20

——— ≡ ODD–SIGNATURE REGGEON STATE

Fig. 7.21

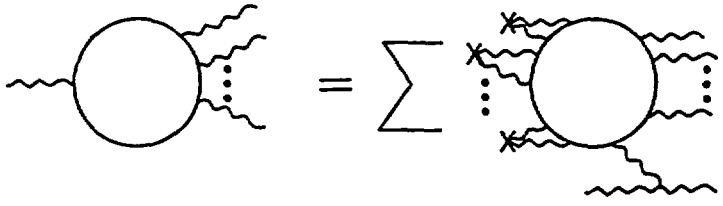

Fig. 7.22